
# The effects of selected proteinase inhibitors on the activity of subilases from psychrotrophic, mesophilic and thermophilic microorganisms

Kristinn Ragnar Óskarsson

**Raunvísindadeild**
**Háskóli Íslands**
**2013**

# The effects of selected proteinase inhibitors on the activity of subilases from psychrotrophic, mesophilic and thermophilic microorganisms

Kristinn Ragnar Óskarsson

16 eininga ritgerð sem er hluti af
*Baccalaureus Scientiarum* gráðu í Lífefnafræði

Leiðbeinandi
Magnús Már Kristjánsson, prófessor

Meðleiðbeinandi
Bjarni Ásgeirsson, prófessor

Raunvísindadeild
Verkfræði- og náttúruvísindasvið
Háskóli Íslands
Reykjavík, júní 2013

The effects of selected proteinase inhibitors on the activity of subilases from psychrotrophic, mesophilic and thermophilic microorganisms

16 eininga ritgerð sem er hluti af *Baccalaureus Scientiarum* gráðu í Lífefnafræði



Raunvísindadeild
Verkfræði- og náttúruvísindasvið
Háskóli Íslands
Hjarðarhaga 2-6
107 Reykjavík

Sími: 525 4600

Skráningarupplýsingar:
Kristinn Ragnar Óskarsson, 2013, *The effects of chosen proteinase inhibitors on the activity of subilases from psychrotrophic, mesophilic and thermophilic microorganisms*, BS ritgerð, Raunvísindadeild, Háskóli Íslands, 71 bls.

Prentun: Háskólaprent ehf
Reykjavík, júní 2013

# Útdráttur

Samspil hindra og próteinasa er mikilvægur þáttur í stjórnun lífvirkni í lífverum, án hindra myndu próteinasarnir brjóta niður vefi og valda skemmdum og jafnvel dauða. Þetta samspil er einnig góður mælikvarði á hvernig prótein-prótein hrif eru að verkum og gefa þannig vísbendingu um eiginleika viðkomandi próteinasa. Í þessu verkefni sem er hluti af stærra rannsóknarverkefni um hitastigsaðlögun próteina, voru þrír subtilísin-líkir serín próteasar (subtilasar) úr ptóteinasa K fjölskyldunni skoðaðir með tilliti til áhrifa mismunandi valinna hindra á eiginleika þeirra. Subtilasarnir sem skoðaðir voru, voru kuldavirkur subtilasi úr kuldakærri-bakteríu af *Vibrio* tegund (VPR), miðlungshitakæri subtilasinn próteinasi K úr sveppnum *Engyodontium album* (PRK) og háhitakæri subtilasinn aqualysín I úr bakteríunni *Thermus aquaticus* (AQUI). Til að kanna hindrunar eiginleika ensímanna voru gerðar samanburðarrannsóknir á þeim gegn níu hindrum, og af þeim níu voru valdir þrír hindrar til enn frekari mælinga en það voru óvómúkóíð úr kalkúnaeggjum (turkey ovomucoild trypsin inhibator (TOM)) og hindrarnir chymostatin (CHYS) og phenylmetylsulfónylflúoríð (PMSF). Óvómúkóíð eru prótein hindrar, en CHYS og PMFS eru lífrænar sameindir sem hannaðar hafa verið sem sértækir hindrar fyrir próteinasa. Reynt var að meta hvort munur væri á hindrunareiginleikum þessara hindra gagnvart próteinösunum þremur sem aðlagast hafa svo mismunandi hitastigum. Tilgátan var sú að meðal þessara náskyldu ensíma myndi kuldaaðlagaða ensímið hindrast hraðast meðal þessara ensíma vegna meiri sveigjanleika myndbyggingar þess sem leiddi m.a. til aukins aðgengis hindra að bindisetum og hvarfstöð ensímanna. Niðurstöður mælinga sýndu hinsvegar gagnstæða fylgni, þ.e. AQUI reyndist hindrast hraðast í tilfelli allra þessara hindra. Útfrá mælingum með PMSF var fundið út að það sem virtist vera ráðandi þáttur í þessum mun gæti verið aukin óreiða sem PRK og $VPR_{\Delta C}$ þyrftu að yfirvinna vegna þess að bygging þeirra er meira opin og sveigjanlegri miðað við myndbyggingu AQUI.

# Abstract

The interactions between proteases and protease inhibitors is an important part of maintaining balance in organisms, without inhibitors proteases would degrade various components and parts of the organism and cause damage and even death. These protease-protease inhibitor interactions are also good models for studying protein-protein interactions and therefore give clues to the characteristics of the chosen protein. In this study which is a part of a larger research project on temperature adaptation of subtilisin-like serine proteinases, or subtilases, three such homologous enzymes from the proteinase K family were studied with regard to inhibition effects by various inhibitors on their activities. The subtilases where a cold adapted protease from a psychrophilic bacterium of a *Vibrio* species (VPR), proteinase K from the mesophilic fungus *Engyodontium album* (PRK) and aqualysin I from the thermophilic bacterium *Thermus aquaticus* (AQUI). A comparative research was carried out on these proteases with respect to inhibition by nine different inhibitors. Based on the observed inhibitory pattern on the enzymes three of these inhibitors were selected for further measurements. These inhibitors were turkey ovomucoid trypsin inhibitor (TOM) and the two synthetic inhibitors, chymostatin (CHYS) and phenylmethylsulfonyl fluoride (PMSF). In order to determine difference in inhibition patterns, the kinetic rate constants were found from activity measurements of the enzymes in the absence and presence of the inhibitors. The hypothesis was that the cold adapted protease would be inhibited at the fastest rate as they have greater molecular flexibility and presumeably more accessibility of the active site residues. In fact the opposite was indeed observed as the observed inhibition rates were fastest in the case of the thermophilic AQUI. From the measurements done with PMSF against the subtilases it was determined that a possible governing factor causing the slower rate of inhibition of PRK and $VPR_{\Delta C}$ is the larger entropic contribution to the activation barrier for inhibition, most likely as the result of larger structural flexibility of these two subtilases in the uninhibited form compared to the thermophilic AQUI.

# Contents

# Figures

# Tables

# Acknowledgements

I would like to thank my professor Magnús Már Kristjánsson for good advice and help during the project. I would also want to thank Lilja Björk Jónsdóttir for endless help and teaching me how the various objects and equipment worked. And I would like to thank everyone else working around me for good conversations and advise.

# 1 Introduction

The biosphere contains a diverse environment from ice-cold regions such as around the Polar Regions, high mountains, ocean floors and so on to hot deserts, geysers and geothermal ducts as observed on the ocean floor, but these places do all support life. The largest portions of organisms are found in cold environments and cold-adapted organisms are the largest part of the biomass produced on Earth which are generated at temperatures around and under 5°C (Siddiqui and Cavicchili, 2006; Casanueva et al., 2010).

The organisms that are found in these extreme environments are microbes of all sorts, and to survive these hostile conditions, organisms have to adapt to different environmental factors such as temperature, pH, concentration of salt and pressure. For life to function the various chemical reactions of organisms have to go smoothly and they are catalyzed by enzymes and the building blocks of life are proteins and so for life to prevail these proteins have to fold correctly and function in the right way. Microorganisms can be classified after their optimum growth temperature and are commonly classified into four groups psychrophilic ($0 < T_{opt} < 20°C$), mesophilic ($20 < T_{opt} < 50°C$), thermophilic ($50 < T_{opt} < 80°C$) and hyperthermophilic ($80 < T_{opt} < 120°C$) (Karshikoff and Ladenstein, 2001).To grasp the diversity of how incredibly resilient life is, reports of organisms surviving at temperatures from -20°C to 121°C have been reported (Feller and Gerday, 2003; Kashefi and Lovley, 2003; Siddiqui and Cavicchili, 2006).

The proteins from these organisms provide an opportunity through comparative research to attempt to understand which structural factors determine their temperature adaptation.

## 1.1 Temperature adaptation of proteins

Enzymes that have to function in cold environments have to overcome the main problem of slower reaction rates than occur at higher temperatures. From comparative research of homologous enzymes adapted to different temperatures it has been shown that the active sites are conserved so the fundamental mechanisms of the reactions are the same. In cold environments there is a lack of evolutionary pressure to produce stable proteins as denaturation of proteins due to temperature is not a major problem resulting in structures that are more flexible to counteract the molecular restrains due to low temperatures. The surface of cold-adapted proteins has been shown to have improved electrostatic potentials which has been theorized to be one of the factors that direct their substrates to the binding- and active-

sites of these proteins which leads to higher $k_{cat}$ and in most cases higher $K_m$ but the flexibility reduces $\Delta H^{\#}$ (activation enthalpy) (D´Amico et al., 2003).

This enhanced flexibility which is often highly connected to the areas around the active site does provide these enzymes with higher activity than that of their thermophilic counterparts though there are known exceptions and it can be said that stability is sacrificed for more activity (Siddiqui and Cavicchili, 2006). Other traits that seem to correlate with cold-adaptation are for example reduced number of salt-bridges (defined as an ion pair with a distance of 2.5 - 4.0 Å), hydrogen bonds, aromatic interactions, and internal hydrophobic interactions and fewer numbers of Pro, Arg and Lys amino acid residues (Almog et al., 2008; Casanueva et al., 2010). Higher levels of polar uncharged amino acid residues have also been observed in cold-adapted enzymes, though these traits aren't found in all cold-adapted proteins it seems as each family has adopted its own way to handle the problems that come with cold temperature (Siddiqui and Cavicchili, 2006) (Kristjánsson, 2013)

Conformational stability can be evaluated from the Gibbs-Helmholtz equation (equation 1)

$$\Delta G(T) = \Delta H_m \left(1 - \frac{T}{T_m}\right) + \Delta C_p (T - T_m) - T\Delta C_p \ln\left(\frac{T}{T_m}\right) \qquad (1)$$

$\Delta G(T)$ is the free energy needed to disrupt the folded state and is 0 at $T_m$ (melting point). $\Delta H_m$ is the enthalpy change at $T_m$ and $\Delta C_p$ is the heat capacity at a constant pressure. With this equation a stability curve can the plotted, where $\Delta G$ is plotted against the temperature (figure 1) (Siddiqui and Cavicchili, 2006).

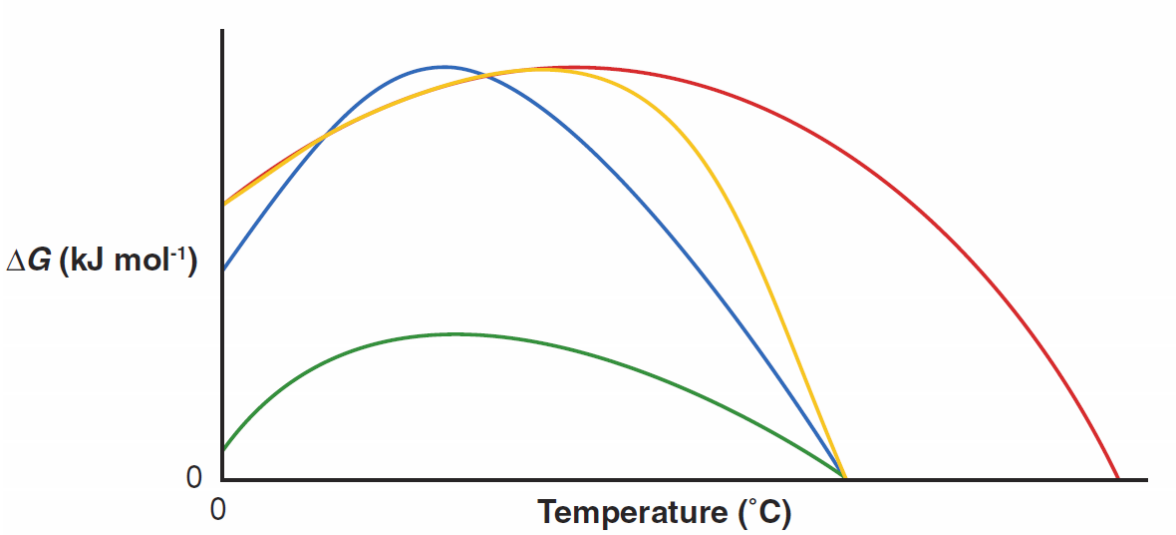


*Figure 1. Hypothetical stability curves for cold-adapted enzymes (blue, green and yellow lines) and thermostable enzymes (red line). The blue, green and yellow lines show possible*

*ways to achieve lower stability, by shifting $T_{max}$ (highest part of the curve) downwards but maintaining $\Delta G$ (blue line), maintaining both $\Delta G$ and $T_{max}$ but with a higher gradient of denaturation (orange line) or by lowering both $\Delta G$ and $T_{max}$ (green line) (Siddiqui and Cavicchili., 2006).*

Enzymes from thermophilic organisms have to adapt to circumstances where high temperatures in the environment put an evolutionary pressure to produce heat-stable enzymes capable to maintain optimal activity at elevated temperatures. Activity however, may have to be sacrificed at lower temperatures to maintain it at high temperatures as the rigidity of their structure does lead to reduced molecular mobility and thus reduced activity (Arnold et al., 2001; Li et al., 2005).

The stability of proteins comes from thermodynamic and kinetic stability, where thermodynamic stability is defined by the enzymes free energy barrier ($\Delta G_{stab}$) and its melting point $T_m$ and kinetic stability is often defined as the half-life at a certain temperature and by elevating these values thermostability can be gained (see figure 1) (Li et al., 2005).

Structural reasons for thermostability have been examined extensively and researchers have not found any indications of any abnormal amino acid (new or modified), new structural motifs or any new covalent modifications to explain the activity and stability at high temperatures. On the other hand there are some aspects in the structure that do correlate with the high thermostability of enzymes from thermophilic organisms, or thermozymes. Higher number of hydrogen bonds, increased number of the amino acids Glu, Lys and Arg, especially in clusters which leads to an increase of salt-bridges as well as other electrostatic interactions, such as charge-dipole and dipole-dipole interactions are observed in thermozymes and are believed to contribute to the net stabilization gain. Disulfide-bridges and metal-binding sites have been shown to lead to thermostabilisation but a clear correlation has not been established in thermophilic proteins (Smith et al., 1999; Li et al., 2005; Kristjánsson, 2012).

Generally thermozymes are believed to have more rigid structures than their mesophilic and cold-adapted counterparts, which is essential for maintaining activity at high temperature. This rigidity is a result of tighter packing of the enzyme´s interior where the hydrophobic packing is high leading to fewer cavities. Fewer Gly residues are often observed which would be stabilizing by leading to a reduction of the entropy of unfolding ($\Delta S$), which is counteracting the stability gained from the elevation of $\Delta H$ form various non-covalent interactions in the protein (Li et al., 2005; Siddiqui and Cavicchili, 2006) as according to the relationship:

$$\Delta G = \Delta H - T\Delta S \quad (2)$$

Where ΔG stands for the free energy barrier between folded and unfolded states of the enzyme and ΔH stands for the enthalpy contributing to ΔG, T stands for the absolute temperature and ΔS is the entropy. Other factors suggested to contribute to the stability of thermozymes is the stabilization of α-helixes dipoles as it is often observed that negatively charged residues are positioned near the N-terminal and positively charged residues near the C-terminal. Also, there is a tendency in thermozymes to have shorter surface-loops with Pro residues which increases their rigidity. This with tighter packing reduces the accessible surface area of the protein, thus minimizing the interactions of the solvent with the protein (Li et al., 2005).

Overall the various properties of natural cold-adapted and thermophilic enzymes see to show a clear trade-off where high stability is traded for lower activity and high activity is traded in for lower stability (see figure 2). A few studies however, have showed that it is possible to make mutants that have shown high activity and higher stability (Arnold et al., 2001).

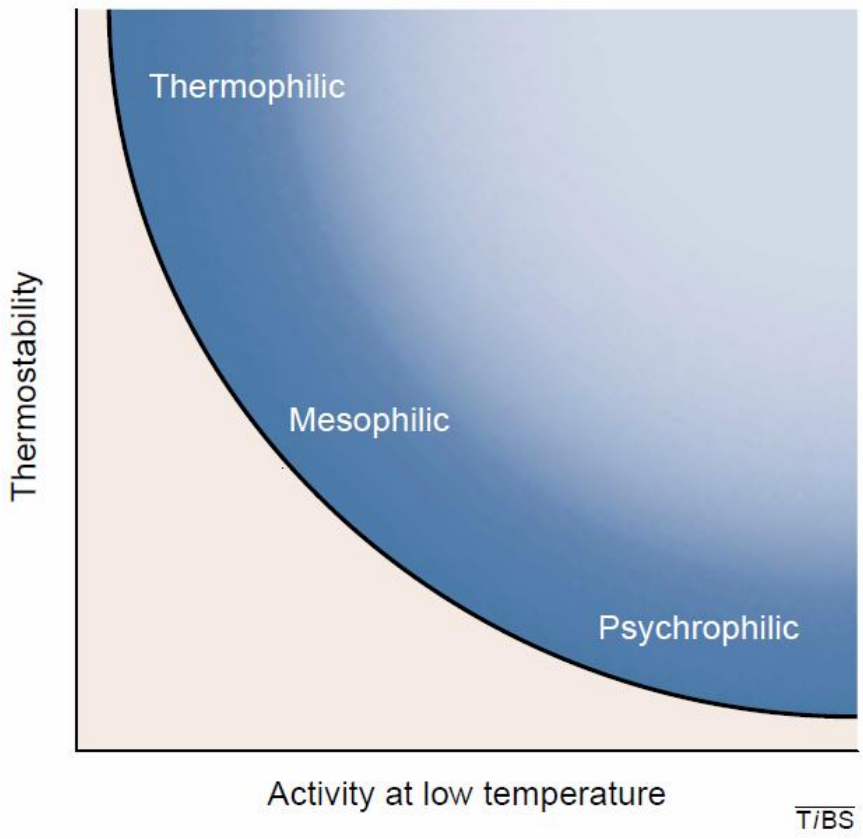


*Figure 2. The correlation between thermostability and activity of homologus enzymes (Arnold et al., 2001).*

## 1.2 Proteases

Proteinases are enzymes that catalyze peptide bond breakdown via hydrolysis and are necessary to accelerate biological pathways to maintain homeostasis and nature has found many various ways to solve that problem (Buller and Townsend, 2013). According to MEROPS database (merops.sanger.ac.uk) proteinases are classified as ten different groups aspartic, cysteine, glutamic, metallo, asparagine, mixed, serine threonine, unknown or compound peptidases and is this classification based on their active site structure and activity.

This class of enzymes is well characterized and can be found in many different organisms and serve diverse roles. Known uses for them in nature are for example in some bacteria that secrete proteinases to manipulate their environment, also proteinases are found in blood-clotting factors (Olson and Chuang, 2002; Oldak and Trafny, 2005). These proteinases have been widely studied, partly because they have proved to be important in industrial applications for example they have been used in laundry detergents. Many industrial processes are conducted at high temperatures and therefore thermostable proteases have been of great interest (Bruins et al., 2001).

### 1.2.1 Serine proteinases

Serine proteinases are proteolytic enzymes that depend upon a serine residue in their active site and belong to many different families of proteins. It has become apparent that these families have different evolutionary origin and can therefore be classified into different clans of families. One way of dividing serine proteinases is to classify them after their catalytic residues (Barrett and Rawlings, 1995). The active site of these enzymes is characterized in most cases by a catalytic triad composed of Asp, His and the essential Ser residue, but other forms of active sites are known (Page and Cera, 2008).

**Table 1**. The diversity of serine proteinases, their structure, catalytic residues and specificity. # = residues acting as nucleophile. *Seven additional families in clan PA of viral orgin apply a nucleophilic Cys to mediate bond hydrolysis (Page and Cera, 2008).

| Clan | Families | Representative member | Fold | Catalytic residues | # | Primary specificity | PDB |
|---|---|---|---|---|---|---|---|
| PA | 12* | Trypsin | Greek-key β-barrels | His, Asp, Ser | 195 | A, D, F, G, K, Q, R, W, Y | 1DPO |
| SB | 2 | Subtilisin, sedolisin | 3-layer sandwich | Asp, His, Ser | 221 | F, W, Y | 1SCN |
| SC | 2 | Prolyl oligopeptidase | α/β hydrolase | Ser, Asp, His | 554 | G, P | 1QFS |
| SE | 6 | D-Ala–D-Ala carboxypeptidase | α-helical bundle | Ser, Lys | 62 | D-A | 3PTE |
| SF | 3 | LexA peptidase | all β | Ser, Lys/His | 119 | A | 1JHH |
| SH | 2 | Cytomegalovirus assemblin | α/β Barrel | His, Ser, His | 132 | A | 1LAY |
| SJ | 1 | Lon peptidase | α+β | Ser, Lys | 679 | K, L, M, R, S | 1RR9 |
| SK | 2 | Clp peptidase | αβ | Ser, His, Asp | 97 | A | 1TYF |
| SP | 3 | Nucleoporin | all β | His, Ser | na | F | 1KO6 |
| SQ | 1 | Aminopeptidase DmpA | 4-layer sandwich | Ser | 250 | A, G, K, R | 1B65 |
| SR | 1 | Lactoferrin | 3-layer sandwich | Lys, Ser | 259 | K, R | 1LCT |
| SS | 14 | L,D-Carboxypeptidase | β-sheet+β-barrel | Ser, Glu, His | 115 | K | 1ZRS |
| ST | 5 | Rhomboid | α-barrel | His, Ser | 201 | D, E | 2IC8 |

These enzymes can be classified as thirteen different clans at least (table 1). Clan PA is the largest of the clans of serine-proteinases and contains digestive enzymes such as trypsin and chymotrypsin which cleave polypeptide chains at the C-terminal side of a positively charged side chains or large hydrophobic side chains respectively. These families share a common ancestor protein with chymotrypsin (family S1) and share its fold. Among other families in this clan are are α-lytic endopeptidase (family S2), sindbis virus core endopeptidase (family S3) and lysyl endopeptidase (family S5) for example. Most members belonging to this clan so far are recognized as endopeptidases and share the order of the catalytic triad residues His/Asp/Ser (HDS) (Barrett and Rawlings, 1995; Page and Cera, 2008).

Clan SB peptidases are prevalent in plant and bacterial genomes but few are known in the animal genomes (Rockwell and Thorner, 2004; Page and Cera, 2008). The archetype of this clan is subtilisin which was first discovered in the Gram positive bacterium *Bacillus subtilis* and is like chymotrypsin one of the first proteins to have their crystal structures determined. The structure of the enzymes of the subtilisin family (family S8) is different from that of the enzymes of proteinases in clan PA. So they must have evolved independently from the chymotrypsin-like serine proteinases in clan PA. The catalytic triad of family S8 contains the same amino acids but in a different order, or Asp/His/Ser (DHS) but has the exactly same geometric organization of these residues in the active sites of the enzymes as observed in clan PA. Subtilisins have been used as a model for protein engineering studies for thermal stability, cold adaptation and stability in non-aqueous solvents through rational mutagenesis and directed evolution (Barrett and Rawlings, 1995; Page and Cera, 2008). This clan also contains another family of proteinases (family S58), the sedolisins where the His general base is substituted by the amino acid Glu and the tetrahedral intermediate is stabilized by a

negative charged carboxyl group rather than partial positive charges and are active at low pH and have proven to be rather useful for protein engineering studies (Barrett and Rawlings, 1995; Page and Cera, 2008).

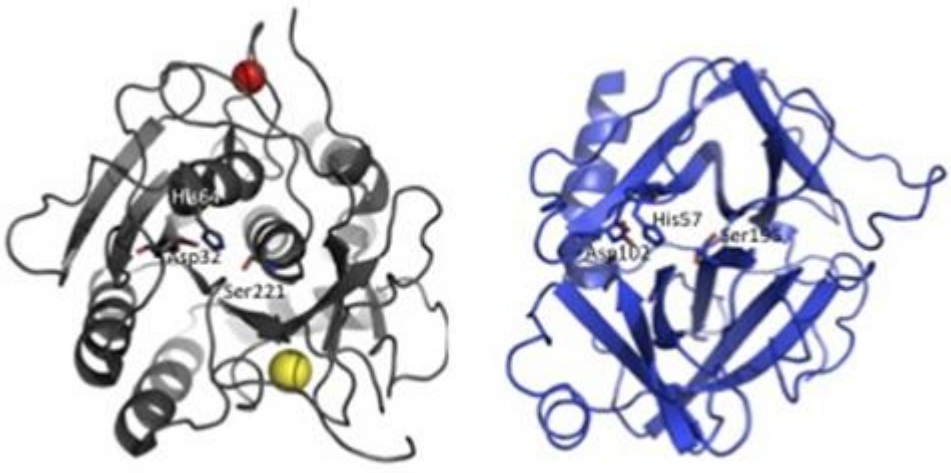


*Figure 3. A comparison of overall three-dimensional structures of Chymotrypsin-like serine protease (to the right) and a subtilisin-like serine proteinase (to the left). The difference in the structure between the enzymes is obvious; chymotrypsin has a β-fold and the subtilisin has a α/β-fold (Kristjánsson, 2012).*

Other clans of serine-proteinases are clan SE which are mostly found in bacteria and contribute to the cell wall metabolism, clan SF containing the LexA repressor from *E.coli* and contributes to the SOS response to DNA damage and also contains the S24 family that is responsible for signal peptidase removal in organisms from all kingdoms of life. Clan SJ which has the unique nature of being ATP-dependent, clan SK together with enzymes form clan PA are responsible for intracellular protein levels in some bacteria. Clans SH, SP, SQ, SR and SS are small clans each containing one family of proteinases and some of them are found in several viral genomes and clan ST known for their ability to hydrolyze peptide bonds within the phospholipid bilayer (Page and Cera, 2008).

### 1.2.2 Subtilisin-like serine-proteinases

Subtilisin-like serine-proteinases (subtilases) of the S8 family can be divided into two subfamilies S8A which contains the typical subtilisin and S8B which contains the eukaryotic subtilase kexin. These subtilases have also been divided into six different families based on the homology in their amino acid sequences. Each family of these six families is named after

a well characterized enzyme from each group as: subtilisin, thermitase, proteinase K, lantibiotic peptidase, kexin and pyrolysin (Kristjánsson, 2012).

Subtilases are mostly produced as multidomain proteins and the variability of their structure and combination is rather high. The subtilisin fold is classified as α/β-fold composed of β-α-β units with parallel beta-sheets. For subtilases this fold has been characterized as a three layer α-β-α-sandwich with the orientation of the beta-strands 2-3-1-4-5-6-7, which contains a rare left-handed crossover connection between strands 2 and 3 and is similar to the Rossmann fold. The connection between the beta-sheets and the α-helices are loops that lie on the surface of the protein (Kristjánsson, 2012).

All prokaryotic subtilases are produced as precursor proteins which are composed of a signal-peptide, an N-terminal prodomain which acts as an intra-molecular chaperone, and an enzyme domain, which are then cleaved off in the activation of the enzyme (Kristjánsson, 2012).

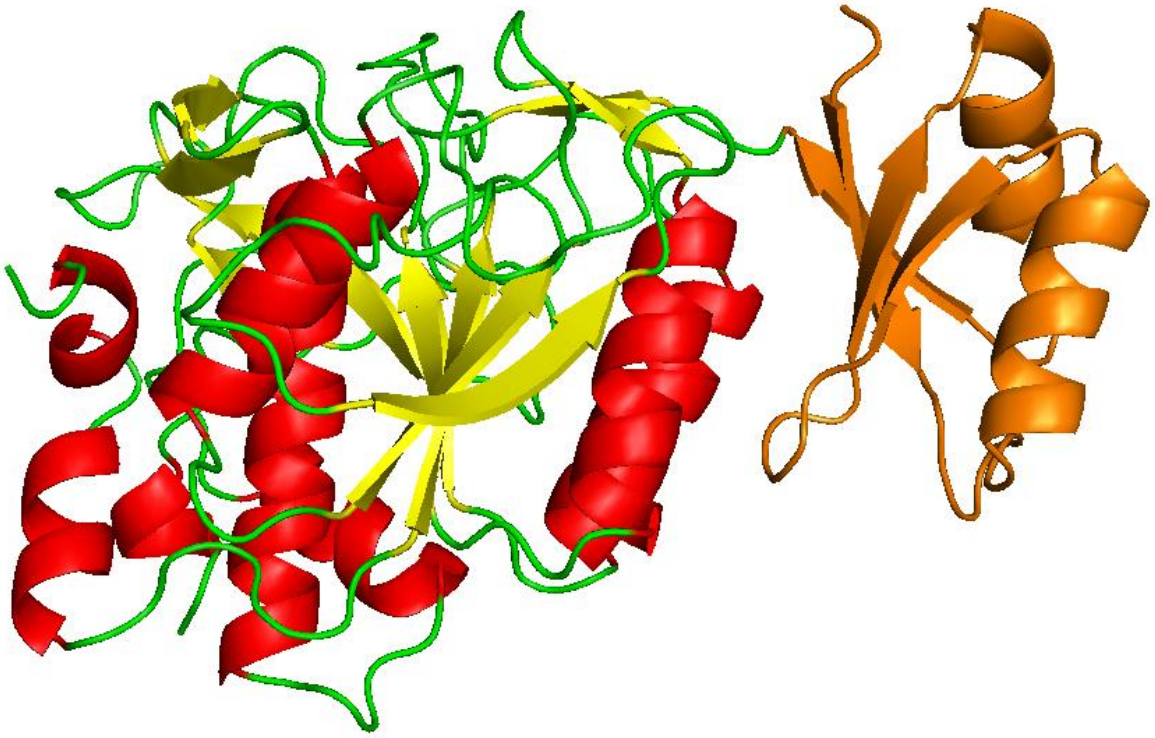

*Figure 4. The structure of the precursor protein of BPN´ (PDB entry 1SPB), the predomain is 77 residues (orange) and does acts an intra-molecular chaperone during the folding process and is cleaved off in the activation of the enzyme. Drawn with PyMOL.*

The prodomain is important in the folding of the enzyme and without it, it would fold very slowly. Cleaving of the prodomain via autolysis in the activation of the protein, contributes to the stability of these proteins as the free-energy barriers which are very high between folded and unfolded structures of the proteins without the prodomain and this makes the unfolding process very slow and therefore the native structure of the enzymes are kinetically stable. This

method for stabilization has been observed in α-lytic-like proteinases as well as in subtilases (Kristjánsson, 2012). Another factor that contributes to the energy barrier is the binding of $Ca^{2+}$ ions in the native state. The "true" subtilisins do usually contain two binding sites for calcium ions but highly different arrangements with respect to calcium binding have been observed, such as in subtilase 3 (SBT3) from tomato which does not bind calcium ions (Ottmann, 2009), and Tk-subtilisin from *Thermococcus kodakaraenis* which has seven binding sites (Tanaka et al., 2007). In total there are 16 different known binding sites in crystal structures of the different subtilases (Tanaka et al., 2007; Kristjánsson, 2012).

The location of the active site in subtilases is in a cleft on the surface formed by two adjacent α-helices and a central β-sheet. The cleft also contains the substrate binding site (see figure 5) (Kristjánsson, 2012).

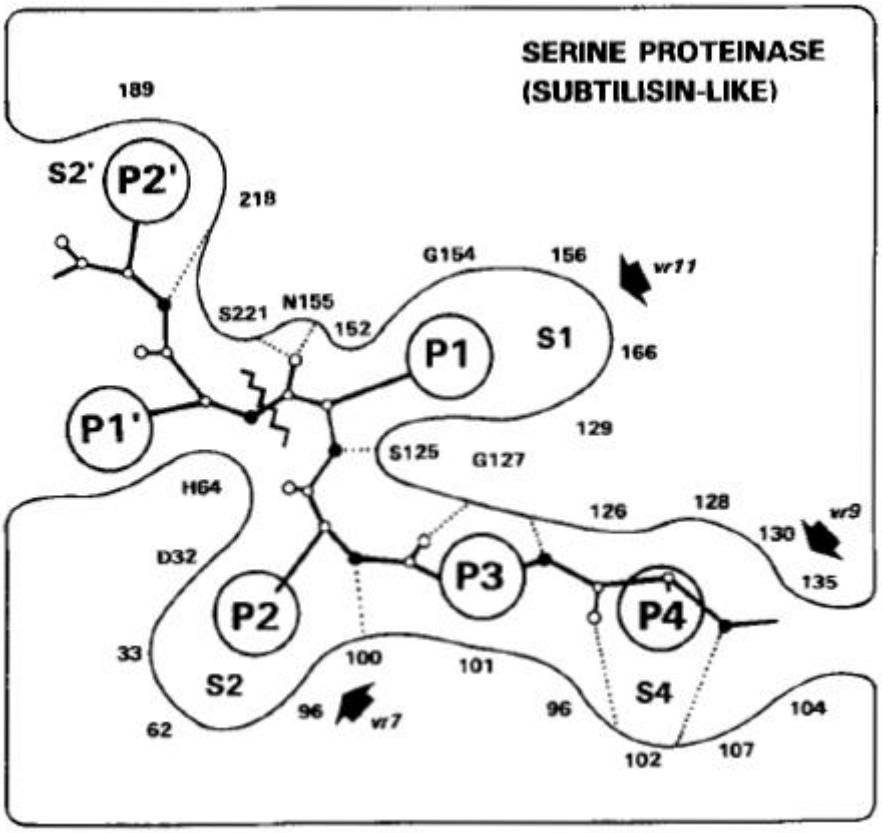


*Figure 5. A schematic drawing of the enzyme-substrate binding for subtilisin BPN´, P1- P2- P2´ and P4 are side-chains of residues of the substrate and S1- S2- S2´- S4 are the corresponding binding sites on the enzyme. The jagged line is the scissile bond that will undergo hydrolysis. Dotted lines show hydrogen-bonds (Siezen and Leunissen, 1997).*

The mechanism for hydrolysis of peptide-bonds for all subtilases is carried out via an acyl transfer mechanism and the formation of a Michaelis complex which is followed by an attack on the carbonyl carbon of the scissile-bond by the serine of the catalytic triad which has enhanced nucleophilic properties due to the adjacent histidine which is acting as a base catalyst. Then a proton donation from the histidine to the newly formed amide-group leads to the dissociation of the first product and a formation of a covalent acyl-enzyme complex. The deacylation occurs via the same mechanism where the nucleophilic attack comes from a water molecule which fills the vacated area where the first product was released from, both these steps are processed thru a tetrahedral intermediate (see figure 6) (Perona and Craik, 1995).

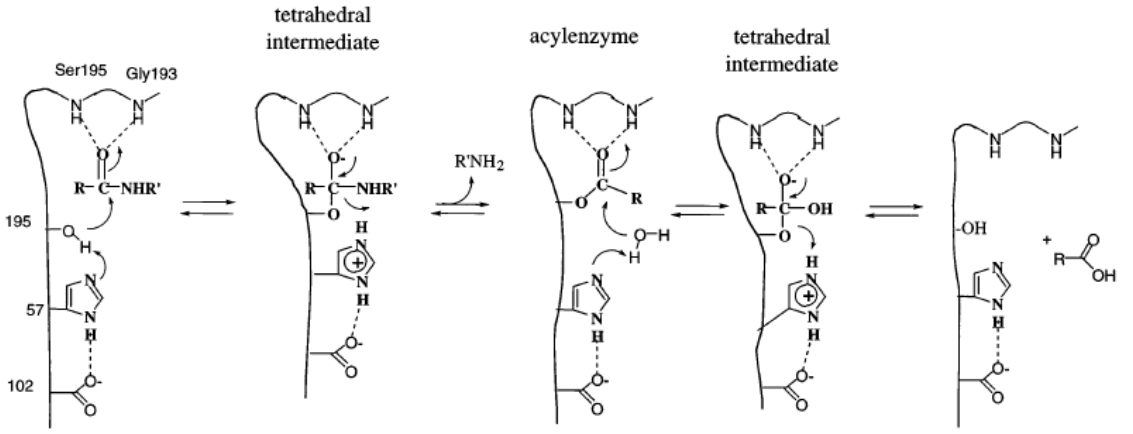


*Figure 6. The reaction mechanism for serine proteases as generally accepted, two main steps are the acyl-enzyme complex and the de-acylation, with a formation of a tetrahedral intermediate (Hedstrom, 2002)*

### 1.2.3 Proteinase K (PRK)

The proteinase K family is named after the subtilisin-like proteinase K (PRK) which is the representative enzyme in this family. This large family of endopeptidases is found in fungi, yeasts, and Gram-negative bacteria and they share a high degree of sequence similarity, or over 37% (Siezen and Leunissen, 1997). This family has been studied extensively and for example includes the thermostable aqualysin I (AQUI) and the cold-adapted proteinase from a *Vibrio* species PA-44 (VPR) been studied for their adaptation to different environments (Kristjánsson et al., 1999, Arnórsdóttir et al., 2002, Arnórsdóttir et al., 2005) (Arnórsdóttir et al., 2007; Sigurðardóttir et al., 2009). All these proteins are produced with large propeptides, or intramolecular chaperones (IMC) that mediate the folding process, as without these IMC the proteins would fold into an inactive molten-globule state (Marie-Claire et al., 2001).

Proteinase K is secreted by the fungus *Engyodontium album* (formerly *Tritirachium album*) which is a mesophilic organism and the molecular weight of the proteinase is 28.930 kDa (Jany and Mayer, 1985) consisting of 279 amino acid residues (Betzel et al., 1988). PRK

contains five cysteines, four of which form two disulfide-bridges and the position of the catalytic triad is $Asp^{39}$-$His^{69}$-$Ser^{224}$ (Müller and Saenger, 1993).

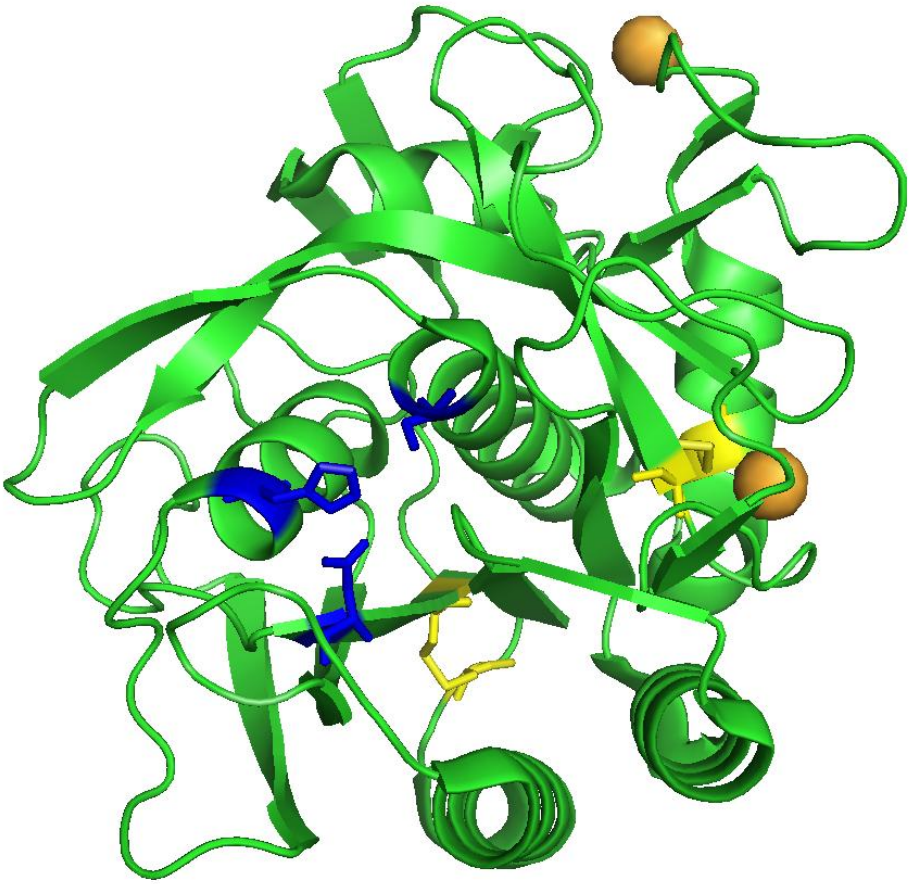

*Figure 7. Proteinase K (PRK) with the catalytic triad $Asp^{39}$-$His^{69}$-$Ser^{224}$ colored in blue, and the two disulfide-bridges are marked as yellow and the calcium ions are bronze (PDB entry 2PRK) Drawn with PyMOL.*

Proteins within this family have been studied extensively. Four calcium binding sites have been indentified in proteinases of the proteinase K family and they are an important factor in the stabilization of proteins in this family. PRK contains two of these calcium binding sites, called Ca1 and Ca2, of which the Ca1 binds calcium stronger. A study conducted to determine the stability contributions of these calcium ion binding sites has revealed a large effect of this calcium binding on the thermal stability of the enzymes (Kristjánsson, 2012). A solution of PRK is stable over a broad pH range or 4.0-12.5 with an optimum activity at pH 8.0 and at pH 8.0 PRK is stable in the temperature range of 25-65°C (Ebeling et al., 1974).

### 1.2.4 The thermostable proteinase K-like proteinase aqualysin I (AQUI) and the cold adapted proteinase K-like proteinase from a psychrotrophic *Vibrio* species (VPR)

AQUI and VPR are members of the proteinase K family, and thus homologs of PRK. AQUI is a thermostable homolog of PRK and the active enzyme contains 279 amino acid residues and has a molecular weight of 28 kDa (Matsuzawa et al., 1988; Sakaguchi et al., 2008). It is produced as a precursor protein with a 113 residue N-terminal propeptide which is considerably longer in comparison to the 77 amino acid residue propeptide of subtilisin BPN´ (Marie-Claire et al., 2001). VPR the cold adapted homologue of PRK and AQUI is also produced with a large N-terminal propeptide consisting of 139 amino acid residues which are cleaved off in the activation process leading to a 291 amino acid residue long protease with a Mr of 29.7 kDa (Arnórsdóttir et al., 2002). AQUI and VPR both also contain over 100 residue long C-terminal domains which are cleaved off autocatalytically on secretion of the enzymes (Figure 8).

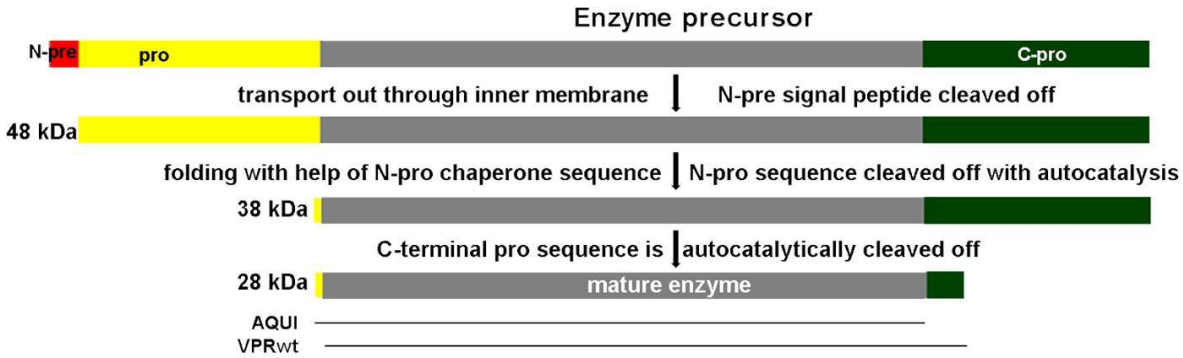


*Figure 8. A schematic representation showing the process of the precursor proteins that of AQUI and VPR upon folding and secretion. A signal peptide is shown in red, the N-terminal prodomain is in yellow, the C-terminal domain is in green and the mature subtilase domain is in grey. The mature AQUI is 15 residues shorter than the wildtype VPR (Kristjánsson, 2012).*

Calcium binding loops are present in both VPR and AQUI and even though it has been shown that they contribute to thermostabilization there is not a direct correlation between the number of calcium binding sites and thermostabilization. VPR contains three binding sites while PRK and AQUI contain two. The position of these calcium binding sites show that AQUI shares its binding sites with VPR and one of the binding sites of VPR and AQUI corresponds to the stronger of the two binding sites in PRK (see figures 7, 9 and 10). VPR contains a third binding site that is found in neither AQUI nor PRK but is known in some other subtilases, but was first described in the structure of thermitase from *T. vulgaris* (Betzel et al., 1990; Tepliakov et al., 1990).

VPR has three disulfide-bridges two of which are positioned close to the calcium binding loops and are also present in AQUI but the third is located at the very end of the C-terminal of

the active enzyme domain (figure 9). These bridges have not been shown to correlate with temperature adaptation but at least one of those disulfide-bridges has been found to correlate with the integrity of the active enzyme structure (Kristjánsson et al., 1999). VPR, as some other cold adapted enzymes has an increased anionic character which has been proposed to contribute to the flexibility of cold adapted proteins. The active site is oriented in the same way as in PRK and is $Asp^{37}$-$His^{70}$-$Ser^{220}$ (Arnórsdóttir et al., 2005; Sigurðardóttir et al., 2009).

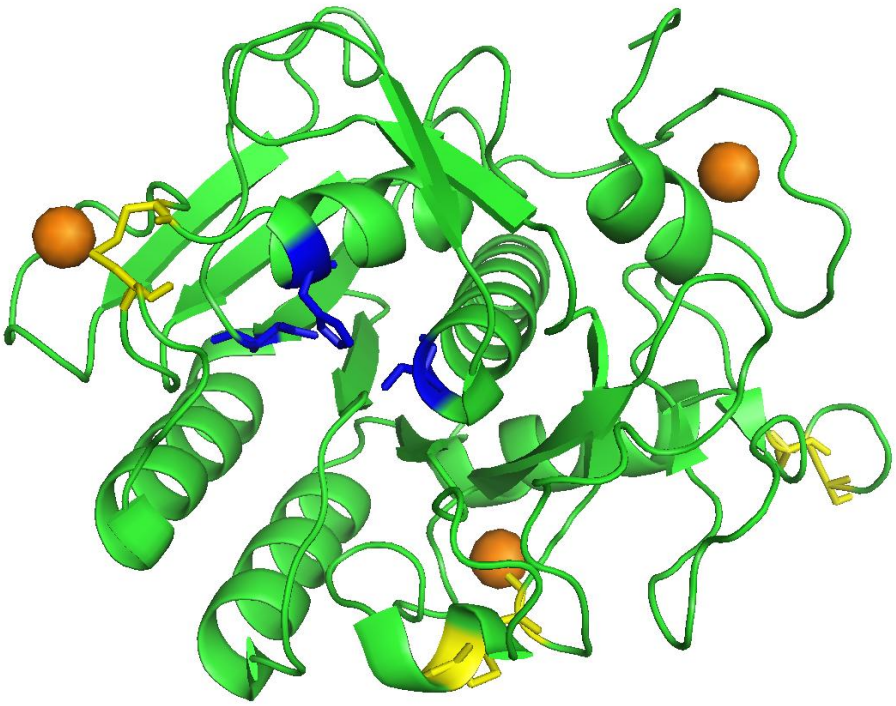

*Figure 9. Structure of VPR with the catalytic triad $Asp^{37}$-$His^{70}$-$Ser^{220}$ colored blue, and the three disulfide-bridges are marked as yellow and the calcium ions are bronze (PDB entry 1SH7). Drawn with PyMOL.*

VPR from the psychrotropic *Vibrio* species is rather stable in the presence of calcium and retains full stability up to 40°C but at temperatures of 50°C or higher the enzyme becomes unstable and starts to unfold, and has a $T_{50\%}$ value of 54°C compared to 69°C that of PRK and 95°C for AQUI (Kristjánsson et al., 1999). VPR has shown higher activity than PRK and AQUI and lower stability at higher temperatures and has been studied extensively with respect to its cold-adaptive properties by the use of site directed mutagenesis (Kristjánsson et al., 1999; Arnórsdóttir et al., 2002; Arnórsdóttir et al., 2005; Arnórsdóttir et al., 2007; Sigurðardóttir et al., 2009).

AQUI is secreted by the Gram-negative extreme thermophile *Thermus aquaticus* YT-1. The enzyme has optimal pH for activity around 10.0, but is active in the pH range of 6-11 and has a maximum activity in the presence of calcium at 80°C (Matsuzawa et al., 1988). AQUI binds two calcium ions that affect the thermostability of the protein, Ca1 site in AQUI corresponds

to the Ca1 in PRK but the second one corresponds to the third site in VPR (Kristjánsson 2012). The catalytic triad is oriented in the same way as in PRK and VPR, $Asp^{39}$-$His^{70}$-$Ser^{222}$ and there are two disulfide-bridges present in the conserved regions, two of which correspond to disulfide-bridges in VPR (see figures 9 and 10) (Arnórsdóttir et al., 2011). Comparing the different properties of AQUI, PRK and VPR with respect to stability and activity at different temperatures indicated that these homologous enzymes show all the traits of temperature adaptation. i.e. the thermophilic, AQUI showing the highest stability at high temperatures but lowest activity, with the opposite being observed for the psychrophilic VPR (Kristjánsson et al., 1999).

Comparison of the amino acid sequence of the three enzymes shows a high correlation or 60% identity for VPR and AQUI and 41% identity between VPR and PRK (Arnórsdóttir et al., 2002).

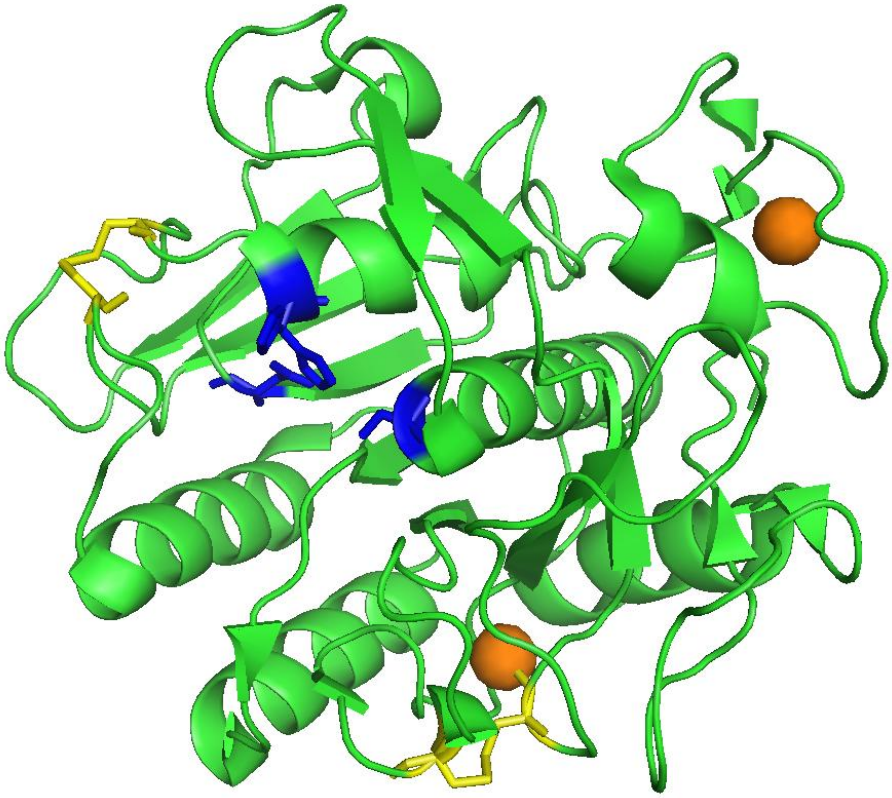

*Figure 10. Structure of AQUI with the catalytic triad $Asp^{39}$-$His^{70}$-$Ser^{222}$ colored blue, and the three disulfide-bridges are marked as yellow and the calcium ions are bronze (PDB entry 4DZT). Drawn with PyMOL.*

The similarities between the structures of AQUI, PRK and VPR makes these enzymes an excellent model to examine what factors in the structure of these proteins contribute to the temperature adaptation (Kristjánsson et al., 1999; Arnórsdóttir et al., 2002; Arnórsdóttir et al., 2005; Arnórsdóttir et al., 2007; Sigurðardóttir et al., 2009; Arnórsdóttir et al., 2011).

## 1.3 Inhibitors

According to the MEROPS database (merops.sanger.ac.uk) inhibitors can be divided into peptidase inhibitors and compound inhibitors. Peptidase inhibitors are proteins that inhibit proteinases and are of great value in both medicine and biotechnology. These inhibitors can be divided into forty eight families. On the basis of their amino acid similarities and on the basis of the three-dimensional structures thirty eight of these families can be divided into twenty six clans of peptidase inhibitors. Inhibitors from eleven families that occur in proteins that contain two or more inhibitor units are classified as compound inhibitors an example of one such inhibitor is turkey ovomucoid that contains three inhibitor units form the Kazal family (Rawlings et al., 2004).

In the past, inhibitors have been classified on the basis of which enzymes they inhibit but the fact that some inhibitors inhibit more than one type of proteinases, makes classification hard. Basing classification on the types of individual inhibitor domains has proven more successful. The way in which inhibitors interact with their target enzymes varies enormously but can generally be divided into two types; trapping reactions and reversible tight-binding interactions. The trapping reactions are specific to endopeptidases because they depend on the cleavage of a peptide-bond in the inhibitor which triggers a volatile conformational change that closes of the active site off the proteinase. In the case of the widespread family of inhibitors, called serpins (serine-like proteinase inhibitors, family I4) the cleavage of the appropriate peptide-bond triggers a very fast acting conformational change that locks the proteinase in an acyl-enzyme complex as the covalent bond can't be hydrolyzed. This type of inhibition is not really reversible as the inhibitor is destroyed in the process and can be called suicide inhibitors (Huntington et al., 2000; Rawlings et al., 2004).

The other main type of inhibition is the reversible tight-binding interactions; this group is made up of proteins that have high affinity for their target enzymes. These inhibitors do exist in their solutions as either "virgin" inhibitors or the "modified" form where the reactive peptide-bond is cleaved (Bode and Hauber, 1992; Laskowski, and Qasim, 2000).These inhibitors bind to their target enzymes in a substrate fashion and can be released either in the virgin or modified form and are therefore truly a part of a reversible reaction. This standard mechanism is best understood for the inhibition of serine-like proteinases. The families that are known to inhibit serine-like proteinases are the families I3A, I8, I12 and I16 (see figure 11 for distribution of inhibitors in the animal kingdom). These families do also inhibit enzymes with other catalytic properties, but little is known why that is, although it has been theorized that these inhibitors do contain other active sites that have different inhibition mechanisms (Rawlings et al., 2004).

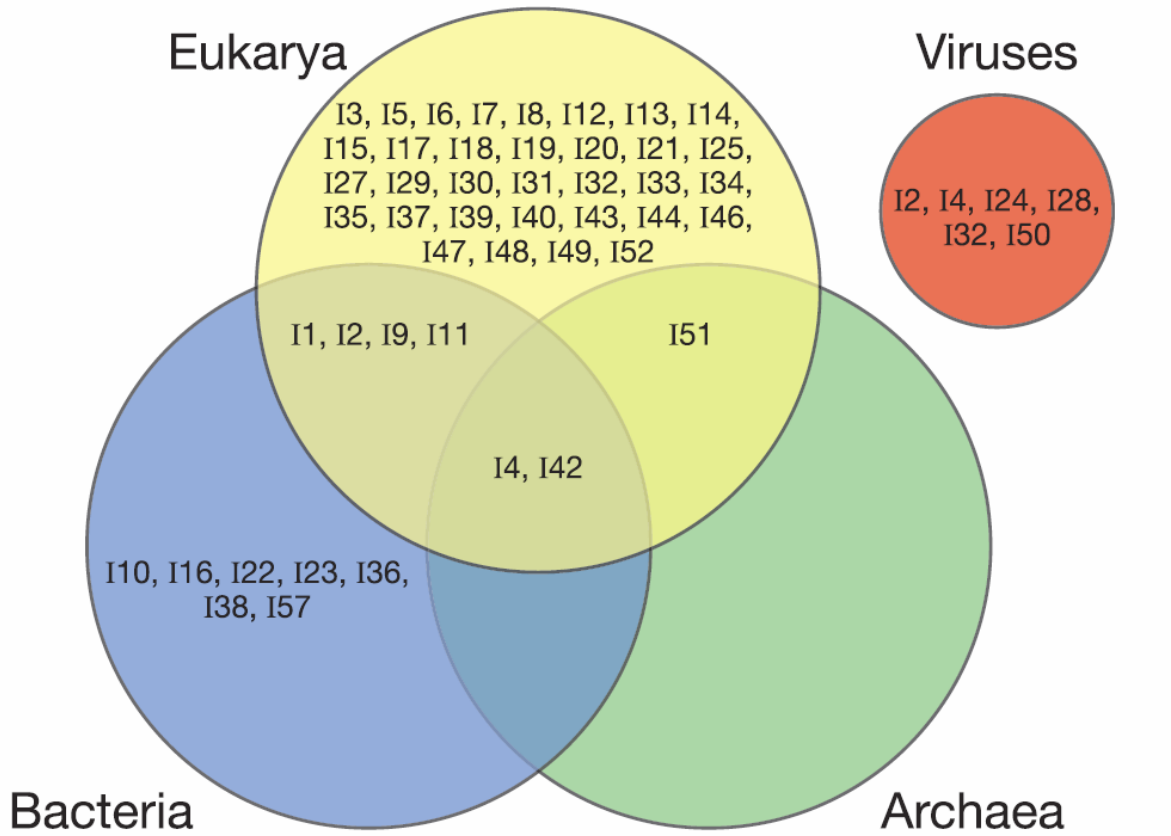


*Figure 11. Summarized data for the distribution of the inhibitor families according to the MEROPS database. Note that the family I4 found in all four groups (Rawlings et al., 2004).*

The best known families to inhibit serine-like proteinases are the serpins, the avian ovomucoids (Kazal-type), the Kunitz-type trypsin inhibitors such as aprotinin and the soybean trypsin inhibitors (Nagase and Salvesen 2001; Laskowski and Kato et al., 1980).

### 1.3.1 Turkey ovomucoid (TOM)

Turkey ovomucoid is a member of the Kazal-type inhibitors and a part of a major group of glycoprotein proteinase inhibitors that are found in avian eggs. This inhibitor is a double-headed inhibitor which consists of three domains where the second domain inhibits trypsin and the third domain inhibits chymotrypsins, elastases and subtilases. These domains are independently active and there is no evidence for noncovalent interactions between them. There are several members of Kazal-type inhibitors that all have a high structural homology and all which have characteristic disulfide-bridges. All these inhibitors show a specific orientation of the loop that binds to the target proteinase (figure 12) and the binding is dependent on the binding of the P1 inhibitor binding site to the S1 binding site on the proteinase (Ibrahim and Pattabhi, 2004)

The third domain of the turkey ovomucoid inhibitor (OMTKY3) is one of the most studied proteinase inhibitor; it has the reactive loop $Lys^{13I}$-$Arg^{21I}$ and has the binding of that reactive

loop to the target enzyme in all studied serine proteinases been reported to be nearly identical no matter of what family or clan the proteinase is from. The interactions of OMTKY3 to the subtilases involve eight main-chain-main-chain hydrogen-bonding and two main-chain-side-chain hydrogen-bonding interactions (figure 12). $Leu^{18I}$ (P1) on the inhibitor is an interesting amino acid in the inhibitor as it interacts with the enzyme in at least four different ways, the N-atom of P1 residue $Leu^{18I}$ interacts with the backbone carbonyl of $Ser^{125}$ (number of amino acid residues as in the subtilisin Carlsberg) with an average length of 3.28 Å and with the O-atom of the side-chain of the catalytic residue $Ser^{221}$ with an average length of 2.93 Å. The O-atom of $Leu^{18I}$ also interacts with two other amino acid residues, the backbone N-atom of $Ser^{221}$ (3.14 Å) and the side-chain N-atom of $Asn^{155}$ in the case of the subtilisin Carlsberg inhibition of OMTKY3, but as mentioned before this seems to be the general way that OMTKY3 inhibits members from the SB clan. OMTKY3 is small and cross-linked it has three disulphide-bridges and consist out of 56 amino acid residues. (Meynes, et al., 2005).

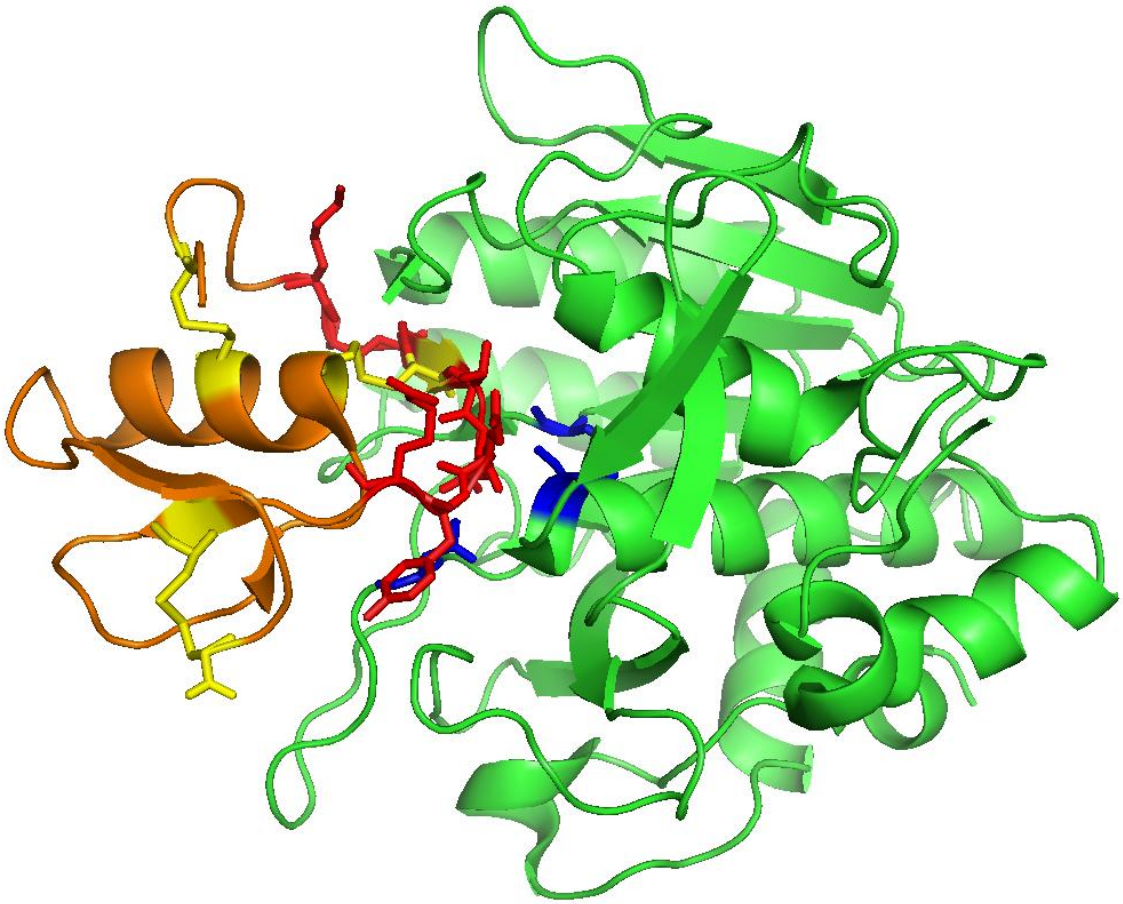

*Figure 12. The subtilisin Carlsberg-OMTKY3 complex, the enzyme is colored green with the three amino acid residues $Ser^{125}$- $Asn^{155}$- $Ser^{221}$ are colored blue. OMTKY3 is colored orange with the reactive loop colored red with the exception of a Cys residue that is a part of a disulfide-bridge which are colored yellow (PDB entry 1YU6). Drawn in PyMOL.*

### 1.3.2 Synthetic inhibitors

Synthetic inhibitors have been designed to inhibit various proteinases and a good example of inhibitors that inhibit serine-like proteinases are for example phenylmethylsulfonyl fluoride (PMSF) and chymostatin (CHYS) which are potent inhibitors of serine-proteinases and cysteine-proteinases especially chymotrypsin-like serine proteinases and subtilisin-like serine proteinases. PMSF has been been widely used since its discovery by Fahrney and Gold in 1963. PMSF reacts with the hydroxyl-group of the serine residue in the active site of the enzyme and binds covalently to it, and the sulfonyl-enzyme complex is then stuck in a structure that resembles the transition-state. Several crystal-structures of enzymes with PMSF covalently bound to the serine residue in the active site have been published including VPR and AQUI (Arnórsdóttir et al., 2005). Chymostatin has not been used as extensively as PMSF. However, it has been reported bound to the residues of the active site in a crystal structure of a cold adapted subtilisin-like proteinase from Antarctic Psychrotroph *Pseudoaleromonas sp.* AS-11 (deposit in the ProteinDataBank, PDB.org (PDB entry 1WVM). The structure of these synthetic inhibitors is made to imitate the natural substrates of the proteinases they are supposed to inhibit and bind specifically to the serine in the active site in the case of serine-proteinases (Kam et al., 2000).

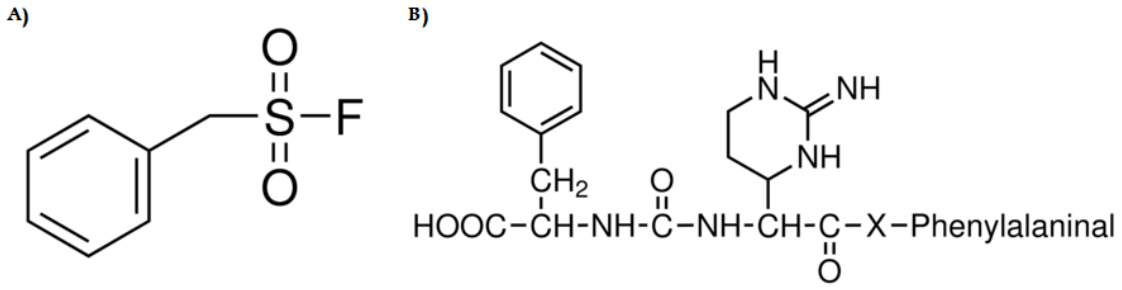


*Figure 13. Figure A) shows the structure of PMSF and figure B) shows the structure of chymostatin, where X stands for Leu, Val or Ile.*

## 1.4 Goals of the project

This study is part of a larger research project being conducted in the laboratory of the instructor (Magnús Már Kristjánsson) that is focused on understanding the molecular basis of temperature adaptation of subtilisin-like serine proteinases from the proteinase K family (AQUI and VPR) and which parts in their structure are affecting their stability and activity at different temperatures. In previous parts of this project, research has focused on differences in certain critical areas in the protein structures that might be contributing to the different thermal properties of AQUI and VPR. Comparative studies where the crystal structures of the enzymes are compared have been carried out to come up with hypotheses about factors contributing their temperature adaptation. To test these hypotheses site directed mutagenesis

has been used. (Kristjánsson et al., 1999; Arnórsdóttir et al., 2002; Arnórsdóttir et al., 2005; Arnórsdóttir et al., 2007; Sigurðardóttir et al., 2009; Arnórsdóttir et al., 2011).

In this project which is a first of its kind conducted on VPR, PRK and AQUI, a comparative study was conducted to establish if there are any differences in the inhibition properties between these enzymes. As has been mentioned, these subtilases originate in microorganisms which have had to adapt to very different temperatures. Interactions of proteins with other compounds, including other proteins are highly temperature dependent, as the strength of non-covalent interactions, which both determine the affinity and specificity in such interactions are temperature dependent, e.g. hydrophobic interactions, hydrogen bonds and salt bridges. This raises questions about how proteins adapt their protein binding interaction such as protein-protein interactions at different temperatures. For example are cold adapted proteins are less dependent on the hydrophobic interaction for binding, than counterparts adapted to higher temperatures, as the driving force for the hydrophobic interaction weakens as the temperature is lowered? Questions about how the stability-flexibility paradigm affects binding at the different temperatures the enzymes have adapted to are also mostly unanswered. Proteinase-proteinase inhibitor interactions are archetypical examples of protein interactions where both specificity and strong binding energy are involved. In this project the aim was finding suitable proteinase-inhibitor models for the subtilases, VPR, PRK and AQUI, and start thermodynamic binding studies attempting to answer some of these questions mentioned. Furthermore, in this study, inactivation rates of the subtilases by highly reactive smaller compound protease inhibitors (PMSF and CHYS) at different temperatures were determined. These inhibitors bind and irreversibly inactivate these enzymes by making covalent links to active site residues. Inhibition rates therefore would reflect accessibility of the active sites in the enzymes and hence their flexibility. By measuring the temperature effect on the inactivation rates would therefore reflect on the how accessibility, and hence flexibility, of the active sites of these enzymes is adjusted at the different temperatures.

# 2 Materials and methods

## 2.1 Buffers

Throughout this study six buffers were used and for convenience all the buffers and their composition are listed in table 2 and their names will be used in the text below.

**Table 2**. List of buffers, their pH and composition.

| ***Buffer A*** | ***Buffer B*** | ***Buffer C*** |
|---|---|---|
| 25 mM Tris<br>10 mM $CaCl_2$<br><br>pH 8.0 | 25 mM Tris<br>10 $CaCl_2$<br>1 M $(NH_4)_2SO_4$<br>pH 8.0 | 25 mM MES<br>10 mM $CaCl_2$<br><br>pH 6.0 |
| **Buffer D** | **Buffer H** | **Buffer P** |
| 25 mM MES<br>10 mM $CaCl_2$<br>500 mM NaCl<br>pH 6.0 | 100 mM Tris<br>10 mM $CaCl_2$<br>pH 8.6 | 100 mM Tris<br>10 mM $CaCl_2$<br>pH 7.8 |

Buffers A, B, C and D were all used in the protein purification steps, while buffers H and P were used in activity measurements during experiments. Buffer P was added to the list as it turned out that the stability of PMSF (phenylmethylsulfonyl fluoride) and chymostatin was much lower at pH 8.6 than at 7.8. All the ingredients of the buffers were from Sigma.

## 2.2 Activity and concentration measurements

Activity of the proteinases was measured using sAAPF-pna (succinyl-Ala-Ala-Pro-Phe-p-nitroaniline) (Bachem). sAAPF-pna was dissolved in either buffer H of P depending on the experiment and the change in absorbance was measured at 410 nm in either Cary 50 Bio UV-Visible spectrometer (Varian), or Heλios α UV-Visible spectrometer from Thermo Eletron Corporation and the molar absorptivity coefficient 8480 $M^{-1}cm^{-1}$ was used to calculate activity units per ml (U/ml) (DelMar et al., 1979). Measurements for AQUI were conducted at 40°C, but at 25°C for both $VPR_{\Delta C}$ and PRK. To maintain a constant temperature the substrate solutions were kept in a water bath at either 40°C or 25°C. Heλios α UV-Visible spectrometer

from Thermo Electron Corporation was also equipped with a ThermoSpectronic Single Cell Peltier system. For assaying enzymes during the purification of the proteins the concentration of sAAPF-pna used was 0.3 mM but in rest of the experiments the concentration was 0.5 mM and activity was measured over 30 or 15 seconds.

To determine concentrations of AQUI, PRK and $VPR_{\Delta C,}$ absorbance at 280 nm was measured and using molar absorptivity coefficients at 280 nm of 34630 $M^{-1}cm^{-1}$ for AQUI, 36580 $M^{-1}cm^{-1}$ for PRK and 34295 $M^{-1}cm^{-1}$ for $VPR_{\Delta C}$, determined as described by (Pace et al., 1995). To calculate the concentrations Beer´s law was used (equation 3), where A is the absorption (without units), ε is the molar absorptivity ($M^{-1}cm^{-1}$) b is the thickness of the cuvette (cm) and c is the concentration (M).

$$A = \varepsilon bc \quad (3)$$

The same method was used to find out the concentration of turkey ovomucoid (TOM) which has the molar absorptivity coefficient at 280 nm of 11555 $M^{-1}cm^{-1}$ (Pace et al 1995).

# 2.3 Protein purification and preparation

## 2.3.1 Purification of AQUI

The purification was carried out essentially as described by Arnórsdóttir et al. (2011). A cell pellet of *E.coli* strain BL-21 containing the gene from *Thermus aquaticus* YT1 (ATCC25104) for AQUI cloned into the plasmid pJOE had previously been prepared by Brynjar Örn Ellertson. The pellet was dissolved in 49 ml of buffer A, 1 ml of lysozyme (50 mg/ml) and 50 µl DNAase (1 µg/ml) were added and the mixture was gently shaken for two hours. The next step was to freeze the solution in liquid nitrogen ($N_{2l.}$) and thereafter allowed to thaw. This freeze/thaw cycle was repeated three times and for the last thawing step it was kept in the cold room at 4°C and shaken over night.

The sample was then heated to 70°C for 60 minutes to cleave the C-terminal domain of the protein and to release the fully active proteinase from the membrane fraction of the cell debris (Arnórsdóttir et al., 2011). The sample was then centrifuged for 20 minutes at 12000 g and 15°C in a Beckman Coulter centrifuge and the supernatant was collected and activity measured to make sure that the protein was still there and active. The solution was then again salted with ammonium sulfate to make it 1 M, and then centrifuged at 15000 g for 20 minutes at 20°C. The supernatant was collected and lastly the sample was loaded into a 50 ml superloop while filtering the sample thru a 0.2 µm filter.

The first column to be used was a 30 ml phenyl Sepharose. Before use the column was washed with three column volumes of filtered buffer B. When the sample had been loaded on

the phenyl Sepharose column the ÄKTA purifier chromatography system was programmed so a gradient from 100% buffer B to 0% and 0% buffer A to 100% with stops at 65% buffer B and 35%, was carried out. The sample peaks which had the highest absorbance at 280 nm and had activity over 1 U/ml were collected. This sample was then heated to 60°C for forty minutes to ensure that the C-terminal propeptide had been cleaved off.

The sample was then dialyzed against buffer C overnight to prepare it for the next step in the purification process, the SPXL cation exchange column. The sample was again loaded into a 50 ml superloop and loaded on the cation exchange-column that had previously been equilibrated with buffer C. The elution program used was a linear gradient of 100% buffer C to 0% and 0% buffer D to 100%. The samples with activity over 3 U/ml where combined and mixed with ethylene glycol to make a 10% solution and frozen in liquid nitrogen in 1 ml portions and stored at -25°C.

Due to a fault in the ÄKTA purifier chromatography system during the cation exchange chromatography step, some leak was observed in the flow when the sample was being loaded and it was very apparent that a significant amount of the protein did not bind to the column. Therefore the decision was collected and run the flow through loaded to another phenyl Sepharose column (15 ml). Before the sample was loaded onto the column it was salted with $(NH_4)_2SO_4$ to make the solution 1 M in $(NH_4)_2SO_4$. The column was washed with buffer B and the sample loaded onto to the column, and eluted with a solution of 55% ethylene glycol in buffer A. This run resulted in a sharp peak which was collected for use in the study. Those samples were also frozen in liquid nitrogen and kept in -25°C.

Before use in different experiments samples of AQUI were dialyzed against the appropriate buffer buffers A, H or P depending on which experiment were being carried out.

### 2.3.2 Purification of $VPR_{\Delta C}$

The purification was carried as described by Kristjánsson et al. (1999) with minor modifications. The gene for $VPR_{\Delta C}$ from *Vibrio* PA44 was cloned into the *E. coli* strain Top 10 contained in the pBAD plasmid (Arnórsdóttir et al., 2002). For this study a cell pellet of *E. coli* was used, the cell pellets previously produced by Ásta Rós Sigtryggsdóttir in this lab. The pellet of *E.coli* was dissolved in buffer A and loaded onto Emulsi-Flex system four times to disrupt the cells. The sample was then centrifuged at 15000 rpm for 30 minutes at 4°C. The supernatant was collected and made 90% $(NH_4)_2SO_4$ and centrifuged again at 16000 rpm for 45 minutes and 4°C and the pellet collected and stored in a freezer at -20°C. These first steps were carried out by Ásta Rós Sigtryggsdóttir.

The pellet was dissolved in buffer A and loaded onto a 15 ml Z-D-Phe-TETA (N-carbobenzoxy-D-phenylalanyl-triethylenetetramine-Sepharose) column equilibrated with buffer A. After the sample had been loaded onto the column it was eluted with buffer A containing 0.5 M NaCl to elute proteins which had bound to the column in a non-specific way. When the absorbance at 280 nm was under 0.05 mAU (milli-absorbance units) it was time to elute the active enzyme from the column. For the elution buffer A containing 2M GdmCl was used. Fractions of 2.5 ml were collected from the column and diluted into 2 ml of a buffer A containing 2 M $(NH_4)_2SO_4$ counteracting the destabilizing effects of GdmCl. The fractions that had activity over 1 U/ml were combined and activity measured.

The collected proteinase sample from the Z-D-Phe-TETA column was loaded onto a 15 ml phenyl Sepharose column which had earlier been washed with buffer B. The column was eluted with a linear gradient of 100% buffer B to 0% buffer B and 0% buffer A to 100%. To elute $VPR_{\Delta C}$ a solution of 50% ethylene glycol in buffer A was used. Two peeks were obtained, and were collected separately on the basis of measured absorbance at 280 nm and the activity. The portions that were collected were diluted to 25% concentration of ethylene glycol. These samples were quick frozen in liquid $N_2$ and kept in a freezer at -25°C. Before use $VPR_{\Delta C}$ was either dialyzed in buffers A, H or P depending on the experiment at hand.

### 2.3.3 Preparation of PRK and the inhibitors

Protease K (PRK) and the inhibitors turkey ovomucoid (TOM), chicken ovomucoid (COM) and two samples of soybean trypsin inhibitor (STI) were all purchased from Sigma. Stock solutions were made for each of the proteins, by weighing out 5 mg of the inhibitors and dissolve them in 4 ml of buffer A. A stock solution of PRK in buffer A (1mg/ml) was also prepared. Samples were made 20 % in ethylene glycol, quick frozen in liquid nitrogen and kept frozen at -25°C until use. Before any experiments these samples were either dialyzed against buffers A, H of P depending on the experiment they were needed for.

## 2.4 Method for SDS-PAGE electrophoresis

The method for SDS– PAGE electrophoresis was preformed as described by Laemmli (King, and Laemmli, 1971). The poly acrylamide gel contents are listed in table 3.

**Table 3**. Contents of the solutions used for preparation of the samples and making of the gels.

| *Solution* | *Contents* |
|---|---|
| Solution A | 1.5 M Tris/HCl, pH 8.9 |
| Solution B | 0.5 M Tris/HCl, 10ml/L TEMED (N,N,N´,N´-tetramethylethylenediamine), pH 6.8 |
| Solution C | 30% acrylamide (30g/ 100 ml), 2.8% bis acrylamide (0.8g/100 ml) |
| Solution D | 10% ammonium persulfate (1 g/ 10ml) |
| Solution E | 0.5 M Tris/HCl, 10% w/v SDS, 50% w/v sucrose, 0.25 M dithiothreitol and 0.02% w/v bromophenol blue, pH 6.8 |
| Solution F | 0.25 M Tirs, 1.9 M glycine, 10 mM EDTA (ethylenediaminetetraacetic acid), 0.5%% SDS (5 g/ L) pH 8.75 |

The glass plates were made ready for use by making sure that no leak was possible and the equipment from BioRAD set up. The gels were made by mixing the solutions together (see tables 4 and 5 for recipes). First the lower gel was made by mixing solutions A, C and distilled water and that deventilated then TEMED (99%) (Sigma) and solution D was mixed with that and poured in-between the glass plates and some distilled water pipetted on top of the gel. When the gel had polymerized the water was poured of. The upper gel was made of solution B, C, D and distilled water. The upper gel was poured on top of the lower gel and with a comb sample pockets were made.

**Table 4**. Recipe for two portions of the lower gel.

| *Solution* | *Quantity* |
|---|---|
| Solution A | 4.5 ml |
| Solution C | 7.5 ml |
| TEMED (99%) | 25 µl |
| Distilled water | 5.9 ml |
| Solution D | 0.1 ml |

**Table 5**. Recipe for two portions of the upper gel.

| *Solution* | *Quantity* |
|---|---|
| Solution B | 1.25 ml |
| Solution C | 0.75 ml |
| Distilled water | 3.2 ml |
| Solution D | 0.5 ml |

The protease samples were prepared by mixing 72 µl of protease and 8 µl of 5 mM PMSF so they wouldn't self digest during boiling, 20 µl of solution E was added to make the total volume 100 µl and the mixture boiled for 5 minutes. The inhibitors where prepared in a similar way 80 µl of inhibitor mixed with 20 µl of solution E and boiled for 5 minutes. After boiling, the samples were loaded into the pockets of the gels in 10 µl portions with a FinnPipette and the gels placed in a container filled with solution F which had been diluted in the portions 400 ml solution F into 1600 ml of water. The electrophoresis equipment (BioRAD PowerPac Basic) was connected and set to 200 V and 30 mA.

The gels were stained in 0.25% w/v Coomassie Brilliant Blue R-250, 45% methanol, 7% acetic acid, and water and kept in that solution over night, later the solutions were changed to three parts methanol, one part acetic and six pars water to distain the gels. Then a picture was taken of the gels and size was measured by the travel length of the samples compared to a ladder (PageRuler$^{TM}$Prestained Protein Ladder #SM0671). To determinate the size of the proteins, a graph of $\log_{10}$ (kDa) obtained from the ladder against the Rf-values (measured by counting the pixels on a photograph taken of the gel) and by using KaleidaGraph a trend-line was calculated and that trend-line was used to calculate the molar mass of the proteins.

## 2.5 Determination of parameters for reversible inhibition of subtilases

### 2.5.1 Inhibitory activity of different inhibitors against subtilases

To determine the inhibition pattern for the three enzymes, a group of nine inhibitors was selected that are known to inhibit trypsin- or chymotrypsin- or subtilisin- like proteases. The inhibitors were turkey ovomucoid trypsin inhibitor type (II-T) (TOM), chicken ovomucoid trypsin inhibitor type (III-O) (COM), chicken trypsin inhibitor from egg white type (IV-T) (ovoinhibitor) (OVOI), bovine pancreatic trypsin inhibitor (type I-P) (BPTI), soybean trypsin inhibitor (type I-S) (STI), trypsin-chymotrypsin inhibitor (Bowman-Birk) (9777), aprotinin from bovine lung (A-1153), chymostatin (C-7268) (CHYS) and phenylmetylsulfonyl fluoride (PMSF).

All the proteases and the inhibitors TOM, COM and STI were dialyzed against buffer H while the rest of the inhibitors were just dissolved in buffer H. For each experiment inhibitors were incubated at concentration of 0.1 mg/ml (0.5 mM for PMFS) with each proteinase, such that the initial activity against sAAPF-pna was approximately 1 U/ml. Samples were incubated for 30 minutes at 25°C before measuring remaining activity. A control sample was also prepared for each protease in which the inhibitor solution was replaced with equivalent volume of buffer H. The activity of the control sample was set as 100% and was used as a reference for the protease-inhibitor samples. Activity was measured using a Helios α UV-Visible spectrometer in the standard assay as previously described. Each sample was measured in triplicate.

### 2.5.2 Time for equilibrium for binding of TOM to proteases

To determine the incubation time required for TOM to reach equilibrium in the binding interaction while inhibiting $VPR_{\Delta C}$, PRK or AQUI, an experiment was carried out where the time dependence of inhibition was measured. Samples of AQUI, PRK, $VPR_{\Delta C}$ and TOM were all dialyzed against buffer H and the ratio between inhibitor and protease was kept approximately 1.5.

The samples were incubated with the inhibitor under the defined conditions and activity was measured at regular intervals over 30-40 minutes and the activity compared to a control sample which contained no inhibitor but the same concentration of protease. All the samples were incubated at 25°C and the activity measured in the standard assay. From this experiment the time for equilibrium was determined. Time curves for each subtilase were measured two to three times.

### 2.5.3 Method to determining $K_{i(app)}$

The definition of $K_{i(app)}$ is derived from the reversible binding relationship between the enzyme and the inhibitor (see figure 14 equation 4) (Bieth, 1995).

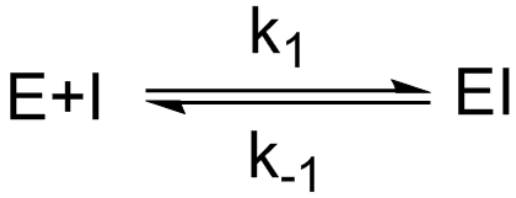


*Figure 14. Approximation of the enzyme - inhibitor interaction (Bieth, J. G., 1995).*

$$K_i = \frac{[E][I]}{[EI]} = \frac{k_{-1}}{k_1} \qquad (4)$$

The relationship for $K_i$ and $K_{i(app)}$ is shown in equation 5, $[S]_0$ stands for the initial substrate concentration) (Bieth, 1995).

$$K_i = \frac{K_{i(app)}}{1 + [S]_0/K_m} \qquad (5)$$

In order to determine the apparent equilibrium constant $K_{i(app)}$ for the inhibition of AQUI, PRK and $VPR_{\Delta C}$ with TOM an experiment was designed to get an estimate for the inhibition constants. In these experiments, samples were made so a constant concentration of the subtilases was used and the effect of different concentrations of the inhibitor TOM on the activity of the enzymes was measured. The concentrations of the inhibitor were between 0 and 4 times molar excess of TOM with intervals of 0.5 molar excess. Before these measurements, the proteases and TOM were all dialyzed against buffer H overnight. Samples of the each protease whit varying concentrations of TOM were incubated for 30 minutes at 25°C and measured for the remaining activity against 0.5 mM sAAPF-pna in the standard assay. The data acquired was then plotted as activity against [TOM] / [protease] ratio, where the activity in the absence of inhibitor (zero times molar excess) was set as 1 (100%), this gave a graphical interpretation of the inhibition. To get an estimate of the apparent inhibition constant $K_{i(app)}$, the data were then plotted as graph with $(v_0 / v_i)$-1 against [TOM] where $v_0$ is the rate of the enzyme reaction in the absence inhibitor between the protease and the substrate and $v_i$ is the rate at varying concentrations of the inhibitor. The slope of the line obtained in those plots is $1/K_{i(app)}$ according to the relationship given in equation 6 (Bieth,1995).. Each sample was measured three times and these sets of measurements were conducted one to two times.

$$\frac{V0}{Vi} = 1 + \frac{[TOM]}{Ki(app)} \qquad (6)$$

## 2.6 The effect of TOM on Michaelis-Menten kinetics

To determine the effect of the inhibitors on the kinetic properties and hence the type of inhibition taking place between TOM and the proteases, the Michaelis-Menten kinetic parameters were determined, in the presence and absence of inhibitor. The proteases and TOM had previously been dialyzed overnight against buffer H and then samples were prepared as either the protease in buffer H only, or the proteases in the presence of a tenfold molar excess of TOM. Seven substrate (sAAPF-pna) concentrations were measured in the range between 0.075-1.0 mM. In each set of the experiments the concentrations of the substrate were measured at least in triplicate and there were two sets of measurements for the protease sample without TOM and three sets for samples with tenfold molar excess of TOM. The change in absorbance at 410 nm was measured using a Heλios α UV-Visible spectrometer equipped with a ThermoSpectronic single cell peltier to maintain constant temperature during measurements. The temperature was also measured in the cuvettes using an external termocouple thermometer to ensure that the temperature in the cuvettes was always the same. To determine the accurate substrate concentration, the substrate-enzyme mixtures after each assay were kept for at least 4 hours for complete hydrolysis, though most of the time the samples were kept overnight, and then diluted tenfold and the absorbance at 410 nm measured and the concentration calculated, using the molar absorbtivity constant for sAAPF-pna, 8480 $M^{-1}cm^{-1}$ with a derivation of the Beer´s law (equation 7)

$$\frac{95}{100} * 10 * A410 * \frac{1}{8480 M^{-1} cm^{-1}} * \frac{1000\, mM}{1\, M} = [sAAPF - pna]\, mM \quad (7)$$

To counter the effects of dilution in the cuvette by adding the enzyme the constant 95/100 is added and the factor 10 is added to make up for the fact the solution has been diluted ten times before being measured. To calculate the change in absorption (ΔA/min) a similar equation was used (equation 8)**.**

$$\frac{\Delta A/min}{8480 \mathrm{M^{-1}cm^{-1}}} * 1000 = \frac{mM}{\mathrm{min}} \qquad (8)$$

The data from the measurements of $VPR_{\Delta C}$ and PRK was worked out in KaleidaGraph using nonlinear regression the values to obtain for $K_m$ and $V_{max}$, the values for $k_{cat}$ (equation 9) and $k_{cat}/K_m$ were calculated (Dowd and Riggs, 1965)

$$\frac{Vmax\ \left(\frac{mM}{min}\right)}{[Enzyme](mM)} * \frac{1\ (\text{min})}{60\ (sec)} = kcat\ (s^{-1}) \qquad (9)$$

The data from the measurements of AQUI were processed differently because it came apparent that the high value of $K_m$ and the fact that $V_{max}$ was not reached at 1 mM concentration of sAAPF-pna that the nonlinear regression wouldn't work as well, so to interpret the data Lineweaver-Burk method was used to obtain $K_m$ and $V_{max}$, $k_{cat}$ and $k_{cat}/K_m$ were obtained the same way as before.

## 2.7 Rate of irreversible inhibition of proteases

To measure the difference in rates of irreversible inhibition of the proteases, two inhibitors were chosen, i.e. chymostatin and PMSF as they do bind into the active site of the enzyme in an irreversible manner. The enzymes were dialyzed against buffer P while chymostatin was dissolved in DMSO (dimethyl sulfoxide) and PMSF was dissolved in isopropanol. Activity was measured using sAAPF-pna in the standard assay.

To measure the inactivation rate constants for inhibition for each of the proteases, four samples were prepared for each set of measurements, one sample as a control that had equal volume of the inhibitor solvent but without the inhibitor. The other three had the inhibitor. To start the reaction the inhibitor was added and at the same time the stopwatch was turned on and as quickly as possible, the activity was measured and that was done until the remaining activity was less than 10% of that of the control samples without inhibitor. These experiments were only carried out at room temperature for chymostatin but for PMSF this was done at 10°C, 20°C, 30°C and 40°C (also at 15°C for $VPR_{\Delta C}$) to obtain data for Arrhenius-graphs.

The data from the activity measurements was plotted against time (in seconds) and fitted with a exponential trend-line to find the activity at time 0, the average of those values and the ones obtained from the sample with no inhibitor was set as activity 1 (100%) to get relative values. The data was then plotted as a (pseudo)first order rate data, by taking the natural logarithm (ln) of the activity and plot that against the time (in seconds) which gave a straight line with a slope which equals –k (pseudo first order rate constant) (see equation 10) (Azizian, 2004).

$$\ln\left(\frac{Vi}{Vo}\right) = -k * t\ (seconds) \quad (10)$$

In the case of PMSF these experiment were carried out at few different temperatures to get the value of k at these temperatures and by using the Arrhenius equation the activation energy of the inhibition can be calculated (see equation 11).

$$k = Ae^{-E_a/RT} \quad (11)$$

Where k is the pseudo-first order rate constant of inhibition, A is the pre-exponential factor which for first order reactions has the unit $s^{-1}$, $E_a$ is the activation energy, R is the universal gas constant and T is the temperature in Kelvin degrees. From the linear plot ln(k) against 1/ (T) (Kelvin degrees), $E_a$, the activation free energy for the reaction can be obtained from the slope, $-E_a/R$.

To calculate the free energy barrier for the irreversible inhibition of the subtilases equation 12 was used.

$$\Delta G^{\ddagger} = RT\ ln\left(\frac{k_B T}{k_{app}\, h}\right) \quad (12)$$

Where R is the universal gas constant, $k_B$ is the Boltzmann constant, h is the Planck´s constant and $k_{app}$ is the observed rate. $\Delta H^{\ddagger}$ - RT, one can calculate the enthalpy from the activation energy. Then it is possible to calculate $\Delta S^{\ddagger}$ for the reaction by the relationship given in equation 13.

$$\Delta G^{\ddagger} = \Delta H^{\ddagger} - T\Delta S^{\ddagger} \quad (13)$$

Then the contributions of the enthalpy and entropy to the free energy barrier can be calculated.

# 3 Results and discussions

## 3.1 Protein purification

### 3.1.1 Purification of AQUI

Purification of AQUI was carried out as described by Arnórsdóttir et al. (2011). The first step in the purification was to bind AQUI to a phenyl Sepharose column and eluting with a negative gradient of buffer B, exchanging it for buffer A (figure 15).

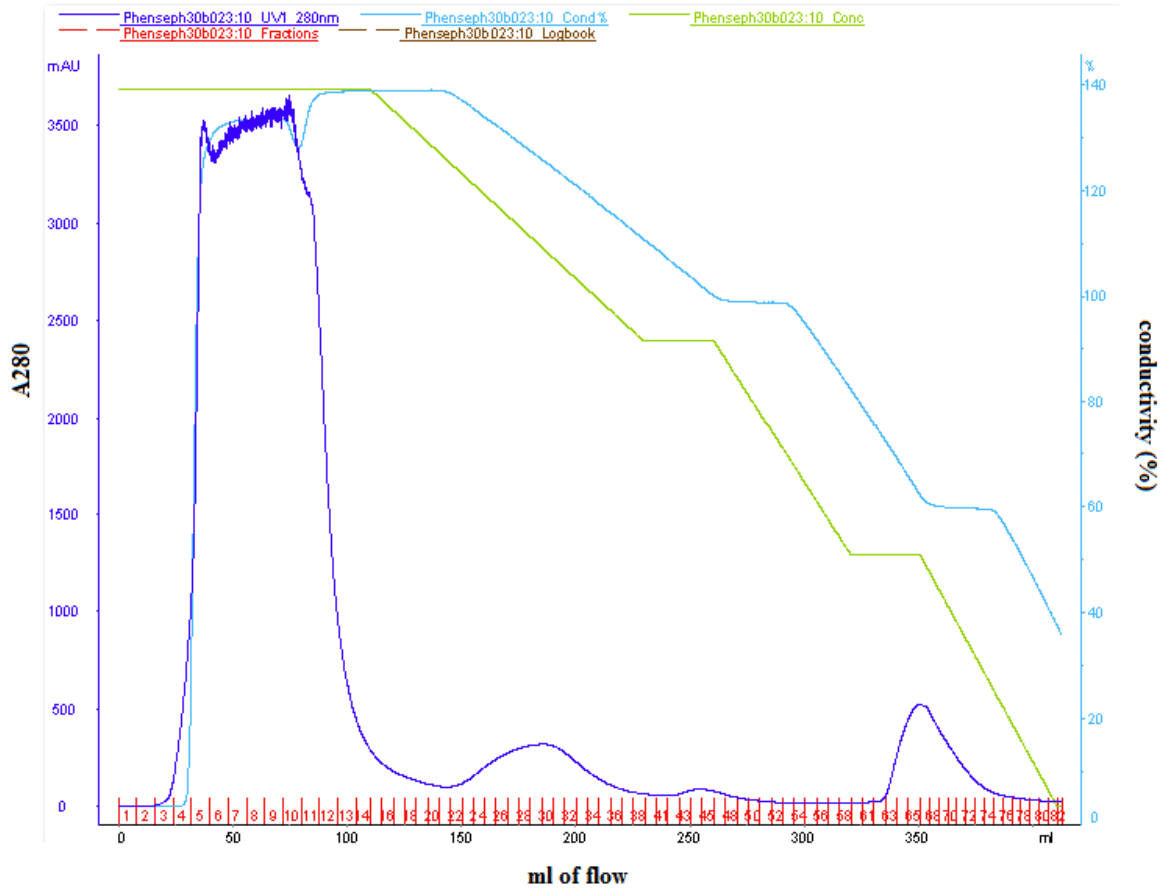


*Figure 15. The results of the phenyl Sepharose column run during the purification of AQUI. The dark-blue line shows the absorption at 280 nm in the units mAU (milliAbsorption units on the left Y-axis) from the ÄKTA purifier chromatography system and on the X-axis is the elution volume in ml. The light-blue line shows the conductivity (% arbitrary scale, right Y-axis) of the eluant. The column was washed with buffer B and a gradient of 100% buffer B to 0% and 0% buffer A to 100% with stops at 65% and 35% buffer B.*

Activity was measured in all eluted peaks, but only the last peak fractions had any activity (at 45% to 30% buffer B). Fractions that had activity over 1U/ml were collected and combined

(Table 6). The other peaks did not have any notable activity so the high absorption there must be due to other proteins and cell parts.

The second step in purification was to run the collected fractions of AQUI from the phe-Sepharose column on a SPXL-cation exchange column using a gradient of 100% buffer C to 0% and 0% buffer D to 100%. (See figure 16)

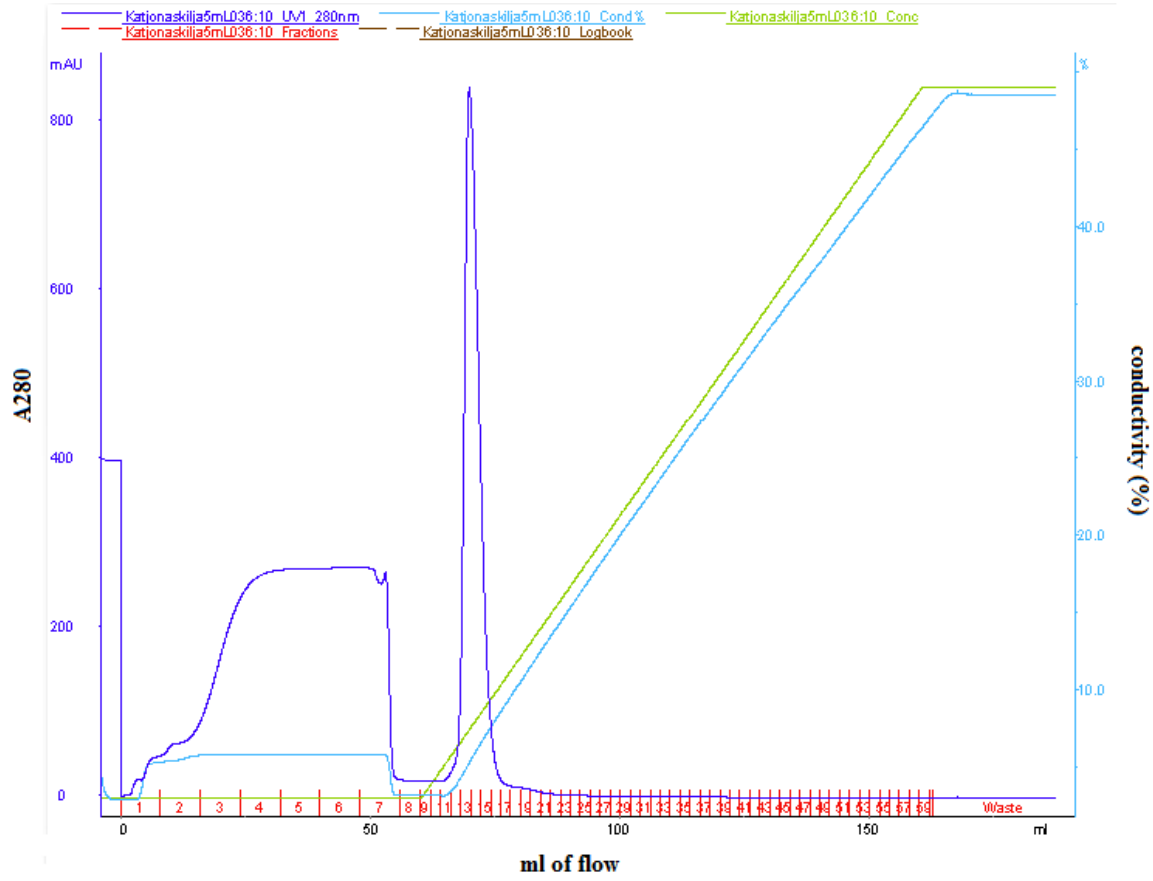


*Figure 16. The results from the SPXL-cation exchange column run during the purification of AQUI. The dark-blue line shows the absorption at 280 nm in the units mAU (milliAbsorption units on the left Y-axis) from the ÄKTA purifier chromatography system and on the X-axis is the elution volume in ml. The light-blue line shows the conductivity (% arbitrary scale, right Y-axis) of the eluant. The column was washed with buffer C and liner gradient from 100% buffer C to 0% and 0% buffer D to 100% used to elute AQUI.*

According to the purification scheme for AQUI (figure 16) most of the enzyme should bind and elute from the column in the sharp major peak that elutes just after the start of the linear salt gradient. It turned out however, that not all the of the enzyme did bind to the column, as a significant fraction of the enzyme activity was found in the flow through fractions so the broad flow through peak was assayed for activity and it was observed that much of the enzyme activity was there, the total volume was 40.0 ml with the activity 2.3 U/ml so in total there were 92 U. The sharp high peak was assayed for activity and all fractions that had

activity over 4 U/ml combined and gave 5.9 ml with the mean activity of 5.5 U/ml or in total 32 U.

The collected fractions from the flow through of the SPXL-cation exchange column were thereafter loaded on to a smaller phenyl Sepharose column, previously equilibrated with buffer B and AQUI was eluted with 55% ethylene glycol in buffer A (see figure 17).

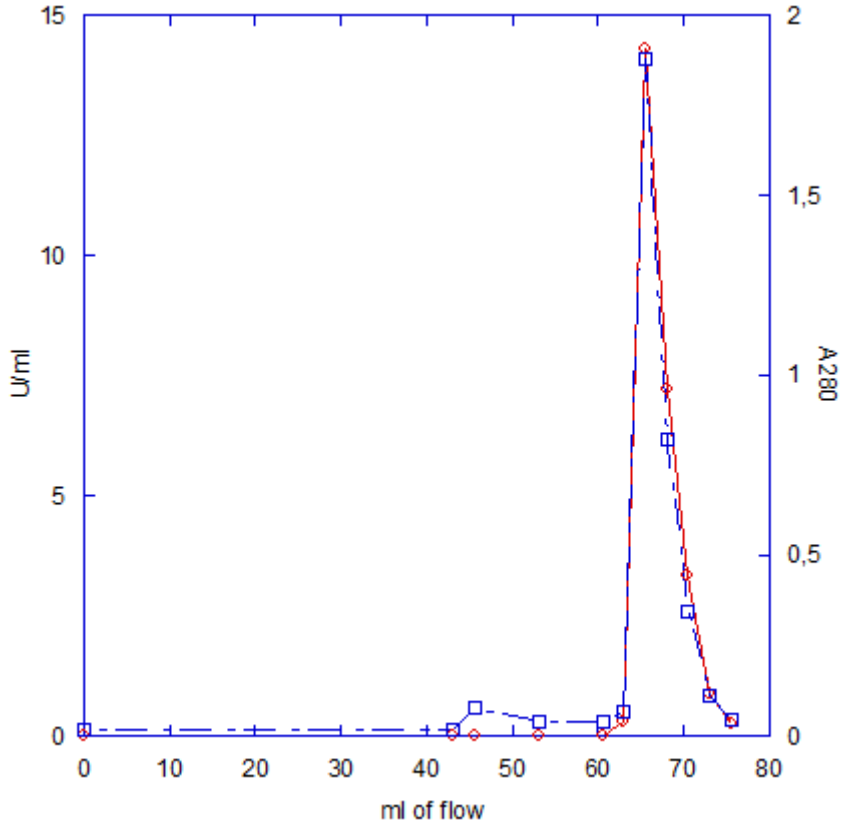


*Figure 17. The results from the second phenyl Sepharose column run in the purification steps of AQUI. The blue-dotted line shows the absorption at 280 nm (the right Y-axis) and the red-line shows the activity (U/ml, on the left Y-axis) measured with 0.3 mM sAAPF-pna. The X-axis shows the eluant volume in ml. The elution solution with 55% ethylene glycol was started at 40 ml of flow.*

To give an approximation of the purifications steps the results were set up in a purification table, where the summarized recovery of activity for each step in the purification for AQUI is shown (see table 6). The total yield in the end was 61% compared to the activity measured before the first phenyl-Sepharose column.

**Table 6**. A purification table for the purification steps of AQUI.

| *Purification steps* | *Volume (ml)* | *Activity units (U)* | *Yield (%)* |
|---|---|---|---|
| Before phenyl – Sepharose column | 44.0 ml | 145.2 U | 100 % |
| After phenyl – Sepharose column | 43.1 ml | 125.0 U | 86 % |
| After cation exchange column | 5.9 ml | 32.5 U | 22 % |
| After the second phenyl – Sepharose column | 6.7 ml | 56.4 U | 39 % |
| Total yield of the cation exchange column and the second Sepharose column | 12.6 ml | 88.9 U | 61 % |

### 3.1.2 Purification of $VPR_{\Delta C}$

The purification of $VPR_{\Delta C}$ was done as described previously by Kristjánsson et al. (1999) with the change, however, that the first step in the purification was that the redissolved pellet was loaded on a Z-D-Phe-TETA affinity column (see figure 18) instead of running it first on a phe-Sepharose.

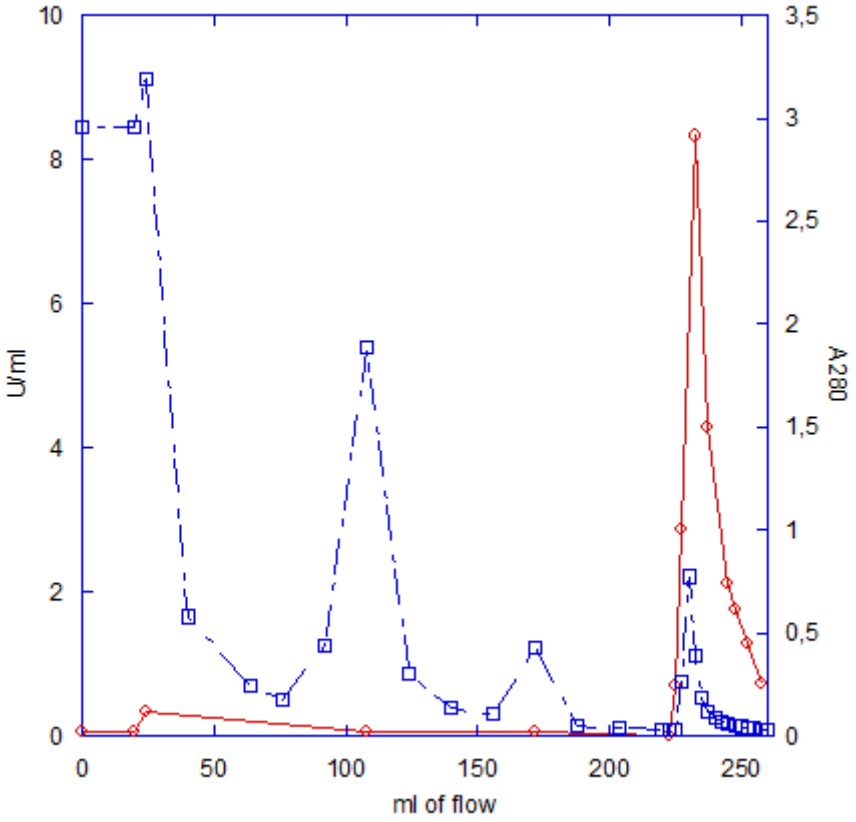


*Figure 18. The results from the Z-D-Phe-TETA specific column run in the purification steps of $VPR_{\Delta C}$. The blue-dotted line shows the absorption at 280 nm (on the right Y-axis) and the red-line shows the activity (U/ml, on the left Y-axis) measured with 0.3 mM sAAPF-pna. The X-axis shows the elution volume in ml. Buffer B containing 0.5 m NaCl was added at 90 ml of eluant and the elution solution of Buffer A containing 2 M GdmCl was added at 220 ml flow.*

The peaks from the Z-D-Phe-TETA specific column were collected and combined and activity measured. The peak at 225 ml eluant showed activity. That peak was made 0.5M $(NH_4)_2SO_4$ and bound to a phe-Sepharose column and eluted with 55% ethylene glycol in buffer A to concentrate the protein in the sample (figure 19).

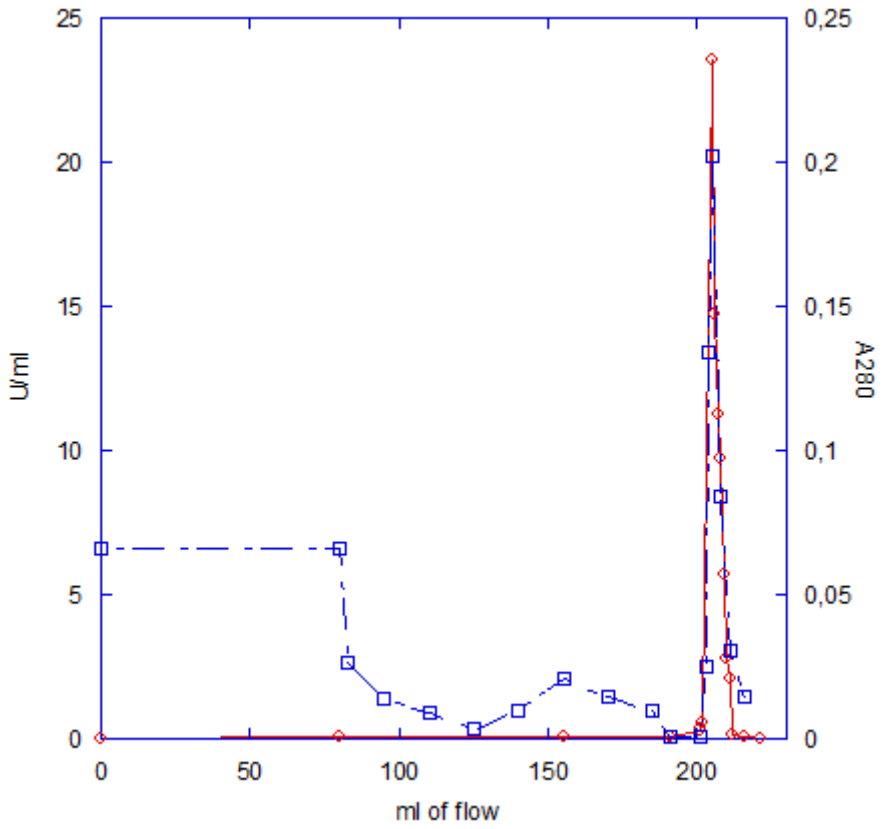


*Figure 19. The results from the phenyl-Sepharose column run in the purification steps of $VPR_{\Delta C}$. The blue-dotted line shows the absorption at 280 nm (on the right Y-axis) and the red-line shows the activity (U/ml, on the left Y-axis) measured with 0.3 mM sAAPF-pna. The X-axis shows the elution volume in ml. A gradient of 100% buffer B to 0% and 0% buffer A to 100% was started at 80 ml and the elute solution (50% ethylene glycol in buffer A) was started at 190 ml flow.*

To give an approximation of the purifications steps the results were set up in a purification table, where the summarized recovery of activity for each step in the purification for $VPR_{\Delta C}$ is shown (see table 7). The total yield in the end was 50% comparing to the activity measured before the Z-D-Phe-TETA column.

**Table 7**. A purification table for the purification steps of $VPR_{\Delta C}$.

| *Purification steps* | *Volume (ml)* | *Activity units (U)* | *Yield (%)* |
|---|---|---|---|
| Before Z-D-Phe-TETA column | 15 ml | 375.0 U | 100 % |
| After Z-D-Phe-TETA column | 58.8 ml | 200.0 U | 53 % |
| After phenyl Sepharose column | 13.2 ml | 188.0 U | 50 % |

## 3.2 SDS-PAGE electrophoresis

To check the purity of the purified proteinase samples of $VPR_{\Delta C}$ and AQUI, as well as the PRK as purchased from Sigma, SDS-PAGE electrophoresis was conducted on them. In addition to samples TOM, COM and two samples of STI from different producers were also run on the same electrophoresis gels, to check their purity (see figure 20).

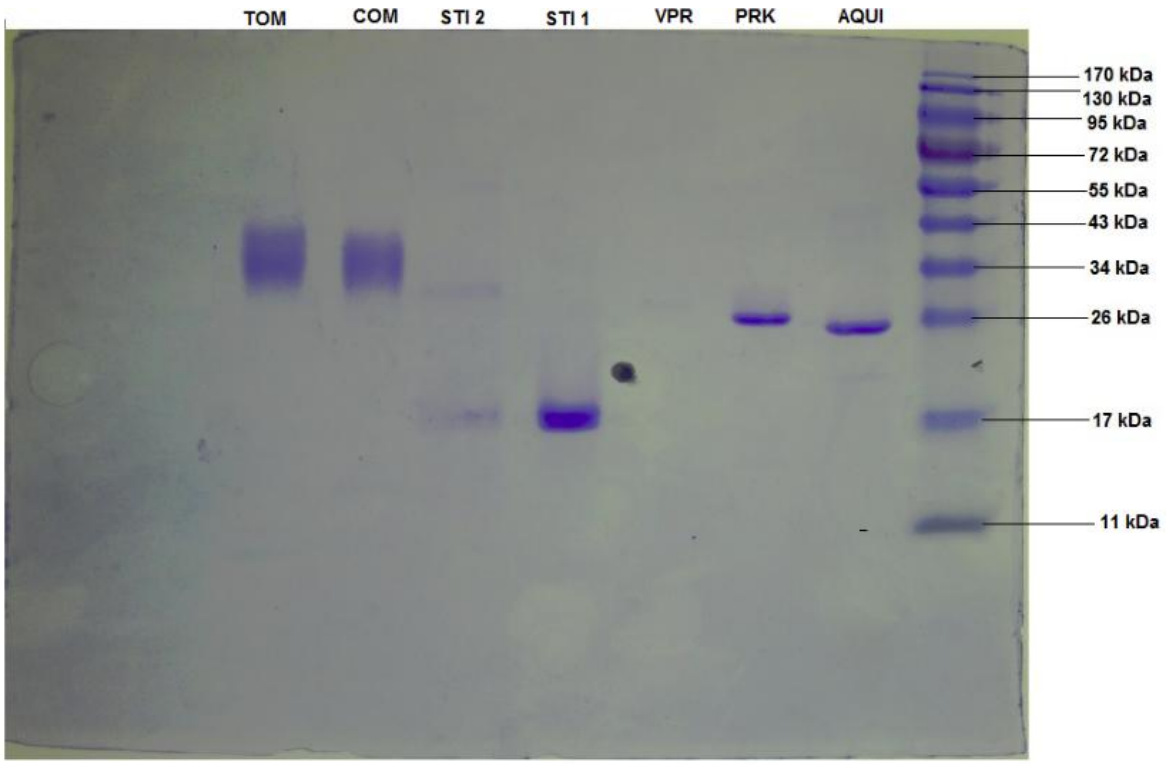


*Figure 20. SDS-PAGE electrophoresis of protein samples used in this study. In the first lane from the right was the ladder PageRuler™Prestained Protein Ladder #SM0671, and then the next one to the left was AQUI and then PRK, $VPR_{\Delta C}$, STI 1, STI 2, COM and TOM.*

From the SDS-PAGE gels it was decided that the samples of the proteases were pure enough and the sample called STI 1 was to be used in this study but not STI 2 as additional bands could be observed in STI 2 sample. The samples of TOM and COM showed relatively broad bands which can most likely be attributed to some glycosylation of these protein inhibitors which can interfer with the electrophoretic mobility.

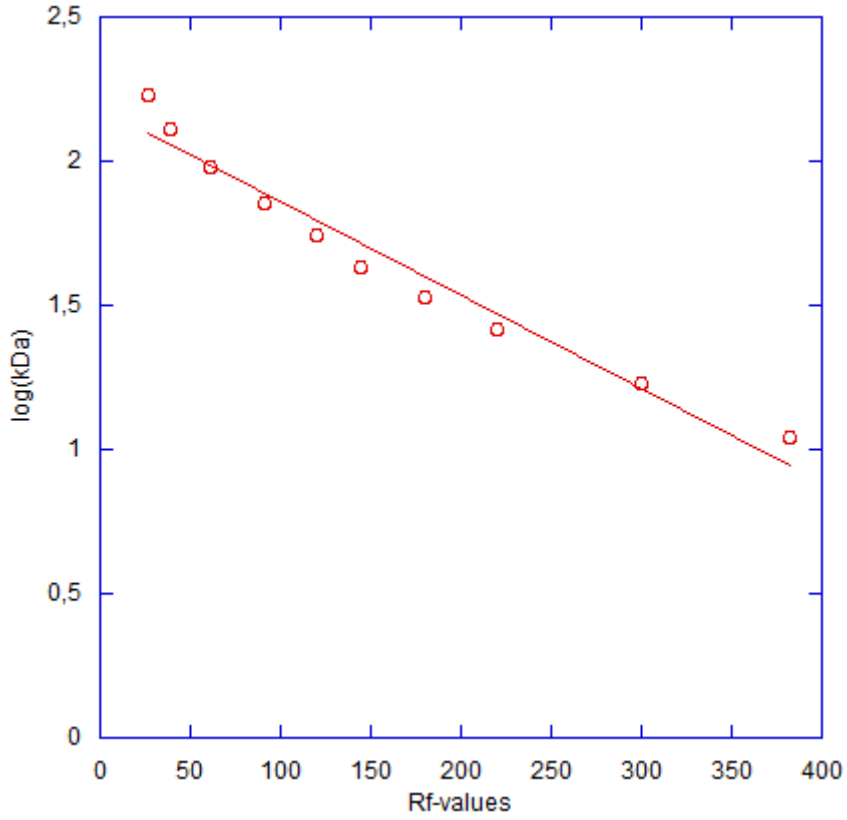


*Figure 21. The line used to calculate the trend-line (Y = 2.1832 – 0.0032337X) that was used to calculate the molecular masses of the samples. The X-axis shows the Rf-values measured by counting the pixels in a photo of the gel and the Y-axis shows the logarithm (base 10) of the molar masses in kDa (kilo Daltons).*

By using the trend-line calculated from figure 21 and by inserting the Rf-values of the samples for Y the molecular masses were determined. The results were that AQUI was estimated to be 27.1 kDa, PRK 27.9 kDa and $VPR_{\Delta C}$ was 30.5 kDa which are all around to values that were expected. STI was measured as 15.4 kDa which pans out comparing them to the reported value 15 kDa but TOM and COM were 37.6 kDa and 38.2 kDa but these values are off from the values given from Sigma, 27 kDa for COM and 20 kDa for TOM probably due to glycosylation.

## 3.3 Inhibitory activity of selected inhibitors

The first step in this study was to look at the effects of selected inhibitors on the activity of the subtilases, $VPR_{\Delta C}$, PRK and AQUI. Nine inhibitors were chosen for this purpose and were considered interesting to look at for further testing. The ones that didn't show inhibitory effects were dropped out of this study but three of the ones that did show inhibitory effects, were chosen for further experimentation (TOM, CHYS and PMSF) (table 8).

**Table 8**. The effect of selected inhibitors on the activity of $VPR_{\Delta C}$, PRK and AQUI. The mean from the three measurements taken of each sample and their standard deviation, relative activity of the samples compared to the control samples. Measured with 0.5 mM sAAPF-pna. In parenthesis are shown the concentrations of the enzymes used.

| *VPR (2.34 μM)* | *Mean (U/ml)* | ***Relative Activity %*** |
|---|---|---|
| Control | 0.97 ± 0.04 | **100%** |
| STI | 1.09 ± 0.08 | **112%** |
| TOM | 0.09 ± 0.02 | **9%** |
| COM | 0.92 ± 0.40 | **95%** |
| Aprotinin | 1.12 ± 0.07 | **116%** |
| BPTI | 1.08 ± 0.04 | **111%** |
| Bowman-Birk | 1.16 ± 0.05 | **120%** |
| OVOI | 0.00 ± 0.00 | **0%** |
| CHYS | 0.00 ± 0.00 | **0%** |
| PMSF | 0.00 ± 0.00 | **0%** |
| PKR (8.86 μM) | Mean | **Relative Activity %** |
| Control 1* | 3.53 ± 0.40 | **100%** |
| Control 2 | 0.93 ± 0.02 | **100%** |
| STI * | 4.18 ± 0.19 | **119%** |
| TOM | 0.06 ± 0.02 | **7%** |
| COM | 0.55 ± 0.01 | **59%** |
| Aprotinin* | 4.60 ± 0.24 | **130%** |
| BPTI | 1.13 ± 0.03 | **121%** |
| Bowman-Birk* | 3.82 ± 0.40 | **109%** |
| OVOI | 0.01 ± 0.01 | **1%** |
| CHYS | 0.01 ± 0.01 | **1%** |
| PMSF | 0.00 ± 0.00 | **0%** |
| AQUI (11,5 μM) | Mean | **Relative Activity %** |
| Control | 1.06 ± 0.08 | **100%** |
| STI | 1.12 ± 0.05 | **106%** |
| TOM | 0.59 ± 0.03 | **56%** |
| COM | 0.73 ± 0.08 | **69%** |
| Aprotinin | 1.12 ± 0.06 | **106%** |
| BPTI | 1.33 ± 0.24 | **126%** |
| Bowman-Birk | 1.18 ± 0.05 | **112%** |
| OVOI | 0.00 ± 0.00 | **0%** |
| CHYS | 0.00 ± 0.00 | **0%** |
| PMSF | 0.00 ± 0.00 | **0%** |

*Marks the samples of PRK measured against the sample called control 1.

The inhibitors that showed the most inhibition were TOM, OVOI, CHYS and PMSF which was expected. Though interestingly some of the samples did show increase in activity which was unexpected but needs further research because the apparent increase is so high that not all of it can be attributed to error in measurements. As expected the results were similar for all the enzymes though COM appears to have more inhibitory activity on PRK and AQUI than it did on $VPR_{\Delta C}$. Another thing that stood out was the lower inhibitory activity of TOM against AQUI, but that can be attributed to the molar ratio [TOM]/ [AQUI] was 0.8 while in the cases of $VPR_{\Delta C}$ and PRK, TOM was in excess because of the chosen parameters for this experiment (see chapter 2.5.1),. That might also indicate that the inhibition activity of COM against AQUI should be even more but that will need more research. On the basis of the results obtained on the inhibitory activity of the nine inhibitors three were selected for further examination, i.e. TOM, CHYS and PMSF.

## 3.4 Rate of inhibition with TOM

To establish the time dependence of inhibition of the three subtilases by TOM, the remaining activity of AQUI, PRK and $VPR_{\Delta C}$ was measured after incubating with the inhibitor under a given set of conditions. This was necessary to determine the time required for the binding of the inhibitor to the protease to reach equilibrium (figure 22).

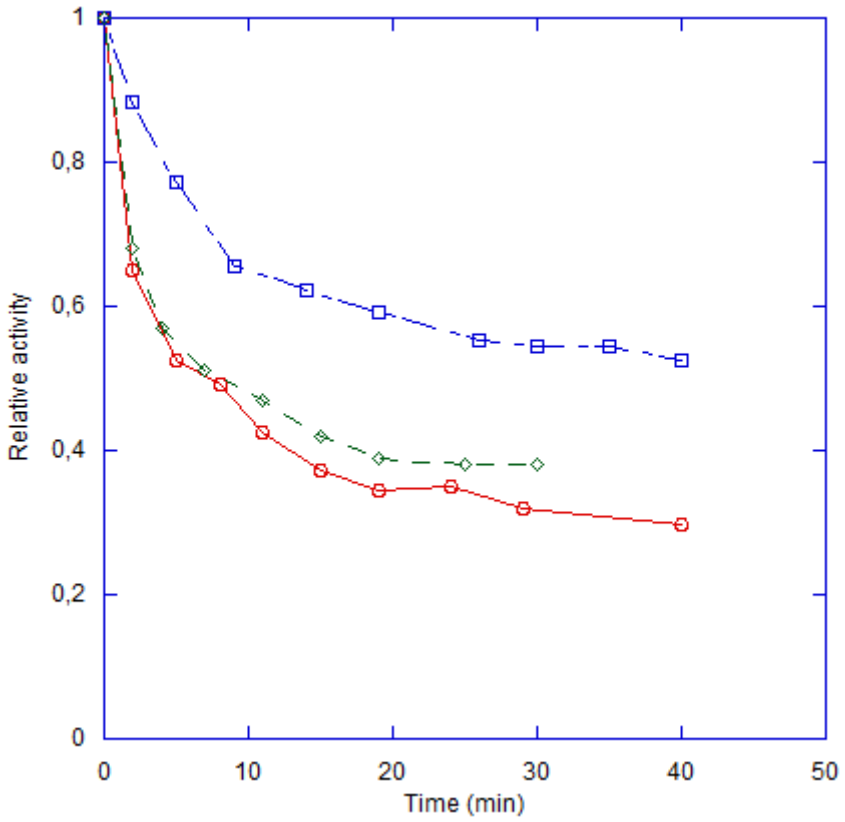


*Figure 22. Time dependence of TOM inhibition of $VPR_{\Delta C}$ (red line with circles (○)), PRK (blue dotted-line with squares (□)) and AQUI (green dotted line with diamonds (◊)). Activity was measured with 0.5 mM sAAPF-pna. $VPR_{\Delta C}$ and PRK were measured at 25°C, AQUI was measured at 40°C, but all samples were incubated at 25°C. The Y-axis shows the relative activity and the X-axis shows the time in minutes.*

In these experiments TOM was used in 1.5 – 2.0 molar excess over the proteinase in the incubation mixture. Under the conditions used the apparent time to reach equilibrium was 30-40 minutes. The difference between the final inhibitions can be explained by the molar ratio as it was not exactly the same in each of the protease samples. The time that it took to reach equilibrium seems to be very similar although the remaining activity in the AQUI samples was at equilibrium at 20 minutes, but in the case of $VPR_{\Delta C}$ and PRK equilibrium was reached later or around 30-40 minutes.

## 3.5 Determination of $K_{i(app)}$

One way to get an estimate of the inhibitory activity if an inhibitor against a protease is to determine the apparent inhibitor constant $K_{i(app)}$ which is the equilibrium constant for the binding reaction (equation 8). $K_i$ is a dissociation constant of the proteinase-inhibitor complex, thus a lower value of $K_i$ the tighter is the binding. It would be of interest to establish if there were any differences in the inhibitor binding properties between AQUI, PRK and

$VPR_{\Delta C}$ to get some insight how different temperature adaptation or thermostabilization could be affecting their binding properties.

One way to obtain an estimate of tightness of binding is to establish the remaining activity of the proteinase after incubation with different molar ratios of the inhibitor ([I]/[E]). Such an experiment was carried out where all the samples were incubated for 30 minutes before measuring as the inhibitory activity was close to equilibrium at that time for TOM against all the proteinases. The results were plotted as relative activity compared to a sample without inhibitors against the various inhibitor / enzyme molar ratio (see figure 23).

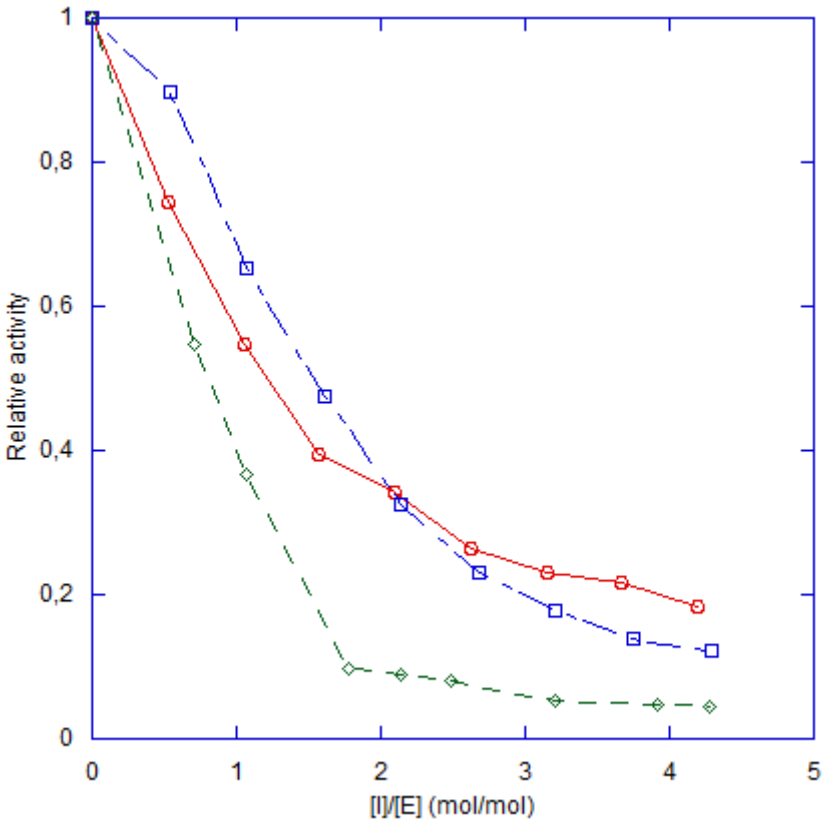


*Figure 23. Effect of different molar ratios of TOM versus $VPR_{\Delta C}$ (red line with circles (○)), PRK (blue dotted-line with squares (□)) and AQUI (green dotted line with diamonds (◊)). The X-axis shows the molar ratio between TOM and the proteases. Y-axis shows the relative activity. Activity was measured with 0.5 mM sAAPF-pna. $VPR_{\Delta C}$ and PRK were measured at 25°C, AQUI was measured at 40°C all samples incubated at 25°C for 30 minutes.*

From these results it is apparent that AQUI binds stronger to TOM than to the other two proteinases. The difference between $VPR_{\Delta C}$ and PRK is not extensive and more research is required to establish the difference if there is any.

With a derivation of equation 8: $((V_0/V_i)-1 = 1/K_{i(app)} * [I])$ a linear relationship should result in a plot were $(V_0/V_i)-1$ was plotted against [I] with a slope equal to $1/K_{i(app)}$ (see figure 24).

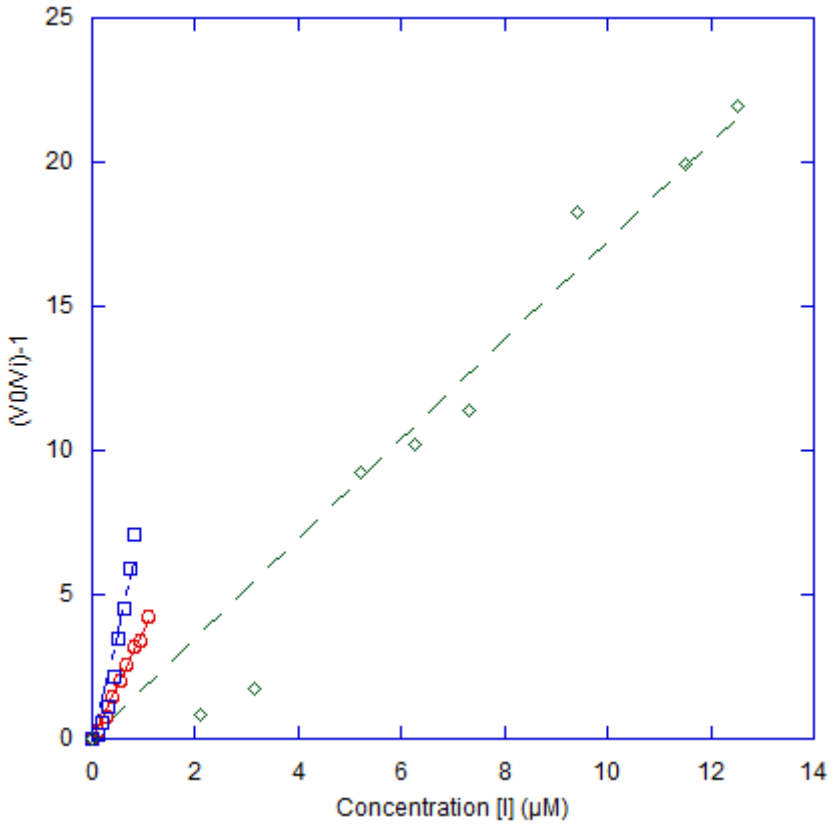


*Figure 24. Effect of different concentrations of TOM versus the rate $(V_0/V_i)-1$ of $VPR_{\Delta C}$ (red line with circles (○)), PRK (blue dotted-line with squares (□)) and AQUI (green dotted line with diamonds (◊)). The X-axis shows the rate $(V_0/V_i)-1$. The Y-axis shows the concentration of TOM. $VPR_{\Delta C}$ and PRK were measured at 25°C and AQUI was measured at 40°C all the samples incubated at 25°C for 30 min. The linear best fits were, Y = 1.7X for AQUI, Y = 7.3X for PRK and Y = 3.8X for $VPR_{\Delta C}$.*

The linear best fits were done in KaleidaGraph and from the slopes of the linear plots the apparent $K_i$ was calculated. $K_{i(app)}$ for $VPR_{\Delta C}$ was 0.26 µM for PRK it was 0.13 µM and for AQUI it was 0.58 µM. In interpreting these results in terms of tightness of binding it is important to take into account the initial enzyme concentration as the ratio of $[E]_0 / K_{i(app)}$ is an important variable in determining the tightness of binding in reversible inhibitors (Bieth, 1995). The $[E]_0 / K_{i(app)}$ ratios were calculated for the proteinases of this study and were found to be 1.0 for $VPR_{\Delta C}$, 1.4 for PRK and 5.0 for AQUI. These results indicate the tightest binding of TOM to AQUI at the same enzyme concentration. This result is interesting as it is

the opposite of what was hypothesized before these experiments, i.e. that the high flexibility and activity of $VPR_{\Delta C}$ would make it more sensitive to inhibition.

## 3.6 Michaelis-Menten kinetics

In order to establish the type of inhibitory effect TOM has on the Michaelis-Menten kinetic parameters of the three proteinases, the rate of the enzyme reaction as a function of the substrate concentration was determined both in the presence of ten-fold molar excess of TOM and in the absence of TOM, measured against the substrate sAAPF-pna. The results were used to produce Michaelis-Menten plots as rate (mM/min) against the concentration of sAAPF-pna (see Figures 25 and 26).

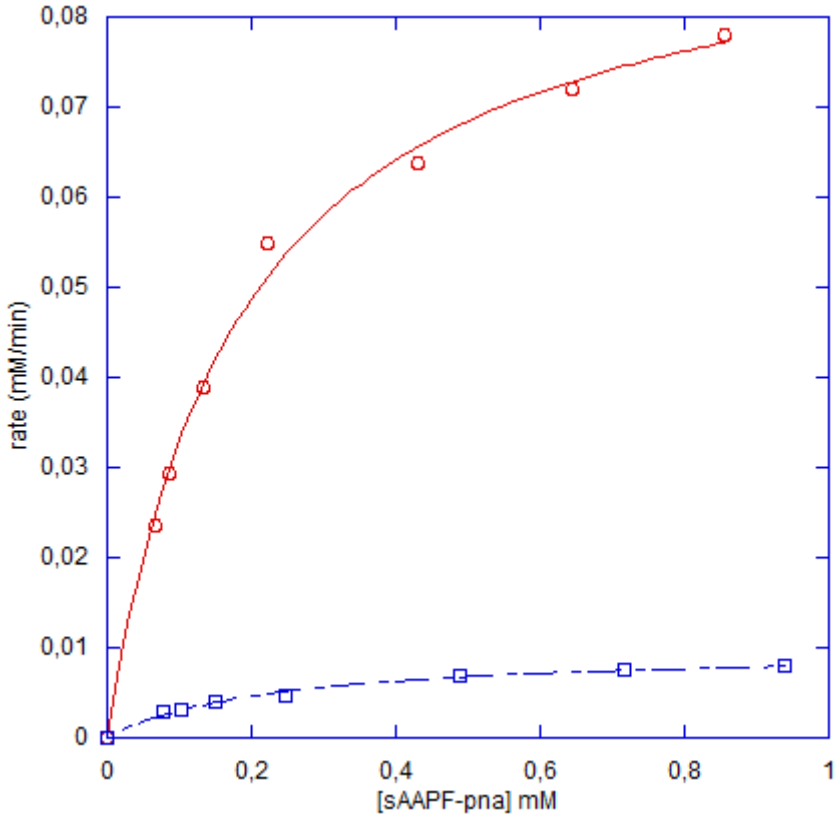


*Figure 25. An example of Michaelis-Menten plot for $VPR_{\Delta C}$ plotted with and without TOM. The red-line represents $VPR_{\Delta C}$ without TOM and the blue dotted-line represents $VPR_{\Delta C}$ incubated with ten-fold molar excess of TOM. Measured at 25°C and incubated at 25°C for 40 minutes. X-axis shows the substrate (sAAPF-pna) concentration in mM and the Y-axis shows rate expressed as mM/min.*

By using non-linear fitting in KaleidaGraph, the constants $K_m$, $k_{cat}$ and $k_{cat}$ / $K_m$ were determined. For $VPR_{\Delta C}$ in the absence of TOM, the values were $K_m$ = 0.181 mM, $k_{cat}$ = 126.6 $s^{-1}$ and $k_{cat}$ / $K_m$ = 702.3 $s^{-1}mM^{-1}$. And the values for $VPR_{\Delta C}$ in the presence of tenfold molar excess of TOM were $K_m$ = 0.180 mM, $k_{cat}$ = 11.6 $s^{-1}$ and $k_{cat}$ / $K_m$ = 65.6 $s^{-1}mM^{-1}$(see table 9

for comparison). In this case it seems that the inhibitor is affecting the turnover number of $VPR_{\Delta C}$ with a tenfold decrease, but $K_m$ stays unaffected.

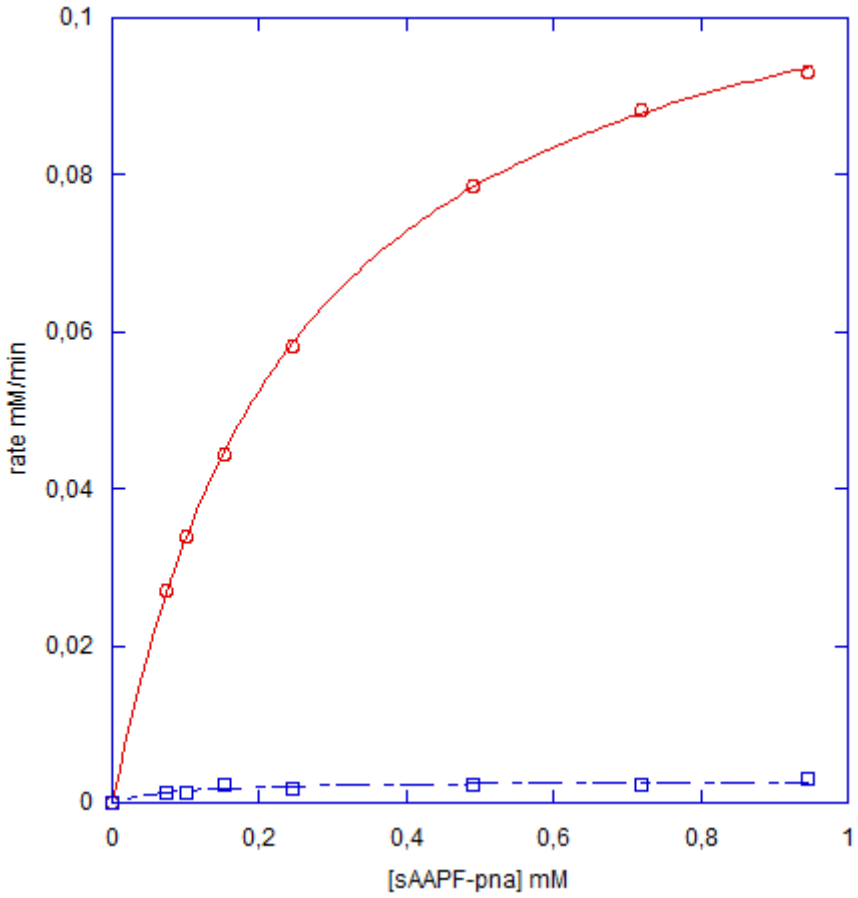


*Figure 26. An example of Michaelis-Menten plot for PRK plotted with and without TOM. The red-line represents PRK without TOM and the blue dotted-line represents PRK incubated with ten-fold molar excess of TOM. Measured at 25°C and incubated at 25°C for 40 minutes. X-axis shows the substrate (sAAPF-pna) concentration in mM and the Y-axis shows rate expressed as mM/min.*

The values for PRK were $K_m$ = 0.282 mM, $k_{cat}$ = 195.7 $s^{-1}$ and $k_{cat}$ / $K_m$ = 605.1 $s^{-1}mM^{-1}$ and in the presence of TOM $K_m$ = 0.181 mM, $k_{cat}$ = 5.9 $s^{-1}$ and $k_{cat}$ / $K_m$ = 34.7 $s^{-1}mM^{-1}$. The interactions are stronger between PRK and TOM than $VPR_{\Delta C}$ and TOM. As in the case of PRK a small decrease in $K_m$ and thirtyfold decrease in $k_{cat}$ (see table 9 for comparison).

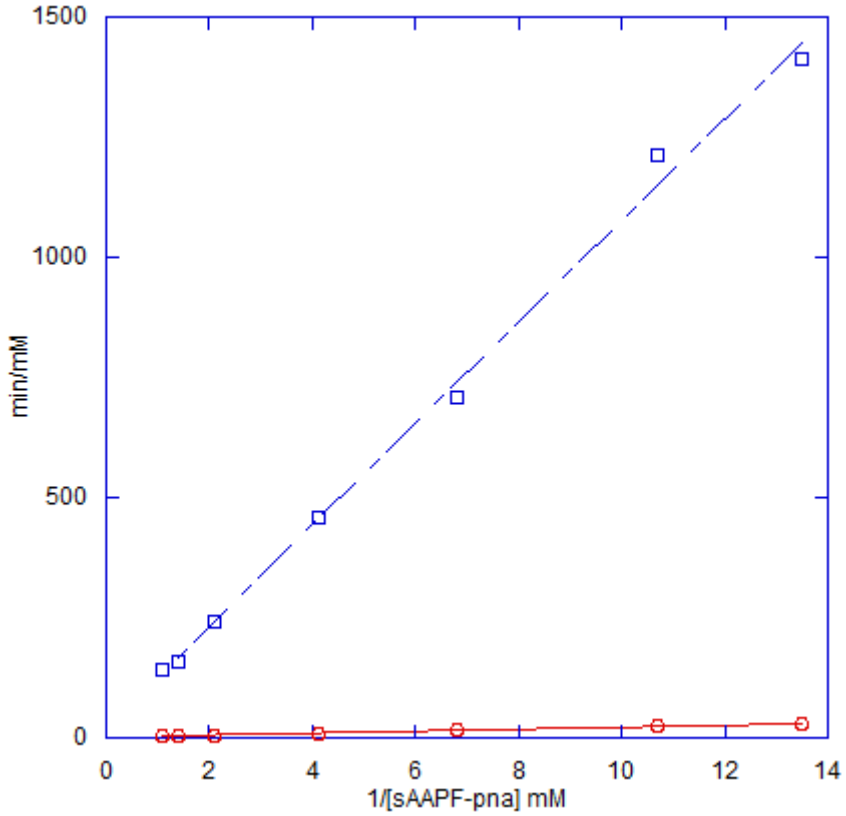


*Figure 27. An example of Michaelis-Menten kinetic measurements for AQUI plotted as a Lineweaver-Burk plot with and without TOM. The red-line represents AQUI without TOM and the blue dotted-line represents AQUI incubated with ten-fold molar excess of TOM. Measured at 40°C and incubated at 25°C for 40 minutes. X-axis shows the substrate (sAAPF-pna) concentration in 1/mM and the Y-axis shows rate expressed as min/mM.*

The Michaelis Menten parameters for AQUI were determined from Lineweaver-Burk plots (see chapter 2.6) (Figure 27). The Michaelis constants were determined to be $K_m$ = 1.1 mM, $k_{cat}$ = 52.9 $s^{-1}$ and $k_{cat}$ / $K_m$ = 47.4 $s^{-1}mM^{-1}$ and in the presence of TOM, but $K_m$ = 4.4 mM, $k_{cat}$ = 6.92 $s^{-1}$ and $k_{cat}$ / $K_m$ = 1.54 $s^{-1}mM^{-1}$ (see table 9 for comparison).

**Table 9**. A comparison of the Michaelis Menten kinetic constants $k_{cat}$, $K_m$ and $k_{cat}/K_m$ for $VPR_{\Delta C}$, PRK and AQUI in the presence and absence of TOM and the standard deviation for each value.

| **$VPR_{\Delta C}$** | **$k_{cat}$ ($s^{-1}$)** | **$K_m$ (mM)** | **($k_{cat}/K_m$) ($s^{-1}mM^{-1}$)** |
|---|---|---|---|
| Without TOM | 126.6 ± 4.9 | 0.18 ± 0.01 | 702.3 ± 2.1 |
| With TOM | 11.6 ± 1.8 | 0.18 ± 0.04 | 65.5 ± 6.4 |
| **Difference (without TOM / with TOM** | **11x** | **0** | **11x** |
| **PRK** | **$k_{cat}$ ($s^{-1}$)** | **$K_m$ (mM)** | **($k_{cat}/K_m$) ($s^{-1}mM^{-1}$)** |
| Without TOM | 195.7 ± 46.0 | 0.28 ± 0.001 | 695.1 ± 165.3 |
| With TOM | 5.9 ± 2.7 | 0.18 ± 0.03 | 31.7 ± 12.7 |
| **Difference (without TOM / with TOM** | **33x** | **1.6x** | **22x** |
| **AQUI** | **$k_{cat}$ ($s^{-1}$)** | **$K_m$ (mM)** | **($k_{cat}/K_m$) ($s^{-1}mM^{-1}$)** |
| Without TOM | 52.9 ± 11.6 | 1.1 ± 0.1 | 47.4 ± 4.0 |
| With TOM | 6.9 ± 2.8 | 4.4 ± 1.0 | 1.5 ± 0.3 |
| **Difference (without TOM / with TOM** | **8x** | **0.25 x** | **32x** |

Comparison of the Michaelis-Menten constants to published values revealed that for $VPR_{\Delta C}$ that $K_m$ was very similar to the published 0.184 mM but for $k_{cat}$ the value was well off from the 68.2 $s^{-1}$ published value which may be attributed to some error in concentration measurements for the enzyme, that also appears in an error in $k_{cat}/K_m$ (Sigurðardóttir, et al., 2009) In the case of AQUI the published values are $K_m$=1.35 mM, $k_{cat}$=71.7 $s^{-1}$ and $k_{cat}/K_m$=48.2 $s^{-1}mM^{-1}$, which are when compared to values obtained here a little higher overall but with $k_{cat}/K_m$ having very similar value (Arnórsdóttir, et al., 2011). The values for PRK are more off for $k_{cat}$ as previously $k_{cat}$ has been measured lower in PRK than $VPR_{\Delta C}$ but the ratio between $k_{cat}/K_m$ is closer to what previously reported (Kristjánsson, et al., 1999; Larsen, et al., 2006).

Comparison of the difference between the Michaelis constants of the proteinases in the absence and presence of the inhibitor TOM a trend that has been revealing itself continues to establish itself, that is it seems that TOM is affecting AQUI more strongly than PRK and $VPR_{\Delta C}$. If the values for the difference of $k_{cat}/K_m$ are examined they are 11-times lower for $VPR_{\Delta C}$ in the presence of TOM, for PRK they are 22-times lower in the presence of TOM and for AQUI the difference is 32- times and are these results in line with those observed before, i.e. AQUI is inhibited most strongly by TOM of these three proteinases. Looking at how the proteinases are being affected it seems that the type of inhibition is a mixed inhibition whereas both higher, lower and the unchanged values of $K_m$ are observed in the presence of TOM compared to the values in the absence of TOM and that $V_{max}$ is greatly affected.

## 3.7 Effect of irreversible inhibitors: chymostatin and PMFS

Both chymostatin and PMSF inhibit the serine proteinases irreversibly by covalently binding to the active serine residue of those enzymes. Difference in reactivity of these closely related homologous enzymes with those inhibitors thus most likely reflect the accessibility of active site residues in those enzymes. Measuring inactivation rates of the enzymes by such inhibitors might provide information on how the difference in the structure that contributes to the temperature adaptation, is affecting the accessibility of the active site.

First order kinetic measurements were conducted for all three proteinases with CHYS and PMSF. The first experiments were conducted with CHYS at room temperature. From those experiments it was established that under these conditions the rate of inhibition was so fast that it wasn't conveniently measurable. These results indicate that CHYS can be used to titrate the active site of all three proteases. To obtain measurable rate constants it was decided to use PMSF for these experiments to see if there were any differences in the irreversible inhibition rates of the three enzymes.

Inactivation rates for each proteinases was measured against several fold molar excess (pseudo-first order conditions) of PMSF over enzyme (100-fold molar excess of PMSF against $VPR_{\Delta C}$ and PRK and 20-fold molar excess of PMSF against AQUI) at selected temperatures between 10°C and 40°C. The samples of $VPR_{\Delta C}$ were incubated at six temperatures 11.2°C, 14.2°C, 20.7°C, 30.2°C, 30.4°C and 40.2 °C. In figure 27 is shown as an example measurement and is of $VPR_{\Delta C}$ at 11.2°C. For PRK the rate constants were measured at 25°C and samples incubated at 10.7°C, 20.9°C, 30.2°C and 39.9°C and for AQUI the rate constants were measured at 40°C and the samples were incubated at 10.3°C, 20.7°C, 30.2°C and 40.0°C (see appendix for figures and values of $k_i$).

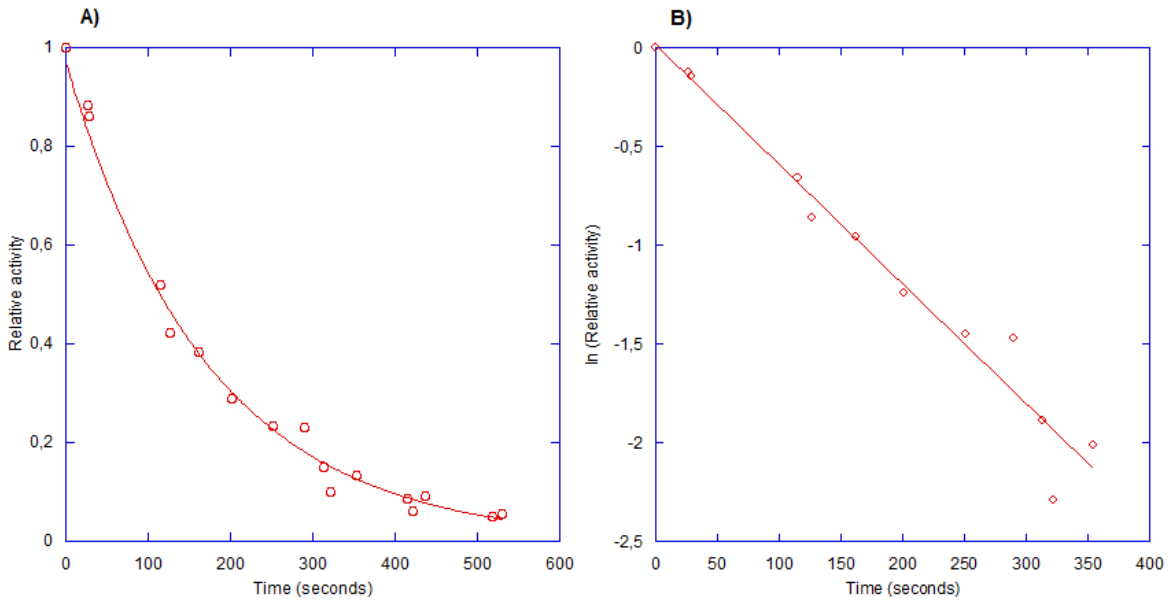


*Figure 28. Inactivation rate for $VPR_{\Delta C}$ in the presence of 100-fold molar excess of PMFS, with incubation at 11.2°C measured with 0.5 mM sAAPF-pna at 25°C. X-axis shows the relative activity on figure A) and ln(Relative activity) on figure B) and the Y-axis shows the time in seconds on both figures. The pseudo first order rate constant for the inactivation $k_i$ = 0.0060 $s^{-1}$.*

The data obtained at all the temperatures and for the three proteinases were similar to that seen in figure 28, and by plotting the data according to equation 12, but leaving out all the data points lower than 10% relative activity for $VPR_{\Delta C}$ and PRK and under 5% relative activity for AQUI, from the a linear representation of the data, the pseudo first order rate constants for the inactivation, $k_i$, were determined for each temperature from the slopes (example figure 28, B)).

By comparing the results for the three proteinases an apparent trend can be observed from these values, i.e. the more thermostable the enzyme is the faster it is being inhibited by the irreversible inhibitor PMSF. In fact, this is a similar trend as was observed in the inhibition with TOM.

These pseudo first order rate constants were then used to set up a Arrhenius plots showing ln (k) against 1000/the absolute temperature (Kelvin degrees) as according to equation 13 which leads to a linear representation of the data giving a slope value = – ($E_a$/R)*1000 (figure 28).

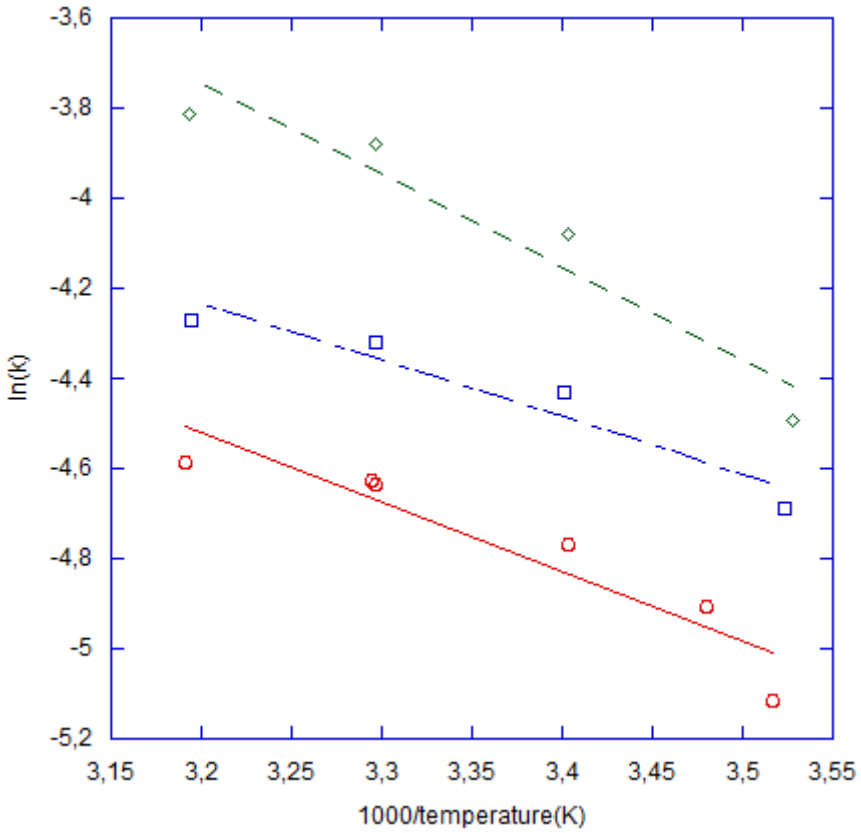


*Figure 29. Arrhenius plots for the irreversible inhibition of $VPR_{\Delta C}$ (red line with circles (○)), PRK (blue dotted-line with squares (□)) and AQUI (green dotted line with diamonds (◊) by PMSF). The Y-axis shows ln(k) (pseudo first order rate constant) and the X-axis shows 1000/the temperature in Kelvin.*

From the Arrhenius plots (figure 29) the activation energy ($E_A$) for inhibition were calculated by multiplying the value of the slope by 1000*R (the universal gas constant = 8.314471 (J/mol*K))

The values obtained for $E_A$ were 12.8 kJ/mol for $VPR_{\Delta C}$, 10.6 kJ/mol for PRK and 17.0 kJ/mol for AQUI. Even though the rate constants for PRK are higher than for $VPR_{\Delta C}$ the activation energy is very similar, but the activation energy for AQUI was somewhat higher than for the other two. The Arrhenius plots were used to calculate the activation parameters for this reaction. From inactivation rate constants one can calculate the $\Delta G^{\ddagger}$, using equation 12 and from the slopes of the plot $\Delta H^{\ddagger}$ can be obtained ($\Delta H^{\ddagger}$ = Ea –RT). From the known values for $\Delta G^{\ddagger}$ and $\Delta H^{\ddagger}$, $\Delta S^{\ddagger}$ can then be calculated. Values for the activation parameters for VPR, PRK and AQUI in the reaction with PMSF, at the different temperatures are summarized in table 10.

**Table 10**. $\Delta G^{\ddagger}$, $\Delta S^{\ddagger}$, $\Delta H^{\ddagger}$ and the value of the pseudo first order rate constant at every temperature that was used for measurements.

| ***VPR$_{\Delta C}$*** | | | | |
|---|---|---|---|---|
| $\Delta G^{\ddagger}$ (kJ/mol) | $\Delta H^{\ddagger}$ (kJ/mol) | $\Delta S^{\ddagger}$ (J/mol K) | Temperature (K) | Rate ($s^{-1}$) |
| 81.6 | 10.4 | 250 | 284.4 | $6.0 * 10^{-3}$ |
| 82.0 | 10.4 | 249 | 287.4 | $7.4 * 10^{-3}$ |
| 83.6 | 10.4 | 249 | 293.9 | $8.5 * 10^{-3}$ |
| 86.0 | 10.3 | 250 | 303.4 | $9.7 * 10^{-3}$ |
| 86.1 | 10.3 | 250 | 303.6 | $9.8 * 10^{-3}$ |
| 88.8 | 10.2 | 251 | 313.4 | $10.2 * 10^{-3}$ |
| **PRK** | | | | |
| $\Delta G^{\ddagger}$ (kJ/mol) | $\Delta H^{\ddagger}$ (kJ/mol) | $\Delta S^{\ddagger}$ (kJ/mol K) | Temperature (K) | Rate ($s^{-1}$) |
| 80.5 | 8.2 | 255 | 283.9 | $9.1 * 10^{-3}$ |
| 82.8 | 8.1 | 254 | 294.1 | $11.9 * 10^{-3}$ |
| 85.3 | 8.1 | 254 | 303.4 | $13.3 * 10^{-3}$ |
| 87.9 | 8.0 | 255 | 313.1 | $14.0 * 10^{-3}$ |
| **AQUI** | | | | |
| $\Delta G^{\ddagger}$ (kJ/mol) | $\Delta H^{\ddagger}$ (kJ/mol) | $\Delta S^{\ddagger}$ (kJ/mol K) | Temperature (K) | Rate ($s^{-1}$) |
| 79.9 | 14.7 | 230 | 283.5 | $11.2 * 10^{-3}$ |
| 81.9 | 14.6 | 229 | 293.9 | $16.9 * 10^{-3}$ |
| 84.1 | 14.5 | 230 | 303.4 | $20.7 * 10^{-3}$ |
| 86.8 | 14.4 | 231 | 313.2 | $22.1 * 10^{-3}$ |

The free energy barriers for all the three proteinases are very similar but it is apparent that $VPR_{\Delta C}$ and PRK do have to overcome more entropic contribution than AQUI to reach their transition state. On the basis of these results it may be proposed that reason for the faster inactivation rates of AQUI, as compared to its homologs adapted to lower temperatures, may at least partly be attributed to a smaller entropic contribution to free energy activation barrier

for the reaction. It can be anticipated that in the case of the more rigid structure of the thermophilic enzyme less entropy needs to be lost in reaching the correct orientation between the reactants in the transition state, than e.g. in the case of the reaction involving the more flexible cold adapted VPR. In the case of the more flexible VPR the more entropy needs to be lost to reach the transition state, which is energetically unfavorable, this entropic contribution raises the activation barrier ($\Delta G^{\ddagger}$), hence slows down the rate of reaction.

# 4 Conclusions

This project was intended to be prelimainary steps for further studies on the inhibition pattern and properties of the three subtilases, the thermophilic, AQUI, the mesophilic PRK and the cold adapted $VPR_{\Delta C}$. Protease-protease inhibitor interactions are prototypical models for protein-protein interactions and it is of interest to examine how these closely related homologous subtilases, adapted to different temperatures responded to different inhibitors. Thus as a first step a series of protease inhibitors were selected and their inhibitory activity against the three subtilases was measured, of the nine inhibitors three (PMSF, CHYS and OVOI) of them did show complete inhibition, TOM and COM did show partial inhibition, but TOM did have considerably more effects on the enzymes than COM. As for the rest of the inhibitors, STI, aprotinin and Bowman-Birk did show an increase in activity that was high enough to indicate that there is something more going on there than just error in the measurement. More experiments on that topic are needed to explain that further.

On the basis of these results, three inhibitors were chosen for further experiments, firstly, TOM was selected to compare the reversible inhibitory and kinetic effects on the subtilases and secondly PMSF and CHYS were used for comparison of the irreversible inhibitory activity.

The first step in the experiment of TOM against the subtilases was to determine the time needed for the binding interaction to reach equilibrium. AQUI seemed to establish equilibrium after 20 minutes but for PRK and $VPR_{\Delta C}$ the time was a bit longer, or 30-40 minutes for equilibrium to establish. These results were used to establish the parameters for the rest of the experiments done with TOM, by incubating all samples for at least 30 minutes at 25°C. The fact that TOM binding to AQUI reached equilibrium before the other two enzymes was the first indication of the higher sensitivity of AQUI against TOM.

To get more direct measurements of how sensitive the three subtilases were against TOM, an experiment was conducted, where the effects of constant concentrations of the subtilases were measured against different concentrations of TOM. In these experiments a more clear difference between AQUI and the other two subtilases was observed, as AQUI was affected considerably more than the other two. The decision was then taken to plot that same data as $(V_0/V_i)$-1 against the concentrations of TOM to determine the apparent equilibrium constant $K_{i(app)}$ to establish the tightness of the binding of TOM to the subtilases. The observed values were; for $VPR_{\Delta C}$ it was 0.26 µM for PRK it was 0.13 µM and for AQUI it was 0.58 µM but by taking the enzyme concentration into the calculations and by using the ratio of $[E]_0$ / $K_{i(app)}$

for comparison the values obtained were 1.0 for $VPR_{\Delta C}$, 1.4 for PRK and 5.0 for AQUI, this means that TOM is binding tightest to AQUI, then PRK and the weakest binding between $VPR_{\Delta C}$ and TOM. Although this follows the order of the enzymes with respect to temperature adaptation, it was in reverse of what was expected.

Michaelis-Menten kinetic measurements were also conducted on the three subtilases in the absence and presence of TOM. The results from the measurements in the absence of TOM gave values that were for AQUI relatively close to the published values but in the case of PRK the values were a bit off to what was expected but that can be attributed to error in concentration measurements of the enzymes. The $k_{cat}$ values were higher than expected, but the ratio of $k_{cat}/K_m$ was closer to what was expected. For $VPR_{\Delta C}$ the $K_m$ value was relatively accurate but $k_{cat}$ was higher than expected. The difference between the values of $K_m$, $k_{cat}$ and $k_{cat}$ / $K_m$ in the absence and presence of TOM showed that $k_{cat}$ did decrease considerably. Differences in $K_m$ however did differ, it did not change for $VPR_{\Delta C}$, it was lower for PRK and did increase by factor four in the case of AQUI that might indicate that the type of inhibition was a mixed inhibition. When comparing $k_{cat}$ / $K_m$, the order was as previously observed did establish itself, the difference for $VPR_{\Delta C}$ was 11-fold, 22-fold for PRK and 32-fold for AQUI. According to these results AQUI is more sensitive to the inhibitor TOM than PRK and affects $VPR_{\Delta C}$ the least.

CHYS was originally chosen to observe the rates of the irreversible first order kinetics but under the conditions chosen for these experiments it was observed that the rate of this inhibition was too fast to readily measure, so for these experiments the serine-proteinase inhibitor PMSF was selected instead. The results were that the rates of inhibition did show the same order as in the case of inhibition with TOM. The data obtained from determining the rates of inactivation at different temperatures were then used to plot Arrhenius graphs to obtain the activation energy ($E_a$) of the inhibition. The values obtained from the plots were 12.8 kJ/mol for $VPR_{\Delta C}$, 10.6 kJ/mol for PRK and 17.0 kJ/mol for AQUI.

From the activation energies obtained from the slopes of the Arrhenius-plots it was decided to calculate the activation parameters, $\Delta G^{\ddagger}$, $\Delta H^{\ddagger}$ and $\Delta S^{\ddagger}$ to get a further insight which factors contributed most to the activation barrier for the reaction of PMSF with the proteinases. From these calculations it came apparent that the faster rate of inactivation of the thermophilic AQUI could be attributed to lower entropic contribution to the free energy of activation, which may be a result of its more rigid molecular structure of its active site, than compared to its homologs VPR and PRK.

# References


Almog, O., Kogan, A., Leeuw, M., Gdalevsky, G. Y., Cohen-Luria, R. & Parola, A. H. (2008). Structural insights into cold inactivation of tryptophanase and cold adaptation of subtilisin S41. *Biopolymers* **89**, 354-359.

Arnold, F. H., Wintrode, P. L., Miyazaki, K. & Gershenson, A. (2001). How enzymes adapt: lessons from directed evolution. *Trends Biochem Sci* **26**, 100-106.

Arnorsdottir, J., Helgadottir, S., Thorbjarnardottir, S. H., Eggertsson, G. & Kristjansson, M. M. (2007). Effect of selected Ser/Ala and Xaa/Pro mutations on the stability and catalytic properties of a cold adapted subtilisin-like serine proteinase. *Biochim Biophys Acta* **1774**, 749-755.

Arnórsdóttir, J., Kristjánsson, M. M. & Ficner, R. (2005). Crystal structure of a subtilisin-like serine proteinase from a psychrotrophic *Vibrio* species reveals structural aspects of cold adaptation. *FEBS J* **272**, 832-845.

Arnorsdottir, J., Magnusdottir, M., Fridjonsson, O. H. & Kristjansson, M. M. (2011). The effect of deleting a putative salt bridge on the properties of the thermostable subtilisin-like proteinase, aqualysin I. *Protein Pept Lett* **18**, 545-551.

Arnórsdóttir, J., Smáradóttir, R. B., Magnússon, Ó. T., Thorbjarnardóttir, S. H., Eggertsson, G. & Kristjánsson, M. M. (2002). Characterization of a cloned subtilisin-like serine proteinase from a psychrotrophic *Vibrio* species. *Eur J Biochem* **269**, 5536-5546.

Azizian, S. (2004). Kinetic models of sorption: a theoretical analysis. *J Colloid Interface Sci* **276**, 47-52.

Barrett, A. J. & Rawlings, N. D. (1995). Families and Clans of Serine Peptidases. *Arch Biochem Biophys* **318**, 247-250.

Betzel, C., Pal, G. P. & Saenger, W. (1988). Synchrotron X-ray data collection and restrained least-squares refinement of the crystal structure of proteinase K at 1.5 Å resolution. *Acta Crystallogr B* **44 ( Pt 2)**, 163-172.

Betzel, C., Teplyakov, A. V., Harutyunyan, E. H., Saenger, W. & Wilson, K. S. (1990). Thermitase and proteinase K: a comparison of the refined three-dimensional structures of the native enzymes. *Protein Eng* **3**, 161-172.

Bieth, J. G. (1995). Theoretical and practical aspects of proteinase inhibition kinetics. *Methods Enzymol* **248**, 59-84.

Bode, W. & Huber, R. (1992). Natural protein proteinase inhibitors and their interaction with proteinases. *Eur J Biochem* **204**, 433-451.

Bruins, M., Janssen, A. M. & Boom, R. (2001). Thermozymes and their applications. *Appl Biochem Biotechnol* **90**, 155-186.

Buller, A. R. & Townsend, C. A. (2013). Intrinsic evolutionary constraints on protease structure, enzyme acylation, and the identity of the catalytic triad. *Proc Natl Acad Sci U S A* **110**, E653-661.

Casanueva, A., Tuffin, M., Cary, C. & Cowan, D. A. (2010). Molecular adaptations to psychrophily: the impact of 'omic' technologies. *Trends Microbiol* **18**, 374-381.

D'Amico, S., Gerday, C. & Feller, G. (2003). Temperature Adaptation of Proteins: Engineering Mesophilic-like Activity and Stability in a Cold-adapted α-Amylase. *J Mol Biol* **332**, 981-988.

DelMar, E. G., Largman, C., Brodrick, J. W. & Geokas, M. C. (1979). A sensitive new substrate for chymotrypsin. *Anal Biochem* **99**, 316-320.

Dowd, J. E. & Riggs, D. S. (1965). A comparison of estimates of Michaelis-Menten kinetic constants from various linear transformations. *J Biol Chem* **240**, 863-869.

Ebeling, W., Hennrich, N., Klockow, M., Metz, H., Orth, H. D. & Lang, H. (1974). Proteinase K from *Tritirachium album* Limber. *Eur J Biochem* **47**, 91-97.

Feller, G. & Gerday, C. (2003). Psychrophilic enzymes: hot topics in cold adaptation. *Nat Rev Microbiol* **1**, 200-208.

Gallagher, T., Gilliland, G., Wang, L. & Bryan, P. (1995). The prosegment-subtilisin BPN' complex: crystal structure of a specific 'foldase'. *Structure* **3**, 907-914.

Hedstrom, L. (2002). Serine protease mechanism and specificity. *Chem Rev* **102**, 4501-4524.

Huntington, J. A., Read, R. J. & Carrell, R. W. (2000). Structure of a serpin-protease complex shows inhibition by deformation. *Nature* **407**, 923-926.

Ibrahim, B. S. & Pattabhi, V. (2004). Crystal structure of trypsin–turkey egg white inhibitor complex. *Biochem Biophys Res Commun* **313**, 8-16.

Jany, K. D. & Mayer, B. (1985). Proteinase K from Tritirachium album limber. I. Molecular mass and sequence around the active site serine residue. *Biol Chem Hoppe Seyler* **366**, 485-492.

Kam, C.-M., Hudig, D. & Powers, J. C. (2000). Granzymes (lymphocyte serine proteases): characterization with natural and synthetic substrates and inhibitors. *Biochim Biophys Acta* **1477**, 307-323.

Karshikoff, A. & Ladenstein, R. (2001). Ion pairs and the thermotolerance of proteins from hyperthermophiles: a 'traffic rule' for hot roads. *Trends Biochem Sci* **26**, 550-557.

Kashefi, K. & Lovley, D. R. (2003). Extending the upper temperature limit for life. *Science* **301**, 934.

King, J. & Laemmli, U. K. (1971). Polypeptides of the tail fibres of bacteriophage T4. *J Mol Biol* **62**, 465-477.

Kristjánsson, M. M. (2012) Thermostable subtilases (Subtilisin-like Serine Próteinases), In *Thermostable Proteins: Structural Stability and Design* (Sen, S., and Nilsson, L., Eds.), 67-104, Taylor and Francis, USA.

Kristjánsson, M. M. (2013) Cold Adapted Subtilases, In *Handbook of Proteolytic Enzymes*, Vol. 1., (Rawlings, N. D., and Salvesen, G. S., Eds.), 3161-3166, Elsevier Ltd.

Kristjánsson, M. M., Magnússon, Ó. T., Gudmundsson, H. M., Alfredsson, G. Á. & Matsuzawa, H. (1999). Properties of a subtilisin-like proteinase from a psychrotrophic *Vibrio* species. *Eur J Biochem* **260**, 752-760.

Larsen, A. N., Moe, E., Helland, R., Gjellesvik, D. R. & Willassen, N. P. (2006). Characterization of a recombinantly expressed proteinase K-like enzyme from a psychrotrophic Serratia sp. *FEBS J* **273**, 47-60.

Laskowski, M. & Kato, I. (1980). Protein Inhibitors of Proteinases. *Annu Rev Biochem* **49**, 593-626.

Laskowski, M. & Qasim, M. A. (2000). What can the structures of enzyme-inhibitor complexes tell us about the structures of enzyme substrate complexes? *Biochim Biophys Acta* **1477**, 324-337.

Li, W. F., Zhou, X. X. & Lu, P. (2005). Structural features of thermozymes. *Biotechnol Adv* **23**, 271-281.

Marie-Claire, C., Yabuta, Y., Suefuji, K., Matsuzawa, H. & Shinde, U. (2001). Folding pathway mediated by an intramolecular chaperone: the structural and functional characterization of the aqualysin I propeptide. *J Mol Biol* **305**, 151-165.

Matsuzawa, H., Tokugawa, K., Hamaoki, M., Mizoguchi, M., Taguchi, H., Terada, I., Kwon, S.-T. & Ohta, T. (1988). Purification and characterization of aqualysin I (a thermophilic alkaline serine protease) produced by *Thermus aquaticus* YT-1. *Eur J Biochem* **171**, 441-447.

Maynes, J. T., Cherney, M. M., Qasim, M. A., Laskowski, M., Jr. & James, M. N. (2005). Structure of the subtilisin Carlsberg-OMTKY3 complex reveals two different ovomucoid conformations. *Acta Crystallogr D Biol Crystallogr* **61**, 580-588.

Müller, A. & Saenger, W. (1993). Studies on the inhibitory action of mercury upon proteinase K. *J Biol Chem* **268**, 26150-26154.

Nagase, H., and Salvesen, G. S. (2001) Inhibition of proteolytic enzymes., Finding, purification and characterization of natural protease inhibitors, In *Proteolytic Enzymes 2nd* ed. (Beynon, R., and Bond, J. S., Eds.), 105-147, Oxford university press.

Oldak, E. & Trafny, E. A. (2005). Secretion of proteases by *Pseudomonas aeruginosa* biofilms exposed to ciprofloxacin. *Antimicrob Agents Chemother* **49**, 3281-3288.

Olson, S. T. & Chuang, Y.-J. (2002). Heparin Activates Antithrombin Anticoagulant Function by Generating New Interaction Sites (Exosites) for Blood Clotting Proteinases. *Trends Cardiovasc Med* **12**, 331-338.

Ottmann, C., Rose, R., Huttenlocher, F., Cedzich, A., Hauske, P., Kaiser, M., Hauber, R. & Schaller, A. (2009). Structural basis for $Ca^{2+}$-Independence and activation by homodimerization of tomato subtilase 3. *Proc Natl Acad Sci U S A* **40**, 17223-17228.

Pace, C. N., Vajdos, F., Fee, L., Grimsley, G. & Gray, T. (1995). How to measure and predict the molar absorption coefficient of a protein. *Protein Sci* **4**, 2411-2423.

Page, M. J. & Cera, E. (2008). Serine peptidases: Classification, structure and function. *Cell Mol Life Sci* **65**, 1220-1236.

Perona, J. J. & Craik, C. S. (1995). Structural basis of substrate specificity in the serine proteases. *Protein Sci* **4**, 337-360.

Rawlings, N. D., Tolle, D. P. & Barrett, A. J. (2004). Evolutionary families of peptidase inhibitors. *Biochem J* **378**, 705-716.

Rockwell, N. C. & Thorner, J. W. (2004). The kindest cuts of all: crystal structures of Kex2 and furin reveal secrets of precursor processing. *Trends Biochem Sci* **29**, 80-87.

Sakaguchi, M., Niimiya, K., Takezawa, M., Toki, T., Sugahara, Y. & Kawakita, M. (2008). Construction of an expression system for aqualysin I in Escherichia coli that gives a markedly improved yield of the enzyme protein. *Biosci Biotechnol Biochem* **72**, 2012-2018.

Siddiqui, K. S. & Cavicchioli, R. (2006). Cold-Adapted Enzymes. *Annu Rev Biochem* **75**, 403-433.

Siezen, R. J. & Leunissen, J. A. M. (1997). Subtilases: The superfamily of subtilisin-like serine proteases. *Protein Sci* **6**, 501-523.

Sigurdardottir, A. G., Arnorsdottir, J., Þorbjarnardottir, S. H., Eggertsson, G., Suhre, K. & Kristjansson, M. M. (2009). Characteristics of mutants designed to incorporate a new ion pair into the structure of a cold adapted subtilisin-like serine proteinase. *Biochim Biophys Acta* **1794**, 512-518.

Smith, C. A., Toogood, H. S., Baker, H. M., Daniel, R. M. & Baker, E. N. (1999). Calcium-mediated thermostability in the subtilisin superfamily: the crystal structure of Bacillus Ak.1 protease at 1.8 Å resolution. *J Mol Biol* **294**, 1027-1040.

Tanaka, S., Matsumura, H., Koga, Y., Takano, K. & Kanaya, S. (2007). Four new crystal structures of Tk-subtilisin in unautoprocessed, autoprocessed and mature forms: insight into structural changes during maturation. *J Mol Biol* **372**, 1055-1069.

Tepliakov, A. V., Kuranova, I. P., Arutiunian, E. G., Frommel, C. & Hohne, W. E. (1990). Crystal structure of thermitase and stability of subtilisins. *Bioorg Khim* **16**, 437-447.

# Appendix

**Table 11**. Name of the AQUI samples, abbreviations, volume and activity as they were before being diluted for the freezer.

| ***Name*** | ***Activity units (U)*** | ***Volume (ml)*** |
|---|---|---|
| KRO1A | 32.5 U | 5.9 ml |
| KRO2A | 32.8 U | 2.3 ml |
| KRO3A | 17.5 U | 2.5 ml |
| KRO4A | 6.1 U | 1.9 ml |
| **Total** | **88.9 U** | **12.6 ml** |

**Table 12**. Name of the $VPR_{\Delta C}$ samples, abbreviations, volume and activity as they were before being diluted for the freezer.

| ***Name*** | ***Activity units (U)*** | ***Volume (ml)*** |
|---|---|---|
| KRO1V | 168.0 U | 7.5 ml |
| KRO2V | 20.0 U | 5.7 ml |
| **Total** | **188.0 U** | **13.2 ml** |

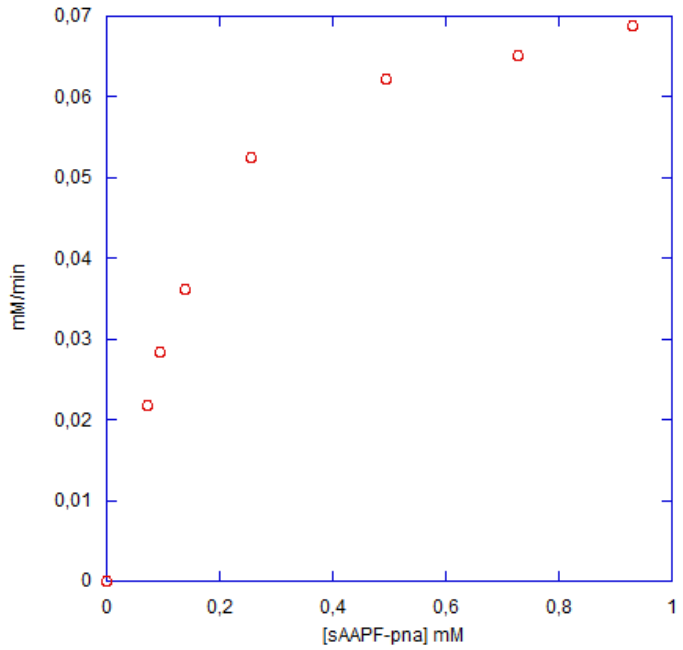


*Figure 30. Measurements done on VPR$_{\Delta C}$ in the absence of TOM plotted as a Michaelis-Menten graph. Measured at 25°C and incubated at 25°C. X-axis shows the substrate concentration in mM and the Y-axis shows rate expressed as mM/min. Measured with sAAPF-pna.*

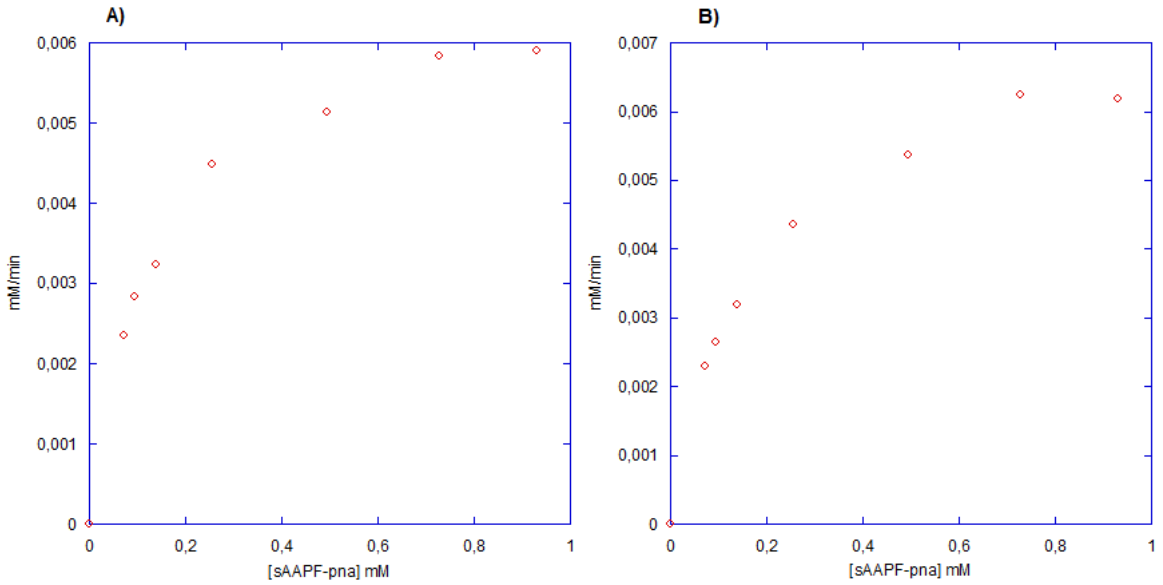


*Figure 31. Measurements done on VPR$_{\Delta C}$ plotted as a Michaelis-Menten graph in the presence of tenfold molar excess of TOM. Measured at 25°C and incubated at 25°C. X-axis shows the substrate concentration in mM and the Y-axis shows rate expressed as mM/min. Measured with sAAPF-pna.*

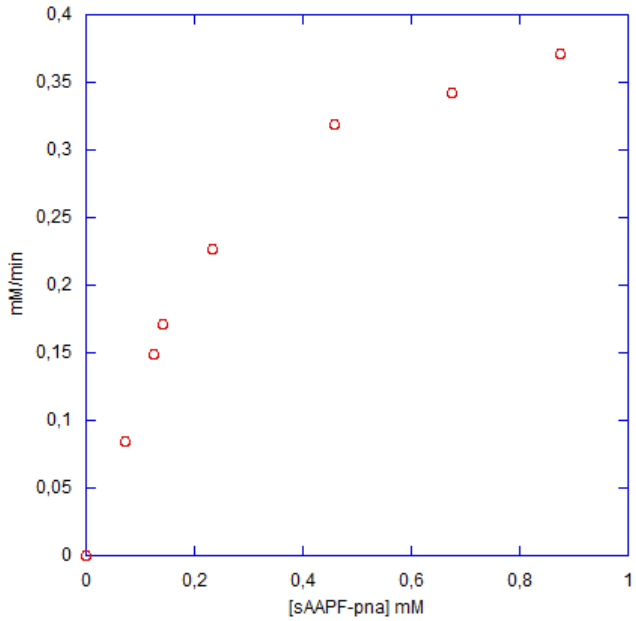


*Figure 32. Measurements done on PRK in the absence of TOM plotted as a Michaelis-Menten graph. Measured at 25°C and incubated at 25°C. X-axis shows the substrate concentration in mM and the Y-axis shows rate expressed as mM/min. Measured with sAAPF-pna.*

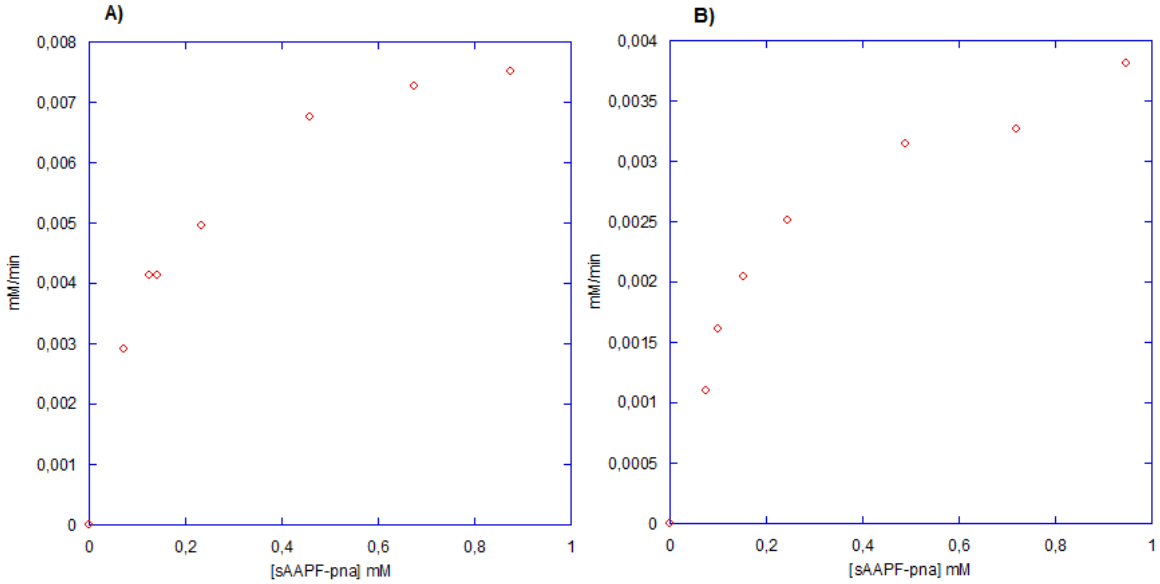


*Figure 33. Measurements done on PRK plotted as a Michaelis-Menten graph in the presence of tenfold molar excess of TOM. Measured at 25°C and incubated at 25°C. X-axis shows the substrate concentration in mM and the Y-axis shows rate expressed as mM/min. Measured with sAAPF-pna.*

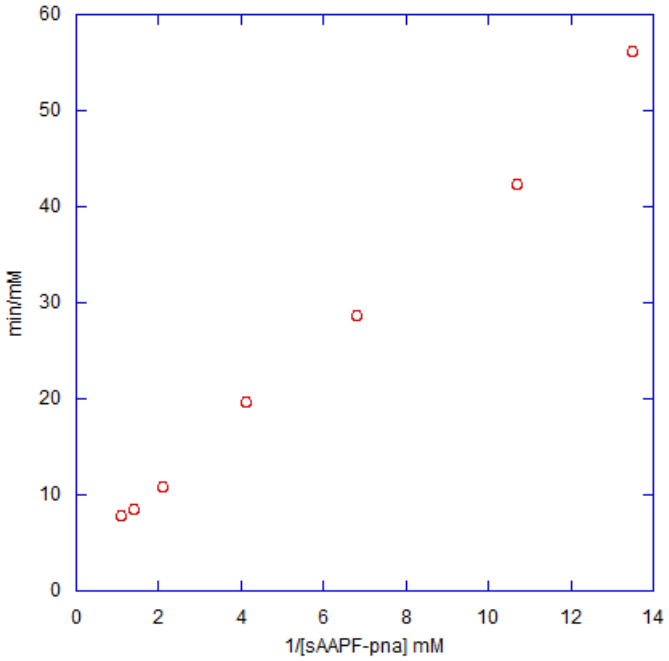


*Figure 34. Measurements done on AQUI in the absence of TOM plotted as a Lineweaver-Burke graph. Measured at 25°C and incubated at 25°C. X-axis shows the substrate concentration in 1/mM and the Y-axis shows rate expressed as min/mM. Measured with sAAPF-pna.*

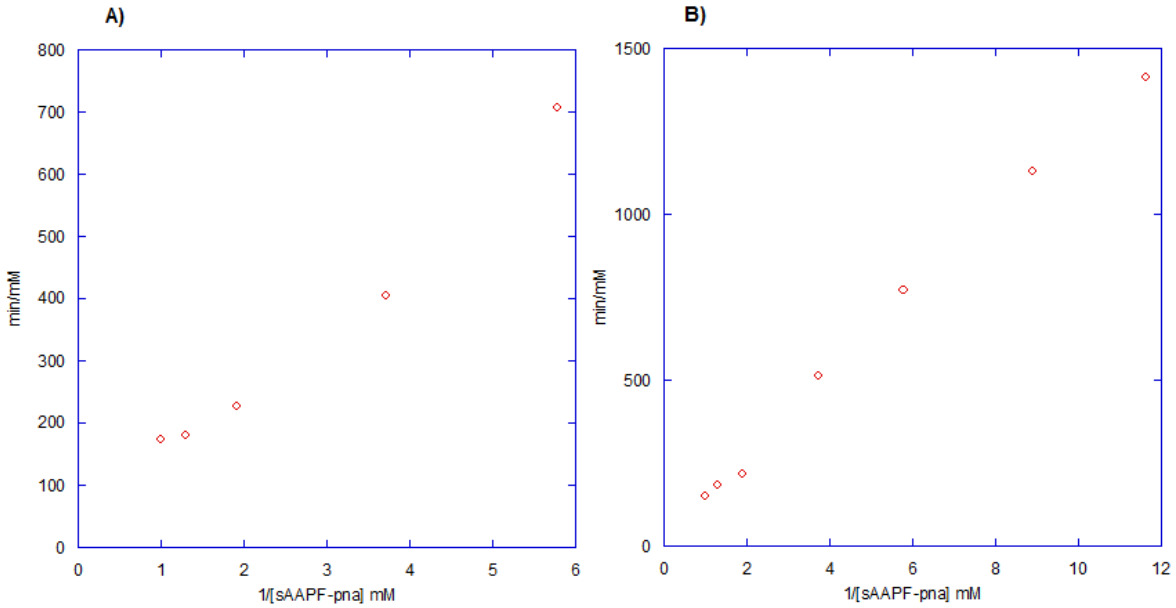


*Figure 35. Measurements done on AQUI plotted as a Linewaver-Burke graph in the presence of tenfold molar excess of TOM. Measured at 40°C and incubated at 25°C. X-axis shows the substrate concentration in 1/mM and the Y-axis shows rate expressed as min/mM. Measured with sAAPF-pna.*

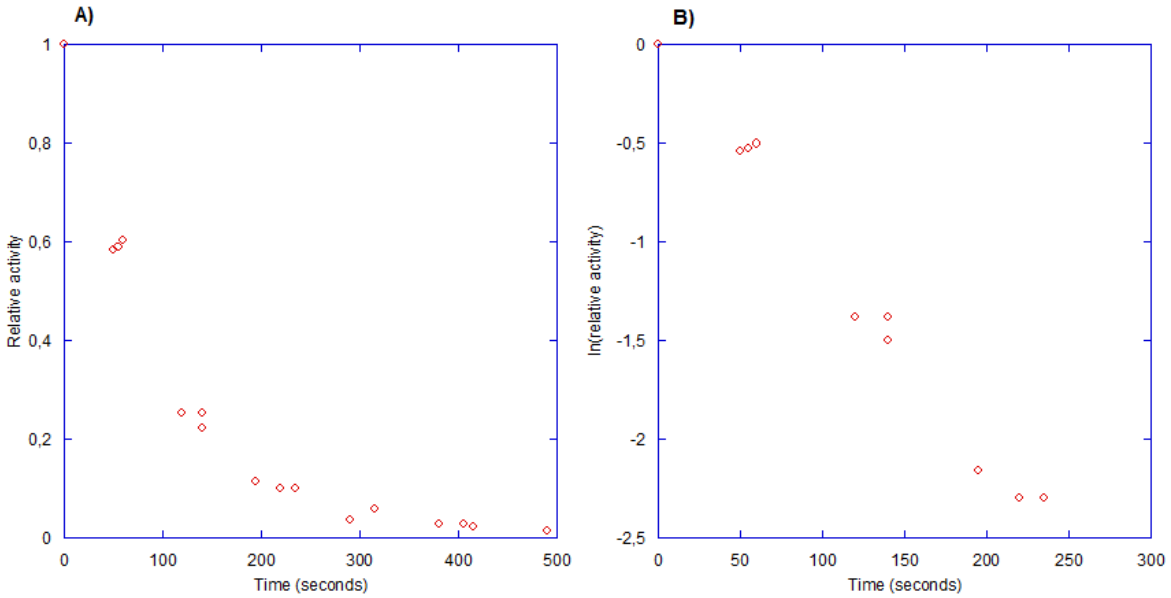


*Figure 36. Rate of inhibition for $VPR_{\Delta C}$ by PMSF measured at 25°C with 0.5 mM sAAPF-pna in the presence of 100-fold molar excess of PMSF incubated at room temperature. Picture A) shows the data represented as relative activity on the Y-axis and time in seconds on the X-axis. Picture B) shows the linear representation of the data, X-axis shows the time in seconds and the Y-axis show ln(relative activity). This graph wasn't used to obtain a rate constant.*

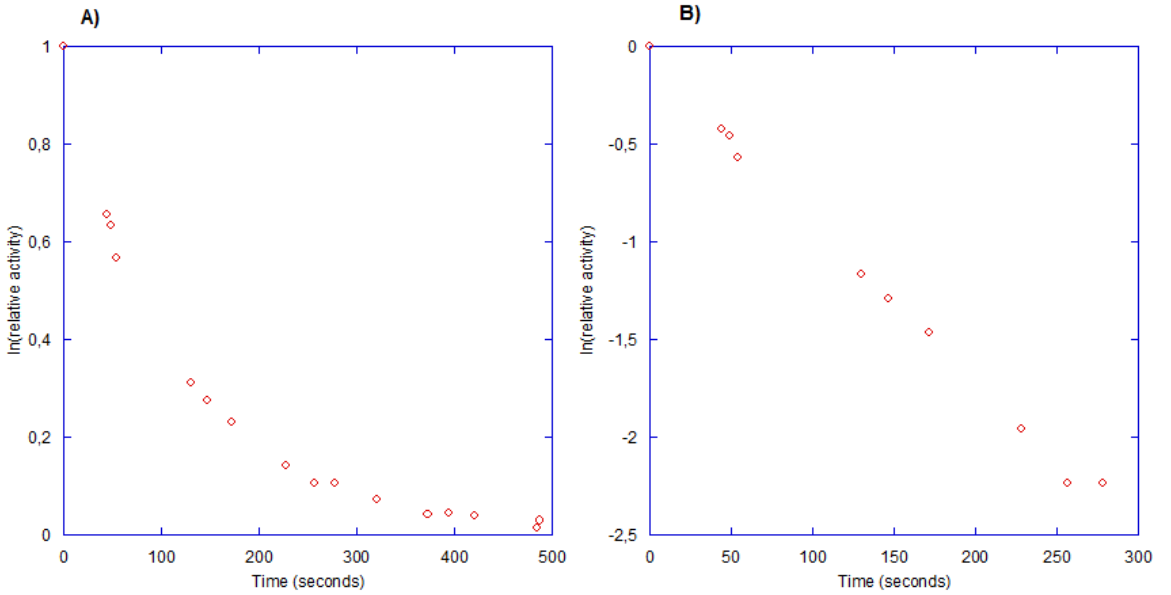


*Figure 37. Rate of inhibition for $VPR_{\Delta C}$ by PMSF measured at 25°C with 0.5 mM sAAPF-pna in the presence of 100-fold molar excess of PMSF incubated at 20.7°C. Picture A) shows the data represented as relative activity on the Y-axis and time in seconds on the X-axis. Picture B) shows the linear representation of the data, X-axis shows the time in seconds and the Y-axis show ln(relative activity). Rate constant obtained was 0.0085$s^{-1}$.*

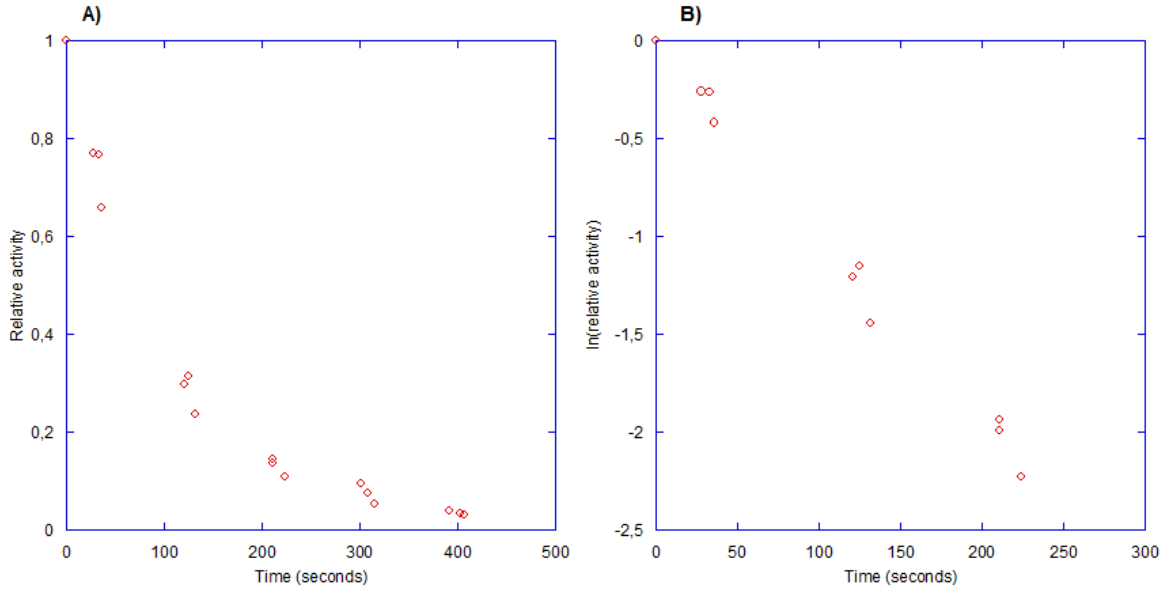


*Figure 38. Rate of inhibition for $VPR_{\Delta C}$ by PMSF measured at 25°C with 0.5 mM sAAPF-pna in the presence of 100-fold molar excess of PMSF incubated at 30.2°C. Picture A) shows the data represented as relative activity on the Y-axis and time in seconds on the X-axis. Picture B) shows the linear representation of the data, X-axis shows the time in seconds and the Y-axis show ln(relative activity). Rate constant obtained was 0.0097$s^{-1}$.*

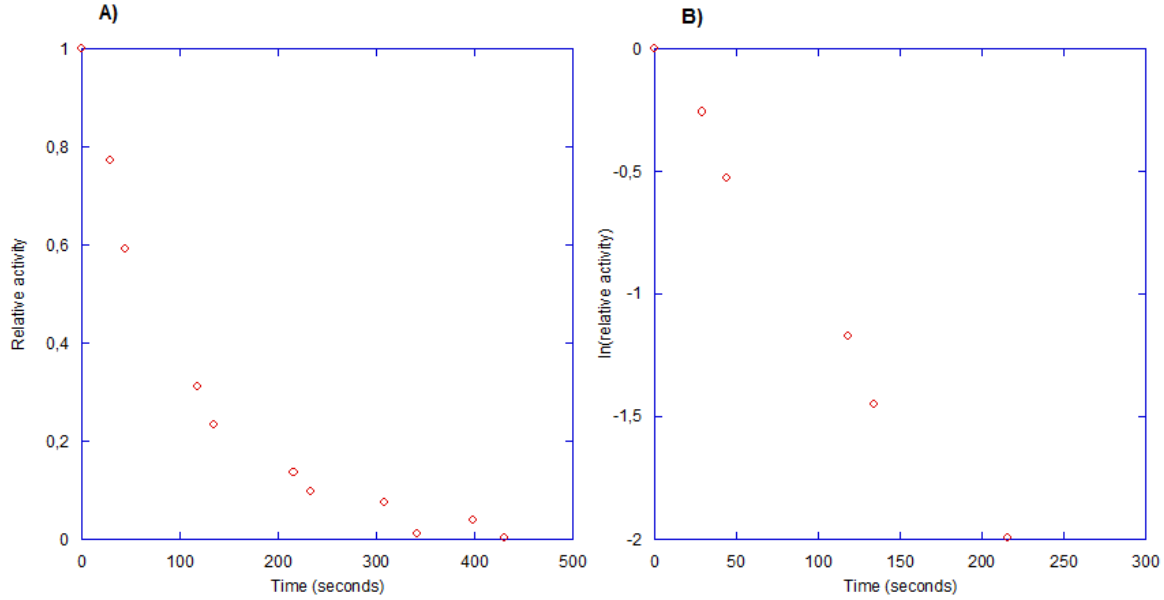


*Figure 39. Rate of inhibition for $VPR_{\Delta C}$ by PMSF measured at 25°C with 0.5 mM sAAPF-pna in the presence of 100-fold molar excess of PMSF incubated at 30.4°C. Picture A) shows the data represented as relative activity on the Y-axis and time in seconds on the X-axis. Picture B) shows the linear representation of the data, X-axis shows the time in seconds and the Y-axis show ln(relative activity). Rate constant obtained was 0.0098$s^{-1}$.*

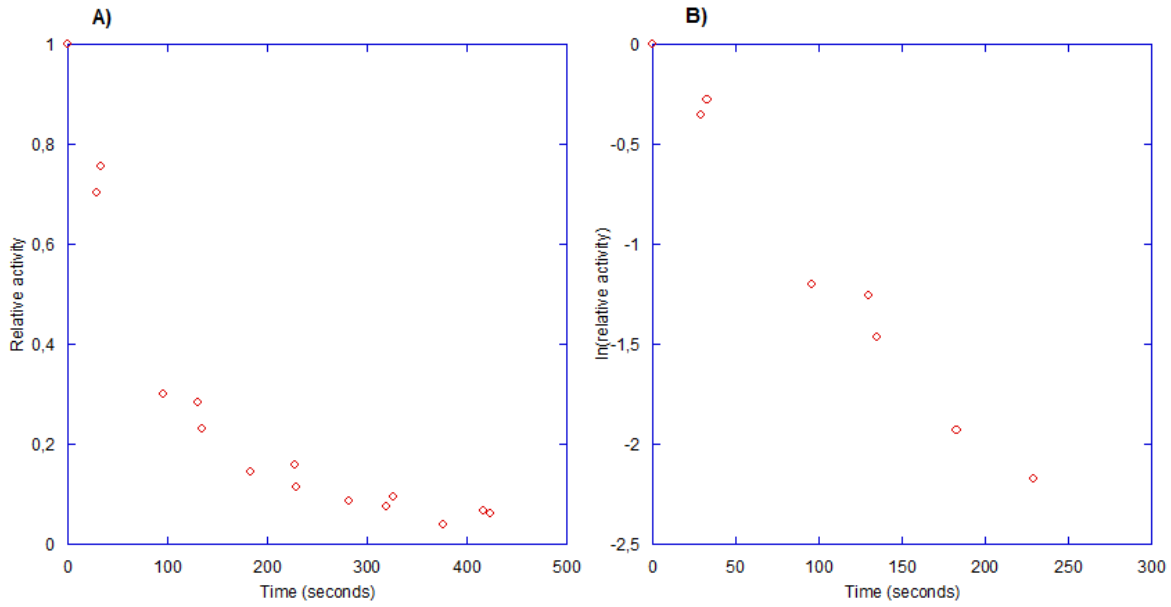


*Figure 34. Rate of inhibition for $VPR_{\Delta C}$ by PMSF measured at 25°C with 0.5 mM sAAPF-pna in the presence of 100-fold molar excess of PMSF incubated at 40.2°C. Picture A) shows the data represented as relative activity on the Y-axis and time in seconds on the X-axis. Picture B) shows the linear representation of the data, X-axis shows the time in seconds and the Y-axis show ln(relative activity). Rate constant obtained was $0.0102s^{-1}$.*

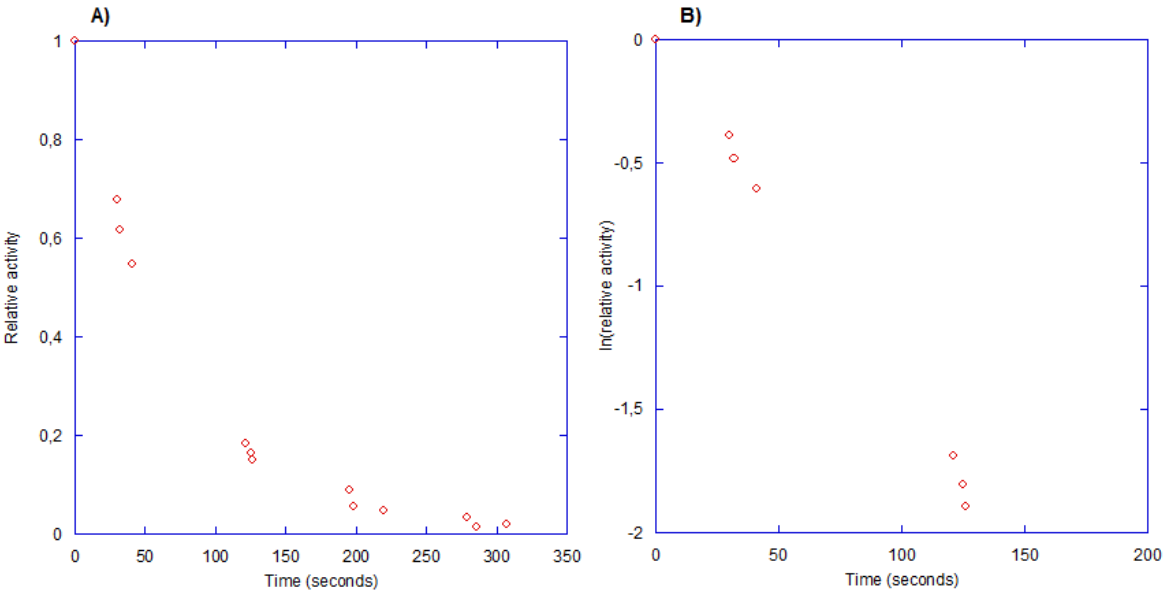


*Figure 41. Rate of inhibition for PRK by PMSF measured at 25°C with 0.5 mM sAAPF-pna in the presence of 100-fold molar excess of PMSF incubated at room temperature. Picture A) shows the data represented as relative activity on the Y-axis and time in seconds on the X-axis. Picture B) shows the linear representation of the data, X-axis shows the time in seconds and the Y-axis show ln(relative activity). This graph wasn't used to obtain a rate constant.*

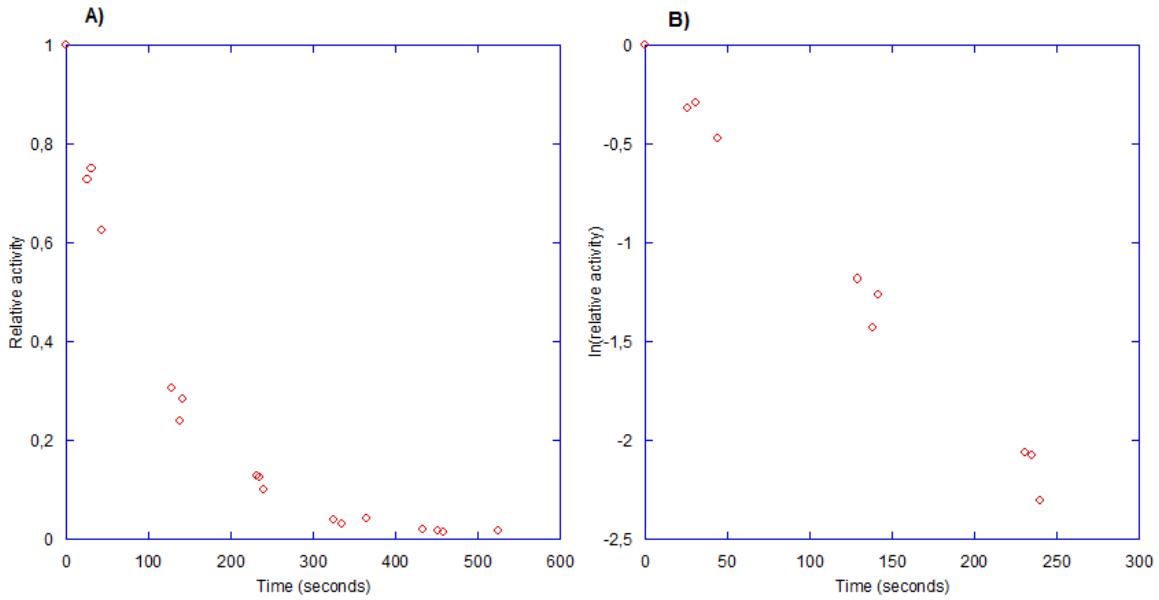


*Figure 42. Rate of inhibition for PRK by PMSF measured at 25°C with 0.5 mM sAAPF-pna in the presence of 100-fold molar excess of PMSF incubated at 10.7°C. Picture A) shows the data represented as relative activity on the Y-axis and time in seconds on the X-axis. Picture B) shows the linear representation of the data, X-axis shows the time in seconds and the Y-axis show ln(relative activity). Rate constant obtained was 0.0092s$^{-1}$.*

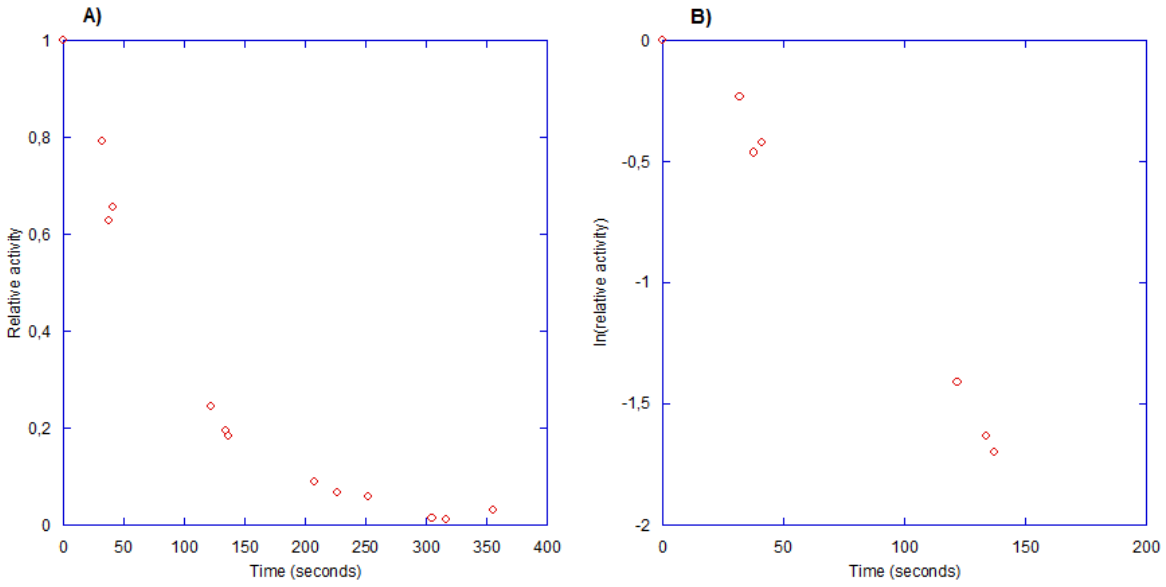


*Figure 43. Rate of inhibition for PRK by PMSF measured at 25°C with 0.5 mM sAAPF-pna in the presence of 100-fold molar excess of PMSF incubated at 20.9°C. Picture A) shows the data represented as relative activity on the Y-axis and time in seconds on the X-axis. Picture B) shows the linear representation of the data, X-axis shows the time in seconds and the Y-axis show ln(relative activity). Rate constant obtained was 0.0119s$^{-1}$.*

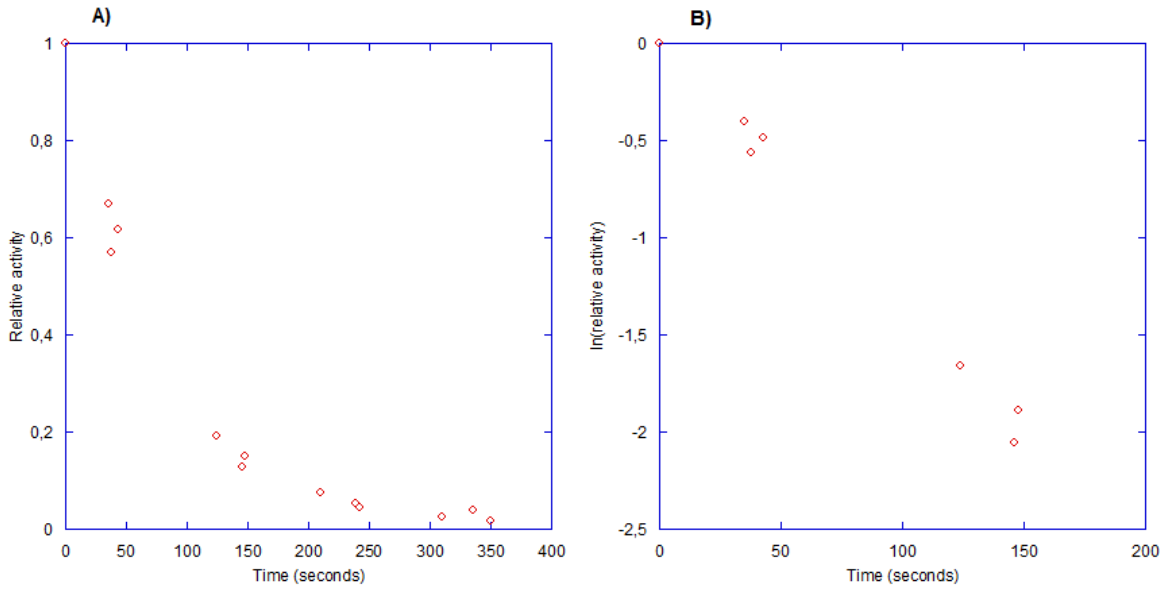


*Figure 44. Rate of inhibition for PRK by PMSF measured at 25°C with 0.5 mM sAAPF-pna in the presence of 100-fold molar excess of PMSF incubated at 30.2°C. Picture A) shows the data represented as relative activity on the Y-axis and time in seconds on the X-axis. Picture B) shows the linear representation of the data, X-axis shows the time in seconds and the Y-axis show ln(relative activity). Rate constant obtained was 0.0133s$^{-1}$.*

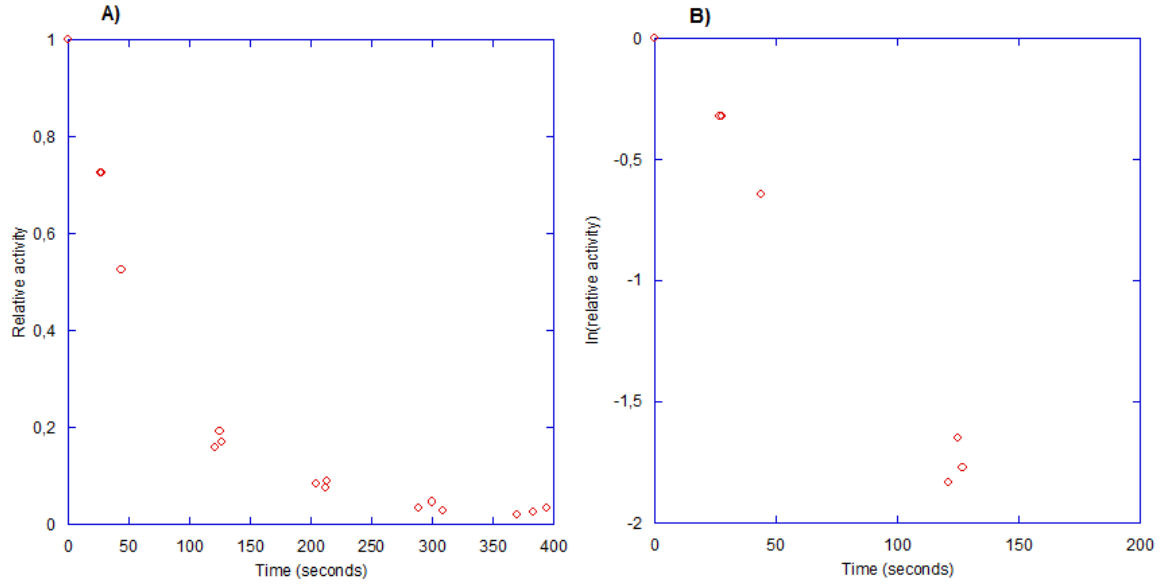


*Figure 45. Rate of inhibition for PRK by PMSF measured at 25°C with 0.5 mM sAAPF-pna in the presence of 100-fold molar excess of PMSF incubated at 39.9°C. Picture A) shows the data represented as relative activity on the Y-axis and time in seconds on the X-axis. Picture B) shows the linear representation of the data, X-axis shows the time in seconds and the Y-axis show ln(relative activity). Rate constant obtained was 0.0140s$^{-1}$.*

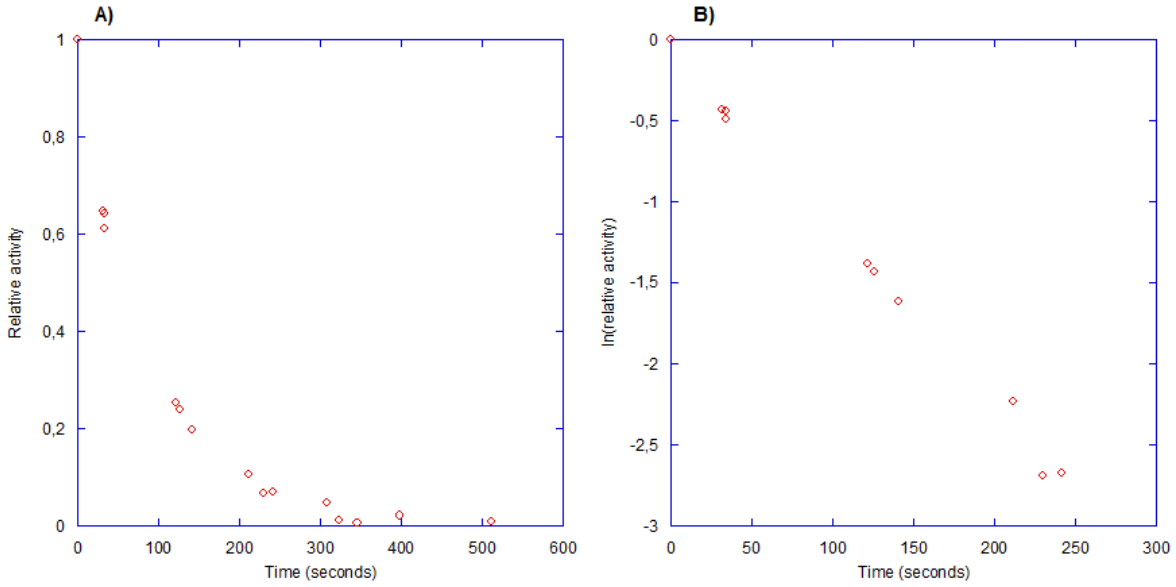


*Figure 46. Rate of inhibition for AQUI by PMSF measured at 40°C with 0.5 mM sAAPF-pna in the presence of 20-fold molar excess of PMSF incubated at 10.3°C. Picture A) shows the data represented as relative activity on the Y-axis and time in seconds on the X-axis. Picture B) shows the linear representation of the data, X-axis shows the time in seconds and the Y-axis show ln(relative activity). Rate constant obtained was 0.0112s$^{-1}$.*

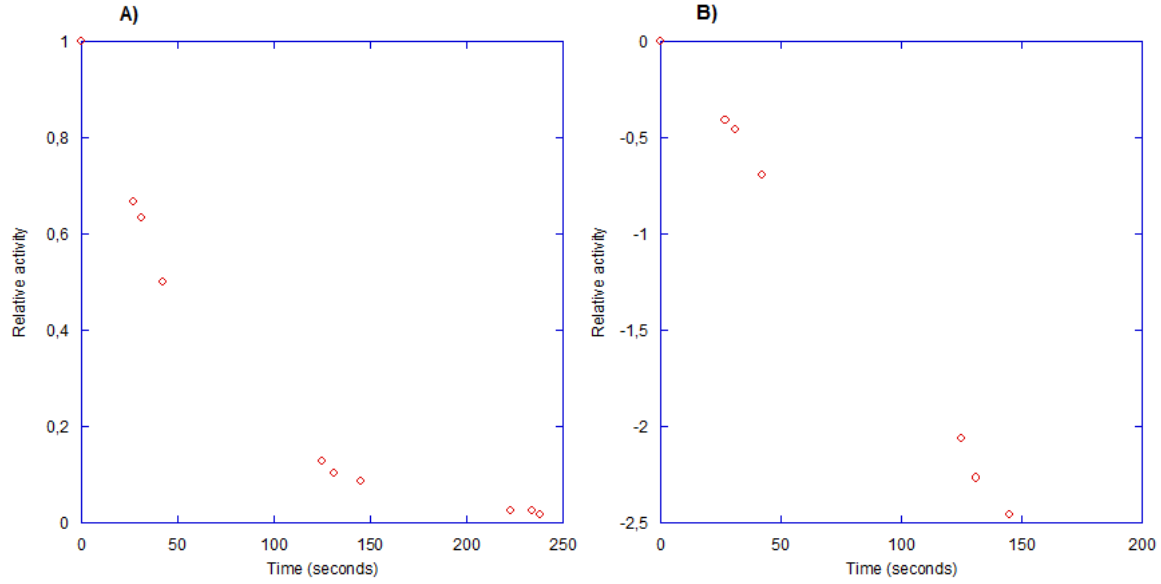


*Figure 47. Rate of inhibition for AQUI by PMSF measured at 40°C with 0.5 mM sAAPF-pna in the presence of 20-fold molar excess of PMSF incubated at 20.7°C. Picture A) shows the data represented as relative activity on the Y-axis and time in seconds on the X-axis. Picture B) shows the linear representation of the data, X-axis shows the time in seconds and the Y-axis show ln(relative activity). Rate constant obtained was 0.0169s$^{-1}$.*

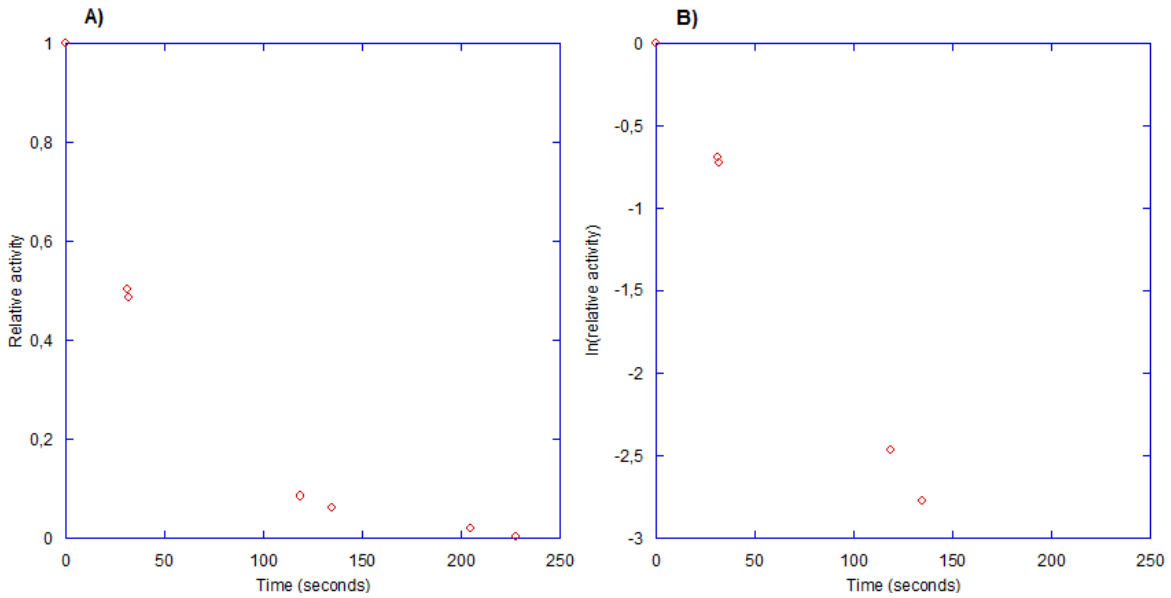


*Figure 48. Rate of inhibition for AQUI by PMSF measured at 40°C with 0.5 mM sAAPF-pna in the presence of 20-fold molar excess of PMSF incubated at 30.2°C. Picture A) shows the data represented as relative activity on the Y-axis and time in seconds on the X-axis. Picture B) shows the linear representation of the data, X-axis shows the time in seconds and the Y-axis show ln(relative activity). Rate constant obtained was 0.0207s$^{-1}$.*

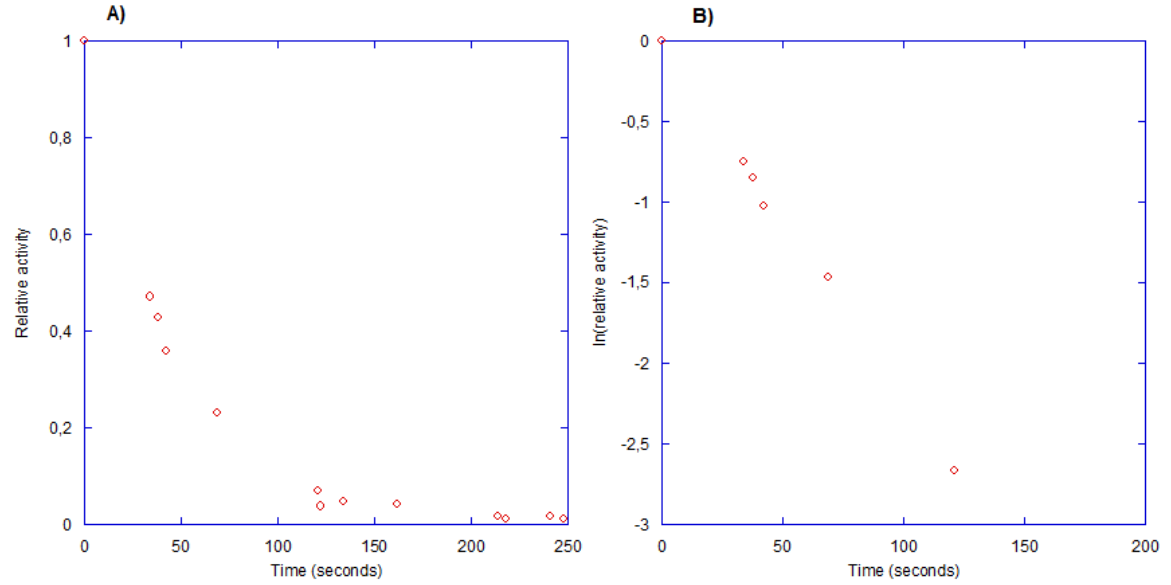


*Figure 49. Rate of inhibition for AQUI by PMSF measured at 40°C with 0.5 mM sAAPF-pna in the presence of 20-fold molar excess of PMSF incubated at 40.0°C. Picture A) shows the data represented as relative activity on the Y-axis and time in seconds on the X-axis. Picture B) shows the linear representation of the data, X-axis shows the time in seconds and the Y-axis show ln(relative activity). Rate constant obtained was 0.0221s$^{-1}$.*